NOAA Technical Report NOS CS 4

TIDAL CONSTITUENT AND RESIDUAL INTERPOLATION (TCARI): A New Method for the Tidal Correction of Bathymetric Data

Kurt Hess
Richard Schmalz
Chris Zervas
Wayne Collier

July 1999
[Revised June 2004]

noaa National Oceanic and Atmospheric Administration

U.S. DEPARTMENT OF COMMERCE
William Daly, Secretary

National Oceanic and Atmospheric Administration
D. James Baker, Under Secretary

National Ocean Service
Nancy Foster
Assistant Administrator

Office of Coast Survey
Captain David MacFarland

Coast Survey Development Laboratory
Bruce Parker

NOTICE

Mention of a commercial company or product does not constitute an endorsement by NOAA. Use for publicity or advertising purposes of information from this publication concerning proprietary products or the tests of such products is not authorized.

TABLE OF CONTENTS

LIST OF FIGURES v

LIST OF TABLES ix

EXECUTIVE SUMMARY xi

1. INTRODUCTION 1

2. TIDAL CONSTITUENT AND RESIDUAL INTERPOLATION (TCARI) 3
   - 2.1. Tide Corrections 3
   - 2.2. Tide Zoning 3
   - 2.3. Astronomic Tides and Tidal Constituents 5
   - 2.4. Spatial Interpolation 5
   - 2.5. TCARI 7
   - 2.6. TCARI Data Requirements 8
   - 2.7. Other Methods of Providing Corrections 9

3. INTERPOLATION BY SOLUTION OF LAPLACE'S EQUATION 11
   - 3.1. Laplace's Equation 11
   - 3.2. Boundary Conditions 12
   - 3.3. Natural Distributions of Corange and Cophase Lines 13
   - 3.4. Solution by Finite Differences 13
   - 3.5. Grid Generation 14
   - 3.6. Rectangular Basin Test Case 15

4. APPLICATION TO GALVESTON BAY 19
   - 4.1. Ship Track Data 19
   - 4.2. Water Level and Model Data 20
   - 4.3. Grid and Weighting Functions 22
   - 4.4. Constituent Interpolation 24
   - 4.5. Residual Water Levels 25
   - 4.6. The Offset and Datum 27
   - 4.7. Sensitivity Tests 27
   - 4.8. Accuracy Tests 30

5. APPLICATION TO SAN FRANCISCO BAY 35
   - 5.1. Ship Track Data 35
   - 5.2. Water Level and Model Data 36
   - 5.3. Grid and Weighting Functions 37
   - 5.4. Constituent Interpolation 37
   - 5.5. Residual Water Levels 41
   - 5.6. The Offset and Datum 41
   - 5.7. Accuracy Tests 43

6. COMPUTER PROGRAMS 47
6.1. PA: Grid Generation 47
6.2. PB: Weighting Function Calculation 52
6.3. PC: Calculation of the Tide Correction 55

7. SUMMARY AND CONCLUSIONS 59
7.1. Summary 59
7.2. Major Results 61
7.3. Production of Ellipsoidally-Referenced MLLW Fields 62
7.4. Future Enhancements 64

ACKNOWLEDGMENTS 65

REFERENCES 65

APPENDIX A. TIDE WAVE SOLUTION 67

APPENDIX B. TIDE DATA FOR GALVESTON BAY 69

APPENDIX C. GALVESTON BAY NUMERICAL CIRCULATION MODEL 73

APPENDIX D. SIMULATED CONSTITUENT FIELDS FOR GALVESTON BAY 85

APPENDIX E. TIDE DATA FOR SAN FRANCISCO BAY 89

APPENDIX F. SIMULATED CONSTITUENT FIELDS FOR SAN FRANCISCO BAY 97

LIST OF FIGURES

Figure 1.1. Schematic showing the depth sounding, D_S; the correction, h^*; the tide zoned correction, h_Z^*, and other survey variables 1

Figure 2.1. The tide zones in Galveston Bay. 4

Figure 2.2. The influence of land on M_2 phases for three nearby gauge locations. 6

Figure 3.1. (a) Grid for rectangular test case. Cells are 0.5 nmi on a side. (b) Grid for the rectangular test region, but rotated 45 degrees 15

Figure 3.2. Solution for *G* in an idealized basin, solving Laplace's Equation with boundary values of O = 100 at point A and O = 0 at point B for two values of *a*. 16

Figure 3.3.Contours created by spatial interpolation of values 100 at point A and 10 at point B. 18

Figure 3.4. Contours created by spatial interpolation of the sine and cosine of values 100 at point A and 10 at point B. 18

Figure 4.1. Galveston Bay locations of ellipsoidally-referenced water level measurements 19

Figure 4.2. Locations, numbers, and names of 14 Galveston Bay water level gauges that supplied data used in this study. 20

Figure 4.3. Grid generated by coastline for solving the LE in Galveston Bay 22

Figure 4.4. Weighting function *g(x, y)* for the water level station at Smith Point (877-0931) . . 23

Figure 4.5. Distribution of M_2 epoch (local) from (a) the numerical model and (b) the LE interpolation method 24

Figure 4.6. Distribution of M_2 amplitude from (a) the numerical model and (b) TCARI 25

Figure 4.7. Residual water levels in Galveston Bay during 1995. 26

Figure 4.8. (a) Offset (m) of MSL minus MLLW, H_O, and (b) tide datum MSL relative to the ellipsoid, H_E. 27

Figure 4.9. Scatter plot showing the corrections determined by tide zoning and those determined by TCARI. The correlation coefficient is 0.861. 32

Figure 4.10. Scatter plot showing the kinematic GPS-measured water levels and the TCARI-predicted water levels, both referenced to the ellipsoid 34

Figure 5.1. Location of water level measurements (denoted by a '+') in San Francisco Bay made by NOS during March and June of 1997. 35

Figure 5.2. Present and past locations of NOS water level gauges in San Francisco Bay where tidal constituent and/or time series data were used. 36

Figure 5.3. TCARI grid for San Francisco Bay. Cell size is 0.25 nautical miles. 38

Figure 5.4. The weighting function, *g(x,y)*, for San Leandro Marina (941-4688) shown as a percentage. 39

Figure 5.5. M_2 amplitudes (cm) as generated by (a) TRIM and (b) TCARI. 40

Figure 5.6. M_2 local epoch (degrees) as generated by (a) TRIM and (b) TCARI. 40

Figure 5.7. Residual water levels at four locations in San Francisco Bay 41

Figure 5.8. Distribution of the MSL-to-MLLW offset (m) in San Francisco Bay as generated by TCARI. 42

Figure 5.9. Distribution of ellipsoidally-referenced MSL datum (m) computed with the TCARI method in central San Francisco Bay. 43

Figure 5.10. Scatter plot showing 939 ellipsoidally-referenced, measured water levels and the TCARI-predicted water levels for the same time and location 44

Figure 5.11. Tide zones for San Francisco Bay. 45

Figure 6.1. Galveston Bay region showing coastline data (solid lines), the grid window (dashed lines), the ocean boundary (dotted lines), and the location of the water cell. . . . 48

Figure 6.2. Control file used to provide input to Program A and Program B as applied to Galveston Bay. Only data above the dashed line is read. 50

Figure 6.3. Typical records from a coastline file 51

Figure 6.4. All records from the ocean boundary file for Galveston Bay. 51

Figure 6.5. The Station file, showing tide station locations and other data for Galveston Bay . . 52

Figure 6.6. Sample portion of a grid file. 53

Figure 6.7. Sample portion of the *g* field file. 55

Figure 6.8. Tidal constituent data for a single station in a NOS standard format. 56

Figure 6.9. A portion of the equilibrium arguments and lunar node factors file 56

Figure 6.10. File with the residual file names. 56

Figure 6.11. Control file for Program C. 57

Figure 6.12. Sample of the Program C output file 58

Figure 7.1. TCARI's ellipsoidally-referenced MLLW field (m) in Galveston Bay. 63

Figure 7.2. TCARI's ellipsoidally-referenced MLLW field (m) for San Francisco Bay 64

Figure C.1. Curvilinear grid used in the three-dimensional hydrodynamic model study of Galveston Bay 74

Figure D.1. For K_1, distribution in San Francisco Bay of epoch from the model (a) and TCARI (b), and amplitude from the model (c) and TCARI (d). 85

Figure D.2. For O_1, distribution in San Francisco Bay of epoch from the model (a) and TCARI (b), and amplitude from the model (c) and TCARI (d). 86

Figure D.3. For P_1, distribution in San Francisco Bay of epoch from the model (a) and TCARI (b), and amplitude from the model (c) and TCARI (d). 87

Figure F.1. TRIM and TCARI fields for K_1 phase and amplitude 97

Figure F.2. TCARI fields for S_2 phase and amplitude. 98

Figure F.3. TCARI fields for O_1 phase and amplitude. 98

Figure F.4. TCARI fields for P_1 phase and amplitude. 99

Figure F.5. TCARI fields for N_2 phase and amplitude. 99

LIST OF TABLES

RMS differences between predicted water levels (using three methods) and GPS-measured water level.. xii

Table 3.1. For an angle varying from 0 degrees at one end to a range of values at the other end, the maximum difference (degrees) between two solutions. 18

Table 4.1. Tide and related data used in the Galveston Bay ship track data comparison. 21

Table 4.2. Results of the benchmark run and the sensitivity tests. Errors are in cm. 28

Table 4.3. Results from the use of hourly or 6-minute observed data for the calculation of the residual water levels. 29

Table 4.4. Results for full TCARI, total water level interpolation, and ignoring the residual water level. Errors are in cm. 29

Table 4.5. Results from the accuracy tests. GPS measured water levels were compared to water levels observed at four gauges. In TCARI, the predicted water levels were compared to those measured in Huff and Gallagher. 30

Table 4.6. Errors (cm) based on water levels estimates using tide zoned corrections. Results are for preliminary tide zoning (one station), final zoning with five stations, and final zoning with eight stations. 31

Table 4.7. Results from comparing errors in water level estimates using spatially-interpolated discrete tide zoning corrections and TCARI 33

Table 4.8. Mean and RMS error and standard deviation of the predicted water level as compared to the measured water level in Galveston Bay using various methods of prediction 34

Table 5.1. Mean error, standard deviation, RMS error, and maximum value of the error (the predicted minus the measured) in water levels in San Francisco Bay (cm) for several methods of estimation as compared to the kinematic GPS measurements 46

Table 7.1. Comparison of errors in tide zoning and TCARI in estimating the post-processed water level data 62

Table B.1. Observed tidal constituent amplitudes (mm) in Galveston Bay 69

Table B.2. Observed tidal constituent Greenwich epochs (degrees) in Galveston Bay. 70

Table B.3. Observed tidal constituent local epochs (degrees) in Galveston Bay 70

Table B.4. Methods of harmonic analysis and length of time series 71

Table C.1. Tidal constituent amplitudes, A (cm), and local epochs, K (degrees). Values are shown for the Tide-Only (May 1995) run, NOS accepted values, the error, and values for the Tide Plus Wind run 77

Table E.1. Observed tidal constituent amplitudes (mm) in San Francisco Bay. 89

Table E.2. Observed tidal Greenwich epochs (degrees) in San Francisco Bay. 91

Table E.3. Observed tidal local epochs (degrees) in San Francisco Bay. 92

Table E.4. Methods of Harmonic Analysis and Length of Time Series Used. 94

EXECUTIVE SUMMARY

The Problem The National Ocean Service's (NOS's) hydrographic survey data are processed to give water depth at the point of the measurement. To produce a depth relative to Mean Lower Low Water (MLLW), which is the chart datum, the measured depth must be corrected to account for the departure of the instantaneous water level from MLLW. This departure is due to the astronomic tide, river flow, water density effects, and meteorological influences. At present, discrete tide zoning is used to provide this correction. Discrete tide zoning rests on the simplifying assumption that the water level in an entire zone has a fixed magnitude and phase relationship to the measured water level at a single nearby gauge. However, this method has several drawbacks. It is inaccurate because it cannot account for changes in the type of tide (e.g., diurnal, semidiurnal, or mixed) between stations and it assumes that non-tidal components vary in space and time the same way that tidal components do. It produces a discontinuity when crossing from one zone to the next. Finally, it cannot be used to reference survey data to the GPS ellipsoid.

A New Method of Solution A new method of making this correction takes values at the tide gauges and spatially interpolates them throughout the survey region. The values at the gauges which are spatially interpolated are:

- each tidal constituent's amplitude and phase value,
- the residual, or non-tidal, water level,
- the offset, which is the difference between local Mean Sea Level (MSL) and MLLW, and
- a tidal datum (either MSL or MLLW) relative to the ellipsoid.

The correction for the time and location of the ship is computed by summing the astronomic tide (computed from the interpolated constituents), the interpolated residual, and the interpolated offset. In addition, for a GPS-supported survey, the ellipsoidally-referenced MLLW values can be spatially interpolated and used to determine MLLW depth. The spatial interpolation at the core of this method is carried out by the use of a set of weighting functions that quantify the local contribution from each of the shore gauges. The weighting functions are generated numerically by solving Laplace's Equation on a grid. The new method is called Tidal Constituent And Residual Interpolation (TCARI).

Accuracy of the New Method The TCARI method was tested for accuracy using post-processed kinematic GPS measurements of water level collected by NOS in Galveston Bay, Texas, and San Francisco Bay, California. The measurements themselves had an accuracy estimated to be from 7 (San Francisco Bay) to 9 cm (Galveston Bay). The results (Table) indicate that TCARI was more accurate than either the numerical model or tide zoning. Although TCARI had lower errors than tide zoning, both methods had errors approximately equal to those in the measurements. It is therefore difficult to determine whether the difference between TCARI and tide zoning is significant.

Table. RMS differences between predicted water levels (using three methods) and GPS-measured water level in Galveston Bay and San Francisco Bay.

Prediction Method	Galveston Bay	San Francisco Bay
Numerical Modeling	15 cm	not available
Tide Zoning	9.4 cm	9.8 cm
TCARI	7.5 cm	8.8 cm

Conclusions The following conclusions about TCARI's application can be made:

- TCARI is more objective and somewhat more accurate than tide zoning when compared to post-processed kinematic GPS water level data.

- TCARI is a data-intensive method. Because of this, results should be better in coastal areas that have many historical locations where tidal constituents, tidal datum offsets, and ellipsoidally-referenced tidal datums are known. TCARI generally gives better results with 6-minute observational water levels, rather than hourly, because the non-tidal variation is more accurately represented.

- TCARI can improve tide zoning and tide prediction. TCARI can be adapted to predict the co-range and co-phase lines that are used to establish the tide zones. TCARI also offers a new method of hindcasting tidal variations in coastal areas.

- TCARI can be used to develop ellipsoidally-referenced MLLW fields. Thus TCARI is positioned for use for future NOS surveys, although it needs many stations where ellipsoidally-referenced tidal datums are known.

- TCARI and numerical model fields can be combined to give improved products. Model errors in estimating the ellipsoidally-referenced water levels may be reduced by using the TCARI spatial interpolation scheme to produce the model datum field. Also, constituent fields could be improved by correcting the model-generated constituent distributions with TCARI's spatially-interpolated error fields.

1. INTRODUCTION

Bathymetric survey data collected by ships are estimates of total water depth at the points where the measurements are obtained. Survey depths must be corrected for several effects, one of which is the departure of the instantaneous water level from mean lower low water (MLLW). MLLW is the datum for NOS charts (Figure 1.1). This departure, which is subtracted from the measured depth, is called the 'tide correction' and is due to both the astronomical tide and the non-tidal effects such as wind setup and river runoff. Today, discrete tide zoning is the method NOS uses to provide this correction. Discrete tide zoning rests on the assumption that the water level in a zone has a fixed magnitude and phase relationship to the measured water level at a nearby gauge. However, this method has known inaccuracies and it produces a discontinuity when crossing from one zone to the next. The objective of the present study is to develop a new method of estimating the tide correction which is not linked to discrete tide zones and which relies on separating the astronomical tide from the non-tidal component.

In discrete tide zoning (Gill, 1998), a number of geographic zones are constructed, each covering a portion of the coastal area being surveyed. The tide correction within any zone is computed by multiplying the amplitude of the water level above MLLW measured at a nearby gauge by a range factor and by applying a time difference. Within each zone, the range factor and time difference are considered to be constant. However, since range ratios and time differences are applied to the total observed water level variation (relative to MLLW), this results in a correction which can be inaccurate because it cannot account for changes in the type of tide (e.g., diurnal, semidiurnal, or mixed) between stations and it assumes that non-tidal components vary in space and time the same way that tidal components do.

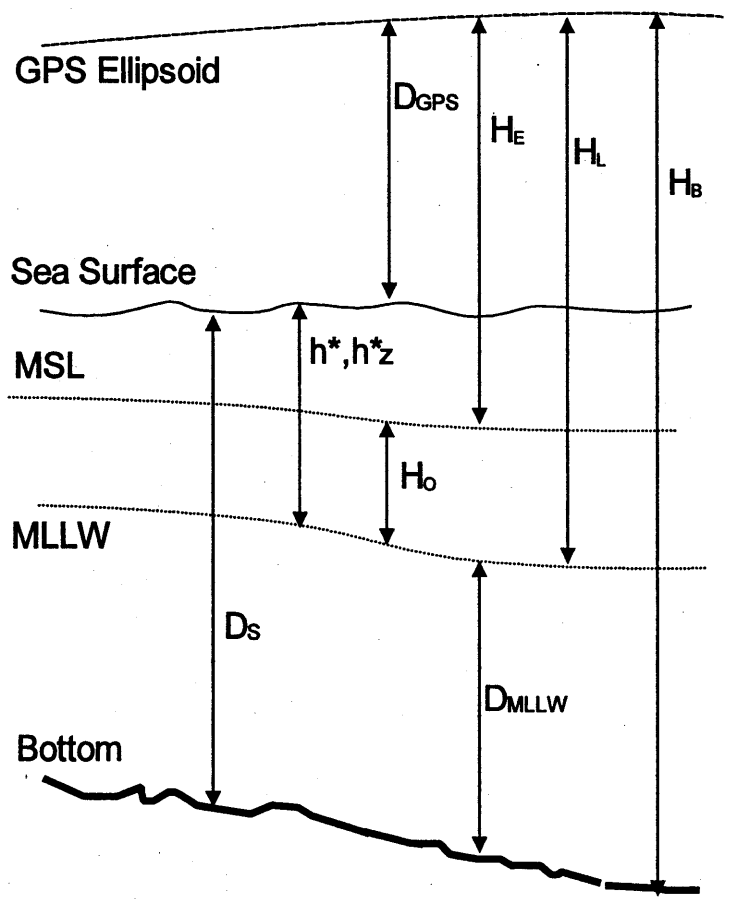

Figure 1.1. Schematic showing the depth sounding, D_S; the correction, h^*; the tide zoned correction, h_Z^*; the sea surface elevation relative to the ellipsoid, D_{GPS}; the offset between MSL and MLLW, H_O; the MSL elevation relative to the ellipsoid, H_E; the depth at MLLW, D_{MLLW}; the MLLW surface relative to the ellipsoid, H_L; and the bottom elevation relative to the ellipsoid, H_B.

The new approach described here is to (1) create an estimate of the local astronomical tide by spatially interpolating the tidal constituents, which have been determined from the harmonic analysis of a time series of prior observations at each

station, to the required location and then reconstructing the astronomical tide by summing the constituents, and (2) create an estimate of the non-tidal component by spatially interpolating the residual water level (observed total water level minus the reconstructed tide). These two components would be summed to give the final, more accurate correction to the bathymetric data. The new method is called Tidal Constituent and Residual Interpolation (TCARI), and is discussed in Section 2.

The approach to spatial interpolation of data required additional research. The method selected for spatial interpolation of the tidal harmonic constituents is obtained by assuming that spatial variation of the amplitude and phase of all tidal constituents obeys Laplace's Equation (LE), the solution of which is found numerically. The method was tested for a rectangular basin (Section 3).

Data from Galveston Bay (Section 4) and San Francisco Bay (Section 5) were used to evaluate the approach. Another spatial distribution of tidal constituents has been generated from the Galveston Bay numerical circulation model, and these were compared to the interpolated constituents. The new estimate of the tide correction will be compared to that generated by the NOS Galveston Bay hydrodynamic model (Section 4 and Appendix C).

TCARI could be used in post-survey data processing and potentially for ship-board data processing. Several programs have been written in Fortran to generate the necessary files and data (Section 6). The use of bathymetric data combined with GPS-measured water level (relative to the ellipsoid) is a technology that is quickly becoming practical. TCARI can easily be used to, for example, estimate the distribution of MLLW (relative to the ellipsoid) throughout the survey area, provided some data are available (Section 7). Discrete tide zoning does not have this capability.

This project supports the Promote Safe Navigation element of the NOAA strategic plan by improving the accuracy of NOAA's nautical charts and reducing processing time. More accurate information on local tides and nontidal water levels will result in more accurate bathymetric data (relative to MLLW) for NOS's nautical charts, and hence more accurate under-keel depth information for shipping and accident avoidance.

2. TIDAL CONSTITUENT AND RESIDUAL INTERPOLATION (TCARI)

2.1. Tide Corrections

As discussed previously, the depth at MLLW, which is the NOS chart datum, is computed from the survey depth sounding, D_S (which has been corrected for variations in ship motion, water density, etc.) by subtracting the tide correction, h^* (in practice, the correction is defined as the negative of h^* so it can be simply added to the sounding value):

$$D_{MLLW} = D_S - h^*. \tag{2.1}$$

The correction consists of three quantities: the astronomical tide, η_A; the residual (non-tidal) effect (such as wind setup), η_R; and the difference between the mean sea level (MSL) and mean lower low water, H_O. Thus

$$h^* = \eta_A + \eta_R + H_O \tag{2.2}$$

At present, h^* is computed by the method of tide zoning. In this paper, the new method called Tidal Constituent And Residual Interpolation (TCARI) is discussed. TCARI is a way of using both the observed water level values at gauges located in the survey area and historical data (the constituents) at the same gauges. Application of the method requires knowledge of astronomical tide prediction, harmonic analysis, and spatial interpolation. Before these topics are covered, discrete tide zoning is briefly summarized.

2.2. Tide Zoning

Discrete tide zoning was developed as a way of estimating water levels at any location in a survey area (Gill, 1998). A desktop computer-based method of drawing the zones was developed by Collier et al. (1999). In discrete tide zoning, a number of geographic zones are constructed, each covering a portion of the coastal area being surveyed. The tide correction within any zone, h_Z^*, at time t is calculated by multiplying the amplitude of the water level above MLLW at a nearby gauge, η_g, by the range factor for that zone, r, and by applying the time difference for that zone, τ, as follows:

$$h_Z^*(t) = r\eta_g(t - \tau) \tag{2.3}$$

Within each zone, the range factor and time difference are considered to be constant.

The tide zoning scheme for Galveston Bay is shown in Figure 2.1. The configuration of each zone is determined by oceanographers in NOS's Center for Operational Oceanographic Products and Services (CO-OPS) by estimating the variations of the tide between two or more NOS water level stations and drawing the zone so that the change in the amplitude of the tide correction between adjacent zones is limited to 0.2 feet and the time change is limited to 0.3 hour. Range and time changes between stations are therefore assumed to be approximately linear. For each zone, CO-OPS estimates a range factor

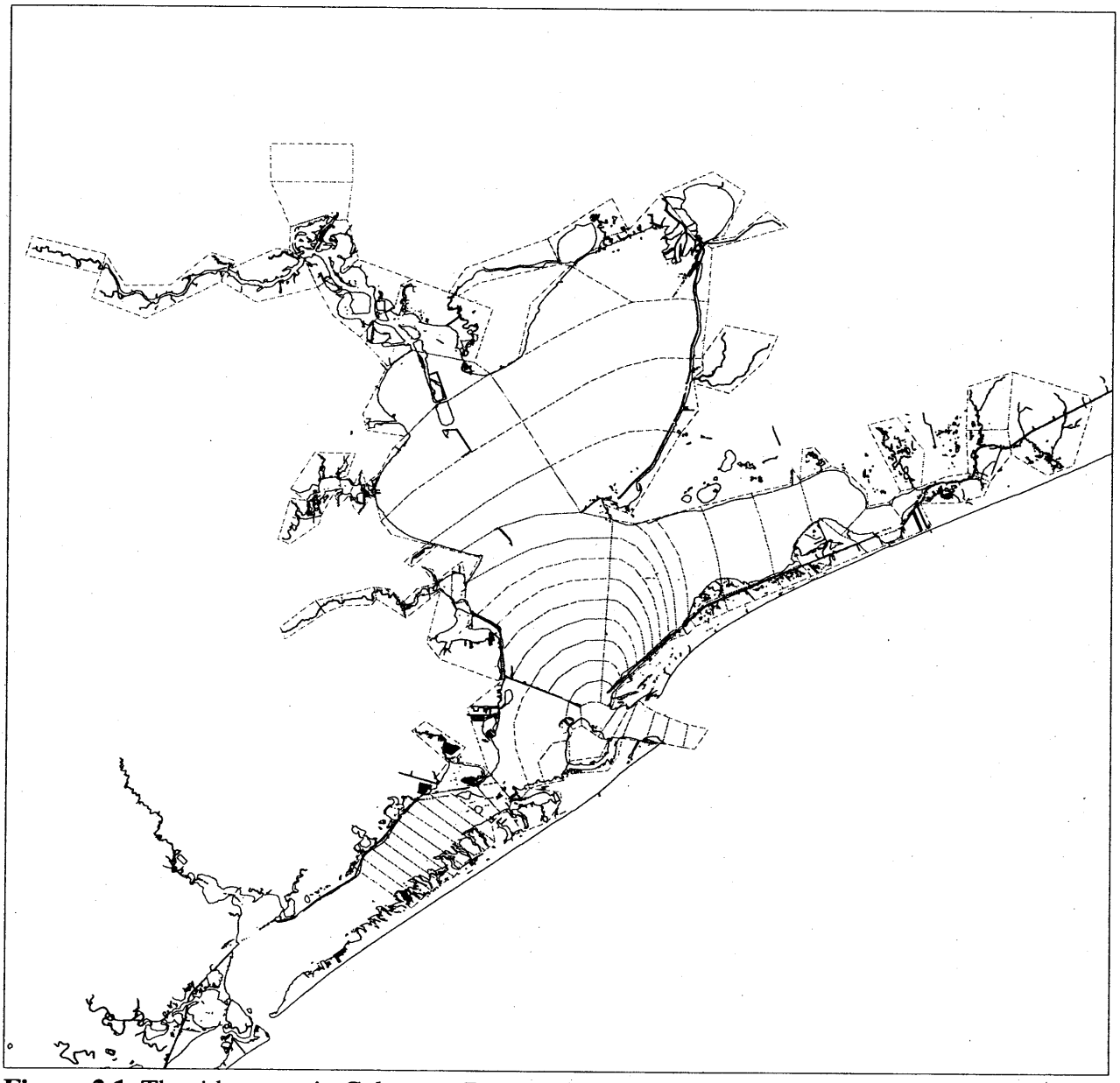

Figure 2.1. The tide zones in Galveston Bay. Within each zone (shown as a polygon), the tide correction has a fixed ratio and time difference relative to the tide measured at one or more water level gauges.

and a time difference for high water and low water in the zone relative to the same variables in one or more reference water level gauges. For preliminary tide zoning, an initial zone configuration is developed and range factors and time differences are generated for (typically) a single, long-term water level station. For final tide zoning, alterations in the polygons may be made and ratios and time differences are generated for (typically) several more stations.

For the automated processing of bathymetric data by NOS's Hydrographic Surveys Division (HSD), the high water and low water ratios are combined into a single value, as are the high water and low

water time differences. The tide correction is obtained by applying the amplitude ratio and time difference to the observed (and smoothed) tide from one or more nearby tide stations to get a local (i.e., ship location) tide.

2.3. Astronomic Tides and Tidal Constituents

The conceptualization of the tide in terms of a set of constituents is fundamental to TCARI. NOS uses the following equation (Schureman, 1958) to predict the astronomic tide, η, relative to mean lower low water (MLLW) at any location and time t:

$$\eta(t) = H_O + \sum_{n=1}^{N} f_n a_n \cos[\omega_n t + (V_o + u)_n - G_n] \tag{2.4}$$

The tide, η, is the sum of a constant offset value (the difference between MSL and MLLW), H_O, and a cosine series of N tidal constituents. For each constituent, f_n is the lunar node factor, ω_n is the angular speed, and V_o+u is the equilibrium argument; these are determined from knowledge of the astronomical motions of the earth-moon-sun system and they apply to all locations. The constituent amplitude, a_n, and Greenwich epoch, G_n, (for predictions in Greenwich, or universal, time) are determined from the analysis of a time series of observations, and apply at a single location. Time is reckoned from the start of the year.

Predictions made using local time require the local epoch. The local epoch, κ'_n, can be found from the Greenwich epoch at any time zone longitude, S, by

$$\kappa'_n = G_n + S\ \omega_n/(15\ degrees/hour) \tag{2.5}$$

where west longitude is negative [note: the above conventions differ from that of Schureman (1958)]. For Galveston Bay, the time zone longitude, S, is -90 degrees, so $S/15$ = -6 hr; for San Francisco Bay, S is -120 degrees, so $S/15$ = -8 hr.

2.4. Spatial Interpolation

The new approach described here depends on a method of spatial interpolation. The common approach (widely used in meteorology) is to create a two-dimensional field from a limited number of observations by the use of a distance-dependent weighting function, w. For example,

$$F(x, y) = \sum_{m=1}^{M} w(d_m) F_m^O \tag{2.6}$$

where $d_m(x, y)$ is the straight line distance between the location of the observation, F^o_m, and the point (at x, y) in the field. w decreases as d increases.

The weighting function approach will produce highly inaccurate results when applied to tidal data because it does not account for the influence of land. An example of the problem is shown in Figure 2.2. The Greenwich phase for the M_2 constituent at High Island in the Gulf of Mexico is 272.4 degrees, while at the nearby Rollover Pass the value is 17.8 degrees and at Smith Point it is 8.6 degrees. The latter two stations are in Galveston Bay. Clearly, any approach that does not account for the existence of the intervening land (in this case the Bolivar Peninsula) or uses the straight line distance between stations will produce inaccuracies.

Therefore, to overcome these difficulties, the approach taken here is to create a set of weighting functions that are the solution of a differential equation that includes spatial derivatives. The equation is solved numerically on a grid. The use of a spatial derivative means that the value at any grid point is directly related to the value at the adjacent grid points. The ultimate effect is to create pathways around land features. The result is a set of new weighting functions, $g(x, y, m)$ that can be used in place of the function w in Eqn. 2.6. The computation of the new weighting functions is covered in Section 3.

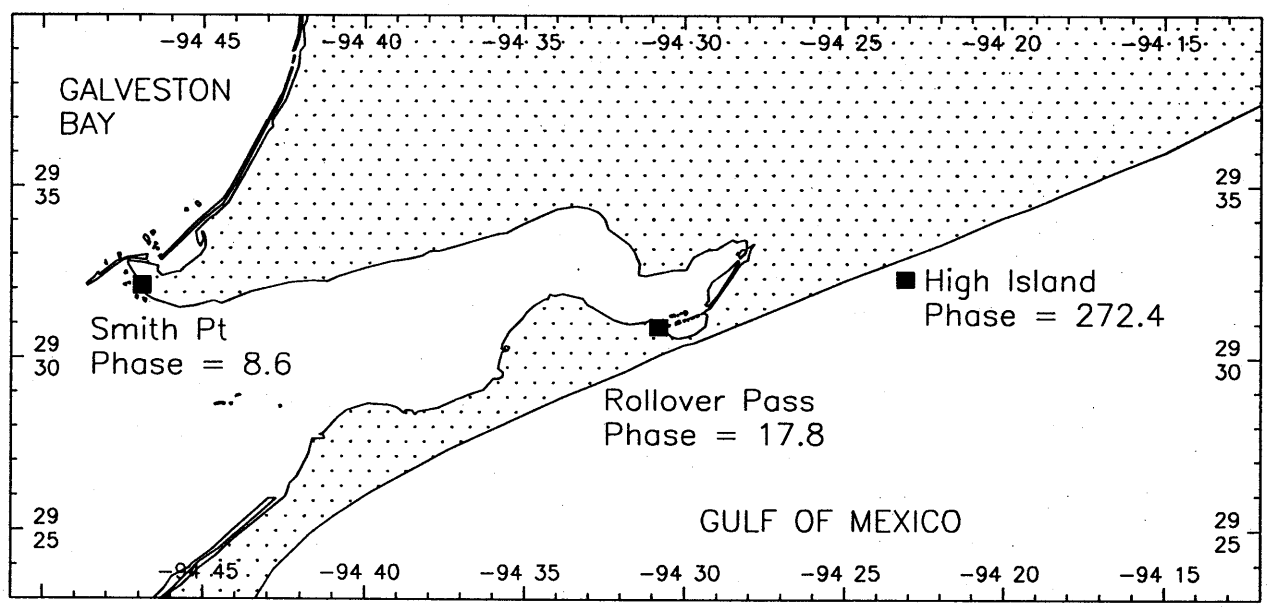

Figure 2.2. The influence of land on M_2 phases for three nearby gauge locations. Although the High Island gauge is located near the Rollover Pass and Smith Point gauges, its phase is quite different. The difference is due to the intervening land (the Bolivar Peninsula) and the land's affect on tide wave propagation.

2.5. TCARI

As explained earlier, the correction h^* at any location can be expressed as the sum of the astronomical tide (η_A), a residual water level component (η_R), and the MSL to MLLW difference (H_O) as

$$h^* = \eta_A + \eta_R + H_O \tag{2.2}$$

For each constituent of the astronomical tide, TCARI creates an interpolated amplitude, A, and epoch, K, which are calculated with the numerically-generated weighting functions, g_c, as follows:

$$A_n(x, y) = \sum_{m=1}^{M_c} g_c(x, y, m) a_{m,n}$$

$$K_n(x, y) = \sum_{m=1}^{M_c} g_c(x, y, m) \kappa_{m,n} \tag{2.7a,b}$$

where $g_c(x, y, m)$ is the weighting function for tidal constituents at location (x, y) for the tide gauge location m, and κ is either the Greenwich or the local epoch. There are M_c locations where tidal constituent data are available. Hence, using the prediction equation 2.4,

$$\eta_A = \sum_{n=1}^{N} f_n A_n \cos[\omega_n t + (V_o + u)_n - K_n] \tag{2.8}$$

The offset (the difference between MSL and MLLW) is also interpolated by

$$H_O(x, y) = \sum_{m=1}^{M_O} g_o(x, y, m) H_{o,m} \tag{2.9}$$

where g_o is the weighting function for offsets for the M_o gauges where the offset, $H_{o,m}$, is known.

Now suppose that there are M_r contemporary water level gauges in the survey area. These stations are not necessarily the same as the first set of M_c, but their constituents must be known. Then the residual component (relative to MSL) at any location is

$$\eta_R = \sum_{m=1}^{M_r} g_r(x, y, m) [\eta_m - \sum_{n=1}^{N} f_n a_{n,m} \cos(\omega_n t + \{V_o + u\}_n - \kappa_{n,m})] \tag{2.10}$$

where η_m is the observed water level (relative to MSL) at gauge m and g_r is the weighting function for the set of M_r gauges.

In order to make comparisons with the post-processed RTK water level measurements in Galveston and San Francisco Bay, an independent estimate of the water surface elevation at any time and location relative to the ellipsoid, D'_{GPS}, is needed. This can be computed by the TCARI method as follows

$$D'_{GPS} = \eta_A + \eta_R + H_E \tag{2.11}$$

where H_E is the ellipsoidally-referenced tidal datum (MSL)

$$H_E(x, y) = \sum_{m=1}^{Me} g_e(x, y, m) H_{E,m} \tag{2.12}$$

Also, TCARI can readily be adapted for survey bathymetric data referenced to the GPS ellipsoid. Let the elevation of the bottom of the water column relative to the GPS ellipsoid be H_B (being comprised of the ellipsoidal distance to the GPS antenna, the antenna-to-sounder distance, and the sounding measurement itself. See Figure 1.1). Then

$$D_{MLLW} = D_B - H_L \tag{2.13}$$

where H_L is the spatially-interpolated value of MLLW relative to the ellipsoid,

$$H_L(x, y) = \sum_{m=1}^{M_e} g_e(x, y, m) H_{L,m} = H_E - H_O \tag{2.14}$$

In sum, TCARI generates either a tide correction or an ellipsoidally-referenced water level by the addition of three components: a astronomical tide which is generated from spatially-interpolated tidal phases and amplitudes, a spatially-interpolated residual (non-tidal) water level, and either the offset (difference between MSL and MLLW) or the ellipsoidally-referenced MSL datum. The generation of the weighting functions is covered in the next Section. Four sets of variables (see Section 2.6) are required at locations in or near the survey area; because tide stations often lack one or more of the four, a separate set of weighting functions is needed for each variable set.

2.6. TCARI Data Requirements

For tide corrections, three sets of variables (tidal constituents, residual water levels, and offsets) are required at locations in or near the survey area. For an ellipsoidally-referenced survey, one additional variable (an ellipsoidally-referenced datum) is needed. Historical tidal constituent data (amplitude and phase) and the offset (the difference between MSL and MLLW) are often available a numerous locations. The residual water level at a location requires both tidal constituents and contemporary observations at the tide gauge at the time of the survey.

Generally speaking, results should improve with the addition of more locations. Since the contemporary measurements are needed for only the residual water level, forehand knowledge of the

spatial patterns of residual water level variability may allow for design of a minimal configuration of gauges. In this study, data collected originally for the purpose of tide zoning was used to assess TCARI; no special data (with the possible exception of the an ellipsoidally-referenced datums) was used. There was also no attempt to determine optimal configurations of water level station locations or lengths of time series that would improve TCARI's accuracy.

2.7. Other Methods of Providing Corrections

Beside discrete tide zoning, there are other methods designed to provide tide correction information. However, these methods have significant drawbacks. One such method is function fitting, which is widely used in meteorology. This method uses an analytical function in two-dimensional space which fits the observations (e.g., Barnes, 1964). This method is not suitable for interpolating tidal data because it cannot account for the large differences in tidal characteristics across land features such as peninsulas.

A second method is numerical circulation modeling (Stawarz and Metzner, 1994; Schmalz, 1996), in which a model is used to determine both the instantaneous water level with respect to MSL and, with a sufficiently long time series, the difference between MSL and MLLW. Although the application of hydrodynamic models is potentially the most accurate approach to determining tidal constituents because these models simulate the dynamics of time-dependent, shallow-water tidal wave motion, in practice numerical circulation models typically require a long time (months to years) to develop to a state where they meet the required accuracies (for examples of accuracy requirements, see National Ocean Service, 1999). In contrast, TCARI was developed so that existing gauge and historical data can be utilized rapidly (on the order of months). In addition, although numerical models are usually calibrated using gauge data, they may not perfectly match the data at the gauges. TCARI, however, uses the gauge data so as to exactly match values where they are available (although this inevitably raises questions about data quality and the spatial density of gauges).

A third method is to generate a tidal datum surface by first selecting a field that has already been referenced to the ellipsoid (the geoid, for example) and then generating a new surface by minimizing the error at the stations with known values (Müller and Groten, 1992). However, the MSL is known to depart significantly from the geoid because of the effects of currents.

3. INTERPOLATION BY SOLUTION OF LAPLACE'S EQUATION

3.1. Laplace's Equation

The method chosen for spatial interpolation is to describe the variable (offset, amplitude or phase) as a two-dimension field, select a field equation that describes the spatial distribution, then compute the numerical solution of that equation. First we let the arbitrary variable *G(x, y)* represent the offset, amplitude, or phase (or any other property). We then assume that the variable obeys the two-dimensional Laplace's Equation (LE)

$$\frac{\partial^2 G}{\partial x^2} + \frac{\partial^2 G}{\partial y^2} = 0 \tag{3.1}$$

and that G matches the observed value at the locations where data are available,

$$G(x_m, y_m) = G_m^o \tag{3.2}$$

The LE was chosen because, in one dimension, it gives a solution that has a constant slope between data points. In two dimensions, the solution between three data points can be a flat plane. A planar solution is desirable because it is the simplest way to interpolate between data points, even though it does not incorporate any tidal physics. Another attractive feature of a numerical LE solution is that information on tidal constituents in one grid point will be related to the values in adjacent grid points, and will thus be able to propagate information around corners. Finally, note that this is the equation in mathematical physics that describes the temperature distribution in an insulated plate of constant thickness and constant heat conduction coefficients.

The LE approach will produce an objectively interpolated field for amplitude and phase, although without including any tidal physics such as wave speed, friction, or depth variation. Since amplitude and phase are computed independently, natural distributions such as amphidromes will not be accurately reproduced. A potentially more accurate approach, which is based on the solution of linearized, single-constituent tide wave equation in a constant-depth basin, solves for amplitude and phase together. A short discussion appears in Appendix A.

Straightforward application of Eqn. 3.1 to a typical geographic area would result in a very large number of fields. In addition to the field for the offset, there would be 74 fields, because for the NOS standard suite of 37 tidal constituents, two fields (i.e., an amplitude field and a phase field) are needed for each constituent. And for the residual water level, a new field would have to be generated for each time a new observation were available; i.e., every 6 minutes. Therefore, to save computer time and memory, the approach was extended by defining a set of weighting functions, g, such that

$$G(x, y) = \sum_{m=1}^{M} g(x, y, m)\, G_m^o \tag{3.3}$$

where M is the number of locations where observations, G^o, are available. The field g then obeys Laplace's equation

$$\frac{\partial^2 g}{\partial x^2} + \frac{\partial^2 g}{\partial y^2} = 0 \tag{3.4}$$

and has a value of either zero or unity at the locations where observed values are available,

$$g(x_i, y_i, m) = \delta_{im} \tag{3.5}$$

That is, for the selected station m, g is unity there but is zero at all the other stations, i. This approach is faster and simpler than solving Eqn. 3.1 because it requires that only one solution field be calculated for each water level station for which there are data. After that, the G field is constructed from Eqn. 3.3 using whatever data is desired. In addition, whenever updated values of the observations become available, there is no need to recompute the g functions.

3.2. Boundary Conditions

Boundary conditions for G and g are needed at water level stations, ocean boundaries, and land boundaries. As discussed above, at station locations where observed values are available, the boundary condition are Eqns. 3.2 and 3.5. The ocean boundary condition is that g has a zero slope in the normal direction,

$$\frac{\partial g}{\partial \varsigma} = 0 \tag{3.6}$$

where ς is the direction normal to the boundary. The boundary condition for G is obtained by substituting G for g in Eqn. 3.6. At land boundaries, the zero slope condition (Eqn. 3.6) is an obvious possibility. However, this condition (which is analogous to a thermally-insulated boundary in the heat flux case) proved to cause the localized packing of contours around the data points, especially near corners, which is not realistic in many cases. Therefore, a second boundary condition was developed. This condition is based on the concept that the variation of g near the shore is determined by the variation in the water level a small distance away from the shore. This is implemented by setting the boundary slope to be proportional to the mean interior slope, i.e.,

$$\frac{\partial g}{\partial \varsigma} = \alpha \overline{\frac{\partial g}{\partial \varsigma}} \tag{3.7}$$

where the overbar represents the spatial average (over the few surrounding cells) of the derivative and the proportionality constant is restricted by

$$0 \le \alpha \le 1 \tag{3.8}$$

This approach allows the zero normal condition to be implemented by simply setting $\alpha = 0$ and the full proportionality condition by setting $\alpha = 1$.

3.3. Natural Distributions of Corange and Cophase Lines

The actual spatial distribution of constant amplitude (corange) and constant phase (cophase) lines will be needed to evaluate the parameter α. In Chesapeake Bay (Browne and Fischer, 1988), cophase lines tended to be normal to the boundary, but if the shore tends to be shallow, then cophase lines curve to give a near-shore phase lag. Corange lines (i.e., lines of constant amplitude) did not show a simple pattern, but were oriented both normal and parallel to the shore. Data on both observed and numerically-simulated tides in Tampa Bay (Zervas, 1993) show again that cophase lines tended to be normal to the shore, but corange lines were oriented both normal and parallel to the shore.

Defant (1961) presents a summary of information on the distributions of corange and cophase lines for the North Sea, the Baltic, the English Channel, the Irish Sea, the Adriatic, the Black Sea, the Persian Gulf, the Indonesian Archipelago, the Eastern China Sea, the Sea of Japan, the Okhotsk Sea, the Gulf of Mexico, the Gulf of St. Lawrence, the North Siberian Shelf. Cophase lines tend to intersect the land at near-normal angles when (1) they are radiating around amphidromic systems and (2) in long, narrow embayments. Corange lines, which intersect and are roughly normal to cophase lines, show evidence of being oriented both normally and parallel to the shore.

Thus it appears that no single value of α will correctly describe all natural distributions. Experimentation will therefore be necessary to settle on a useful value.

3.4. Solution by Finite Differences

The solution to the LE is approximated by the numerical equivalent. For cells equally spaced in each direction, the finite difference form of Eqn. 3.4 at location i, j and iteration k is

$$g^k_{i+1,j} + g^k_{i-1,j} + g^k_{i,j+1} + g^k_{i,j-1} - 4g^k_{i,j} = 0 \tag{3.9}$$

Solving for $g^k_{i,j}$ gives an estimate that solves the equation

$$g^*_{i,j} = \tfrac{1}{4}(g^k_{i+1,j} + g^k_{i-1,j} + g^k_{i,j+1} + g^k_{i,j-1}) \tag{3.10}$$

where g^* is an intermediate solution. Using the method of successive over-relaxation (SOR) (Press et al., 1992), the next estimate (i.e., at iteration $k+1$) is obtained by

$$g^{k+1}_{i,j} = \omega g^*_{i,j} + (1-\omega) g^k_{i,j} \tag{3.11}$$

where $1 < \omega < 2$. The array g is iterated until the following convergence criterion was met:

$$\max\left|g_{i,j}^{k+1} - g_{i,j}^{k}\right| \leq \varepsilon(\max(G_m^O) - \min(G_m^O)) \tag{3.12}$$

Good results were obtained for $\varepsilon = 5 \times 10^{-5}$. The final values of the numerical solution, and in fact convergence itself, was highly sensitive to the exact form of the boundary conditions. Therefore, considerable time was spent in testing different forms.

3.5. Grid Generation

The numerical solution to the Laplace's Equation can only be determined by solving the equations on a grid composed of square cells representing either land or water. The grid is generated from (a) the window in latitude-longitude space, (b) the cell width, (c) the coastline (defined as a set of latitude-longitude pairs), and (d) the location of one water point. No bathymetric data are required.

The process is as follows. First, a geographic window is selected. It is specified by the longitude limits (*lonmax, lonmin*) and the latitude limits (*latmax,* and *latmin*). Then, given a cell width, *wcell* (in nautical miles), a grid of undifferentiated cells is generated by dividing the width into *Imax* intervals and height into *Jmax* intervals, where

$$\begin{aligned} Imax &= \frac{C_o}{wcell}(lonmax - lonmin) \\ Jmax &= \frac{C_a}{wcell}(latmax - latmin) \end{aligned} \tag{3.13}$$

where C_o and C_a convert degrees to nmi. *wcell* should be considered a nominal value. Since *Imax* and *Jmax* are integer values, the division of either the width by *Imax* or the height by *Jmax* will result in actual cell widths that are slightly larger or smaller than *wcell*. This distortion is small (less than 1%) when *Imax* and *Jmax* are large and is ignored in the numerical solution.

Next, the land-water boundary in this grid is determined by checking all cells that (a) contain at least one point in the coastline data file, or (b) are intersected by a line drawn between points defining the coastline. Finally, starting from the known water point, all cells adjacent to it which are not tagged as the land-water boundary are also set to represent water. The remaining cells are therefore land. The land-water boundary cells are set to either land or water.

In general, the generation of grids for complex coastlines requires serious consideration. First, the window must be selected so it covers the entire area of the bay to be zoned. If there is coastal ocean within the window(which is the usual case), the method requires that the coastline file contain data points outside the window; if not, the process of filling land points will run around the end of the coastline and all cells will be turned into water. Cells, which are square, should be small enough so that important features such as entrances and straits will have at least two or three cells across them, although the computation is faster with larger cells.

3.6. Rectangular Basin Test Case

For the test cases, the water area is a simple six-sided region with parallel sides. The six corners are specified by latitude-longitude pairs. For a window bounded by latitudes 28° 54' and 29° 50' and by longitudes -95° 20' and -94° 5' and *wcell* = 0.5 nmi, the resulting grids (one oriented so that its sides are parallel to the borders of the window, and another rotated 45 degrees clockwise) are shown in Figures 3.1a and 3.1b.

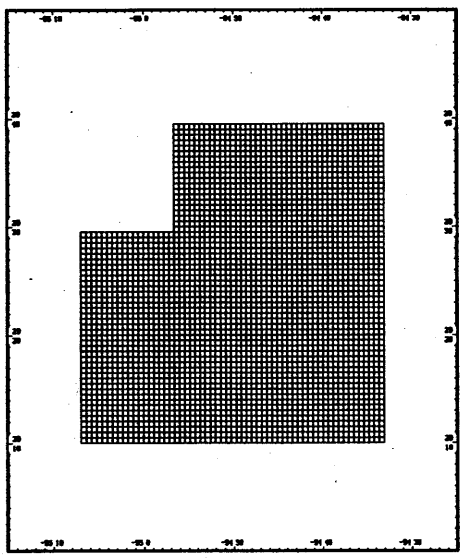

Figure 3.1a. Grid for rectangular test region. Cells are 0.5 nmi on a side.

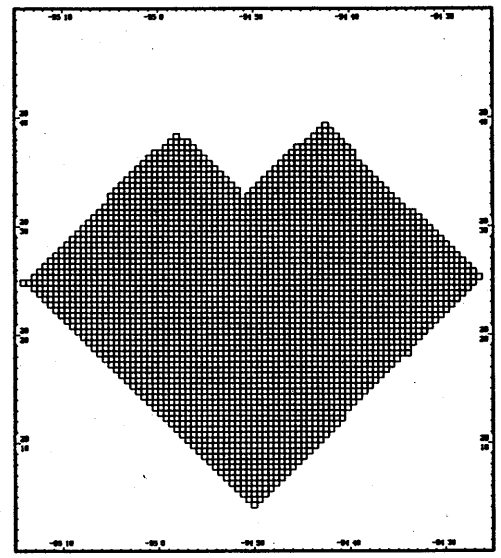

Figure 3.1b. Grid for the rectangular test region, but rotated 45 degrees.

A set of test cases was developed to implement and refine the numerical scheme. The basin has straight sides and occupies a region approximately the size of Galveston Bay. A grid (Figure 3.1a) was then generated which had square cells measuring 0.5 nautical mile on a side. The resulting grid array had dimensions 87 by 100, and approximately 36% represented water. The maximum width and height of the basin was 59 cells. The test cases consist of finding the solution with four different boundary conditions. For each test cast, the boundary values consisted of setting $G^o = 100$ in the lower left corner and $G^o = 0$ on the right side about two-thirds the way up.

For the first test cast, the boundary condition is zero gradient in the normal and tangential directions. The solution for this case ($\alpha = 0$) is shown in Figure 3.2a. The solution was achieved after 698 iterations using $\varepsilon = 1.25 \times 10^{-5}$. Although contour lines intersect the side as required, contours are packed around the two locations where the input values are given (Points A and B in the figure). This undesirable packing results naturally from the solution of the LE and this specific boundary condition, which are analogous to a temperature distribution with thermally-insulated boundaries, and is characteristic of a saddle point.

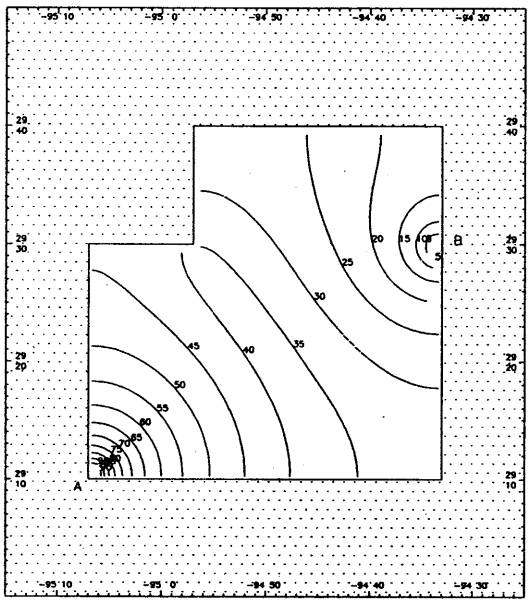

Initial basin, $\alpha = 0.0$

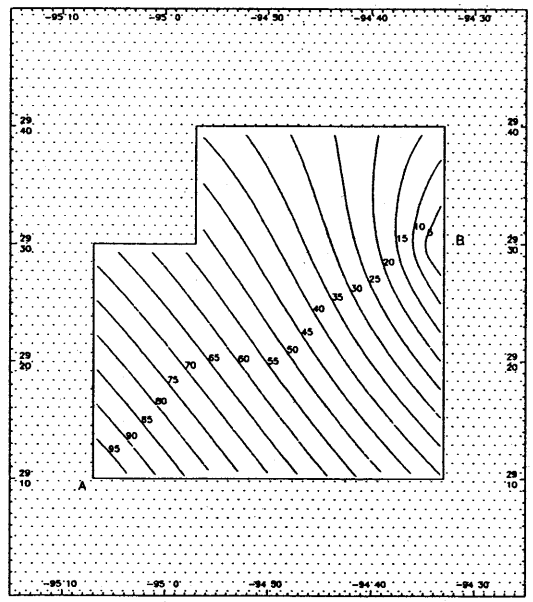

Initial basin, $\alpha = 1.0$

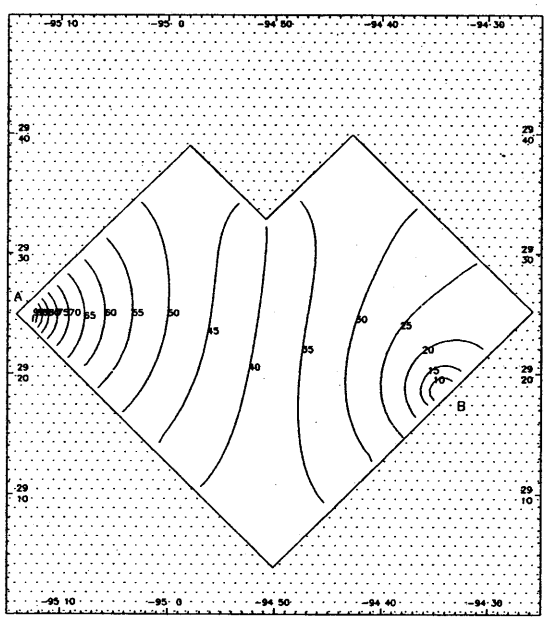

Rotated basin, $\alpha = 0.0$

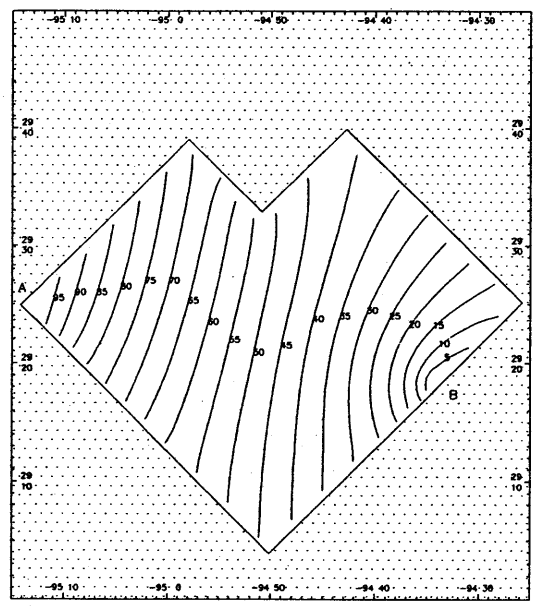

Rotated basin, $\alpha = 1.0$

Figure 3.2. Solution for G in an idealized basin, solving Laplace's Equation with boundary values of $G^o = 100$ at point A and $G^o = 0$ at point B for two values of α.

At the opposite extreme, using the full extrapolation ($\alpha = 1$) produces a different set of contours (Figure 3.2b). This solution required 1419 iterations to complete and results from the condition that the gradient of G in each spatial direction is a constant. This solution is mush less affected by boundary influence than the previous solution. The lines are approximately straight in the lower left corner (Points A), and have nearly uniform spacing; this solution approximates the idealized solution of a flat plane.

A severe test of the numerical solution is to see whether the same solution results when the basin is rotated by 45 degrees. The solution for $\alpha = 0$ (Figure 3.2c) and $\alpha = 1$ (Figure 3.2d) show that the unrotated solution is reproduced to within about 5, which is 5% of the full scale. Maximum displacement of the contours was about 10 cells (5 km) and occurred near the center of the basin. Since this level of error is relatively small,, the numerical scheme is judged to be acceptable. The number of iterations required were 717 and 651 for $\alpha = 0$ and 1, respectively.

In each basin, the contours for $\alpha = 1$ are slightly curved. The curvature can be reduced by taking a smaller value for ε or a smaller grid size, although convergence requires a larger number of iterations. Also, the above distributions were created by solving Eqn. 3.1 for $G(x, y)$ with the boundary input values O=100 at point A and O=0 at point B. An equivalent distribution can be generated by solving the Eqn. 3.4 for $g(x, y)$, then solving Eqn. 3.3 for $G(x,y)$. Comparison of the two solutions shows differences of less than 1% of full scale.

Neither of the distributions shown in Figure 3.2 is entirely realistic as compared to cotide or cophase lines. An intermediate solution, one which has contours approaching normal intersection with the coast but without the packing of contours around the input boundary locations, can be generated by setting α to an intermediate value. The solution for $\alpha = 0.9$ is shown in Figure 3.3.

A final point to consider about the test boundary values ($G^o = 100$, $G^o = 0$) is that, if G^o represents phase angle in degrees, then $G^o = 0$ is equivalent to $G^o = 360$. The solution for this case would be significantly different. One approach is to spatially interpolate the sine and cosine values separately, then add them together. In this case the field G is generated by

$$G(x, y) = \tan^{-1}\left(\frac{\sum_{k=1}^{K} g(x, y, k)\sin(G_k^o)}{\sum_{k=1}^{K} g(x, y, k)\cos(G_k^o)}\right) \tag{3.14}$$

For $G^o = 100$ degrees at point A and $G^o = 0$ degrees at point B, the result is shown in Figure 3.4. The field generated this way has slightly more uniform spacing of contours, and the maximum difference is approximately 5 degrees.

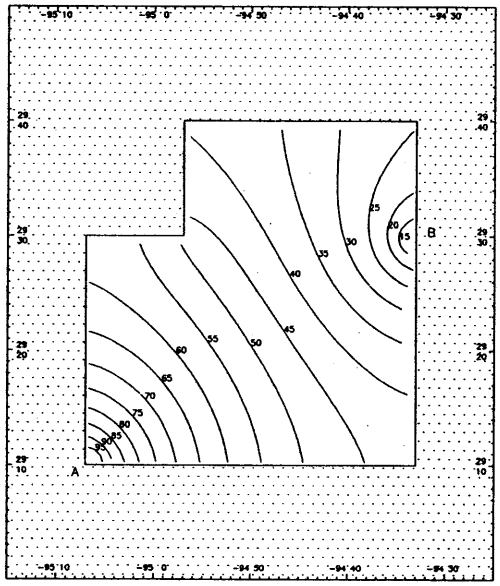

Figure 3.3. Contours created by spatial interpolation of values $G^o = 100$ at point A and $G^o = 10$ at point B ($\alpha = 0.9$).

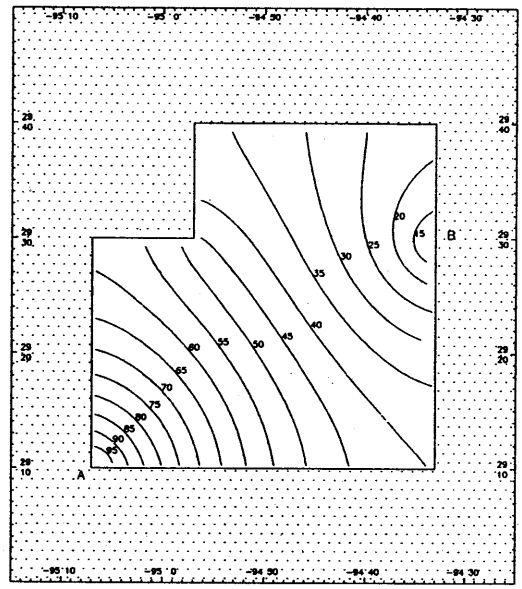

Figure 3.4. Contours created by spatial interpolation of the sine and cosine of values $G^o = 100$ at point A and $G^o = 10$ at point B ($\alpha = 0.9$).

The difference between the two solutions was studied by setting up an analytical case. The angle varied between 0 degrees at one end and a different value (from 20 degrees to 110 degrees) at the other. Two solutions were determined, one by linear interpolation of the angle, the other by linear interpolation of the sine and cosine of the angle and a reconstruction by the arctangent. The table below shows the maximum difference (in degrees) between the solutions as a function of the difference between the end values. The difference in solutions is less than 1 degree when the difference between end values is less than about 58 degrees.

Table 3.1. For an angle varying from 0 degrees at one end to a range of values at the other end, the maximum difference (degrees) between the solutions obtained by (1) linear interpolation between the end angles and (2) linear interpolation between the sine and cosine of the end angles, then reconstruction of the angle by the arctangent.

End Angle	110	100	90	80	70	60	50	40	30	20
Difference in Solution Angles	7.8	5.5	4.0	2.7	1.8	1.1	0.6	0.3	0.1	0.04

4. APPLICATION TO GALVESTON BAY

Galveston Bay was selected as the next test case because it was the site of an intensive water level data collection project during 1995 (Huff and Gallagher, 1996). The Bay has recent tide data, ellipsoidally-referenced water level data (WGS-84), and a numerical circulation model developed by Schmalz (1996).

4.1. Ship Track Data

During the summer of 1995, extensive measurements of water levels referenced to the WGS-84 ellipsoid were made from a small craft traveling around Galveston Bay as part of a NOAA research program (Huff and Gallagher, 1996). The locations where the 618 measurements were made are shown on Figure 4.1. The accuracy of these measurements is discussed in Section 4.8.

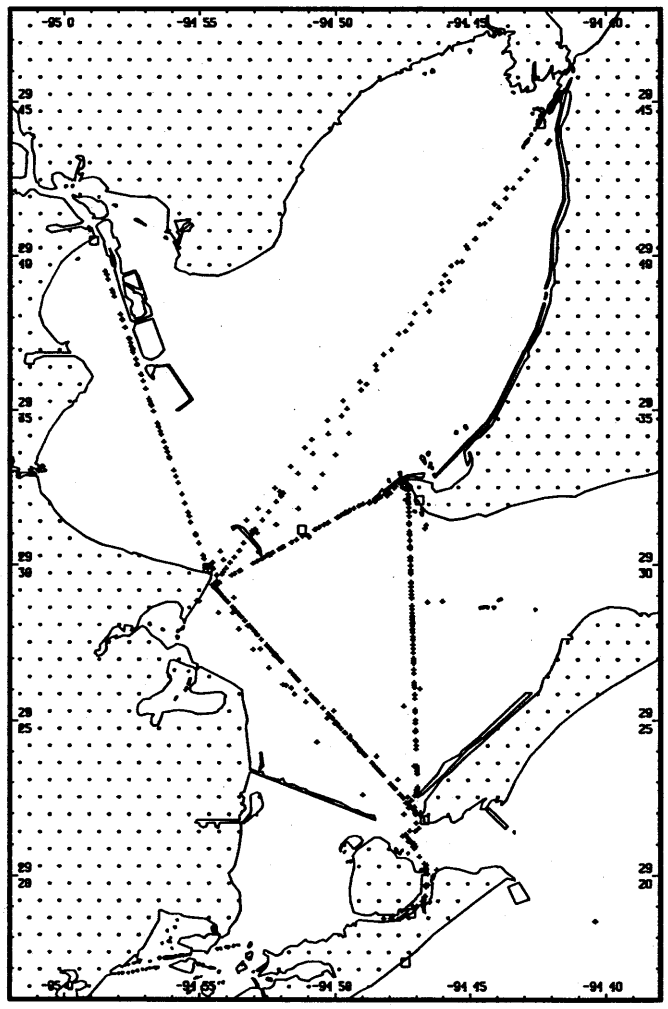

Figure 4.1. Galveston Bay locations (denoted by a '+') of ellipsoidally-referenced water level measurements.

Most of the measurements were made in the mid-bay region along a triangular course with vertices close to operating NOS water level gauges. At each of the observations the time, location (latitude and longitude), water level relative to the ellipsoid, and ship speed are known. The measurements were made on 17 days beginning June 13 (day 164) and ending July 7 (day 188).

4.2. Water Level and Model Data

There are 14 water level stations which had tide data used in this study. Their locations are shown in Figure 4.2. During the NOAA research program, contemporary water level time series

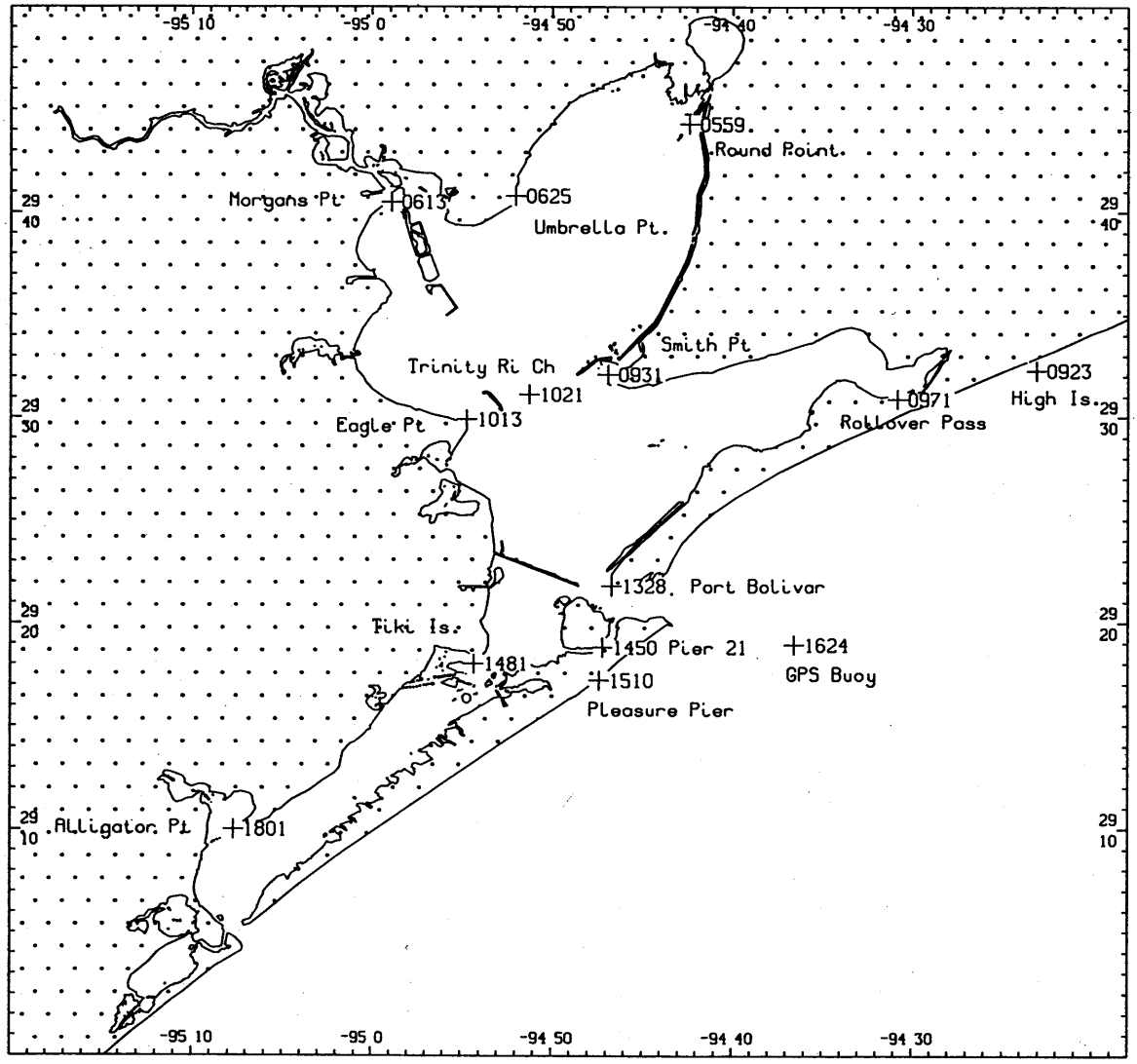

Figure 4.2. Locations ("+"), numbers, and names of 14 water level gauges that supplied data used in this study. The station numbers shown are the last four digits of the seven-digit number; the first three digits are 877.

measurements were made by NOS and the Conrad Blucher Institute (CBI) of Texas A. and M. University at Corpus Christi. These included 12 shore-based stations, a station located on a platform near the Houston Ship Channel (877-1021), and a temporary, offshore location on a GPS-fitted buoy (877-1624). Time series (at both 6-minute and hourly intervals) are available at 10 locations within the Galveston Bay and coastal region, and tidal constituents were available for those stations. In addition, tidal constituent data derived from past measurements were available at the other four stations. Eight stations had a datum (usually Mean Tide Level, which is equivalent to MSL) referenced to the ellipsoid. The data available at each location are shown in Table 4.1. A listing of the tidal constituents and details of the harmonic analysis methods is given in Appendix B.

Table 4.1. Tide and related data used in the ship track data comparison. Columns show the location name, the institute (Ins) which collected the data (NOS or CBI), the station number, the number of constituents available (NC), whether an observed time series (Obs) is available, and the offset H_O and WGS-84 ellipsoidal datum H_E, in meters (H_E values from Schmalz, 1996). na means not available.

No.	Name	Ins	Sta. Num	NC	Obs	H_O	H_E
1	Round Pt.	CBI	877-0559	37	✔	0.213	-29.014
2	Morgans Pt.	CBI	877-0613	37	✔	0.198	-29.053
3	Umbrella Pt.	NOS	877-0625	37	na	na	na
4	High Island	NOS	877-0923	37	na	0.366	na
5	Smith Pt.	NOS	877-0931	37	✔	0.195	-28.845
6	Rollover Pass	NOS	877-0971	37	na	0.213	-28.725
7	Eagle Pt.	CBI	877-1013	37	✔	0.174	-28.775
8	Trinity River Chn.	NOS	877-1021	20	✔	0.177	na
9	Port Bolivar	CBI	877-1328	37	✔	0.214	-28.624
10	Galveston, Pier 21	NOS	877-1450	37	✔	0.253	na
11	Tiki Is.	NOS	877-1481	23	na	na	na
12	Pleasure Pier	NOS	877-1510	37	✔	0.366	-28.537
13	GPS Buoy	NOS	877-1624	25	✔	na	na
14	Alligator Pt.	NOS	877-1801	37	✔	0.092	na

Another part of the NOAA project was the development of a numerical circulation model of the Bay (Schmalz, 1996). The model was calibrated for the survey period and produced tidal constituent amplitudes and phases. These will be discussed in Section 4.4. A description of the model appears in Appendix C.

4.3. Grid and Weighting Functions

Application of the LE method described in Section 3 for interpolation requires the generation of a numerical grid and the subsequent computation of influence functions. The numerical grid was generated using a digital coastline file (Figure 4.3). A cell size (*wcell*) of 0.35 nmi was chosen because it approximates the mean size of the numerical model's cells and it is small enough to include most of the important narrow channels such as the entrance to the Bay. For the longitude limits (*lonmax*=94° 18', *lonmin*=-95° 20'), *Imax*=134, and for the latitude limits (*latmax*= 29° 50', *latmin*=28° 52'), *Jmax*=165. The actual cell width is 0.351 nmi and the height is 0.352 nmi.

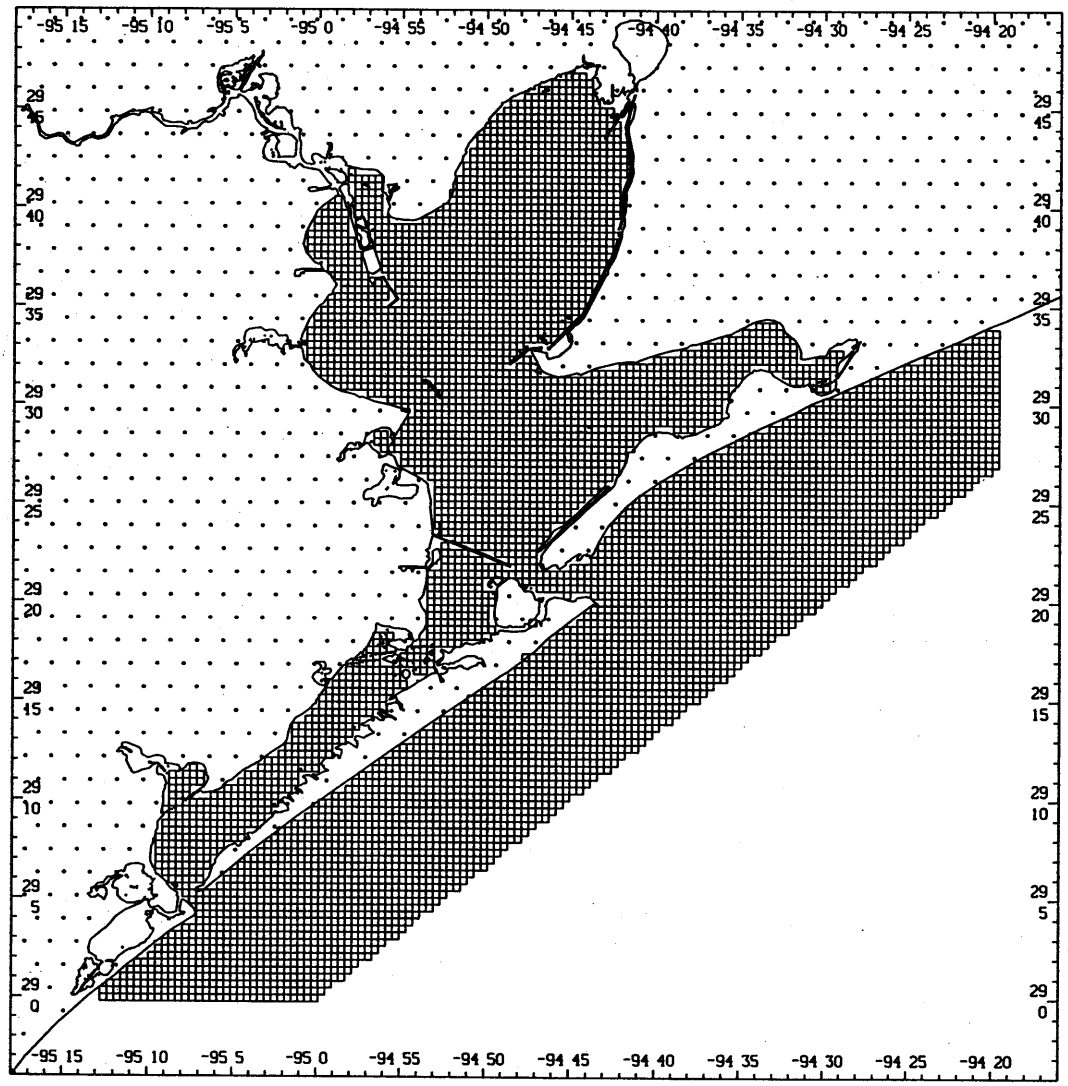

Figure 4.3. Grid generated by coastline for solving the LE in Galveston Bay. Cell widths are 0.35 nmi.

Editing of the grid was necessary. To insure that all the major water bodies were included in the grid, five cells were forced to be water by editing. These included one cell near Tiki Island, two cells near the southeastern end of the Texas City Channel spoil island, and two cells near the southwest entrance to the Bay at San Luis Pass. Also, the positions of a few tide gauges were adjusted by 0.1 or 0.2 nmi to insure that the gauges were not enclosed by land. Finally, although the cell size is not small enough to resolve the Galveston Channel (which separates Pelican Island from the city of Galveston), the Pier 21 gauge (877-1450) was automatically included as a water cell (as are all tide gauge cells).

The weighting functions were computed for each set of variables. For the tidal constituents, all 14 locations were used. For the residual water levels, only 9 of the 10 locations were used: the GPS-fitted buoy observations were not used since there were significant gaps in the data. *G* fields were computed for the offset (the MSL-to-MLLW difference) and the ellipsoidally-referenced MSL datum.

An example of one of the weighting functions is shown in Figure 4.4. The function, *g*, is shown for the tidal constituents at station 877-0931 at Smith Point. The function has the value 100 there and has the value 0 at all other water level locations. There are 12 other distributions, one each for the other water level gauge locations. The function shows at any location throughout the bay what percentage of a field, such as a constituent's phase, is due to the value at the Smith Point gauge.

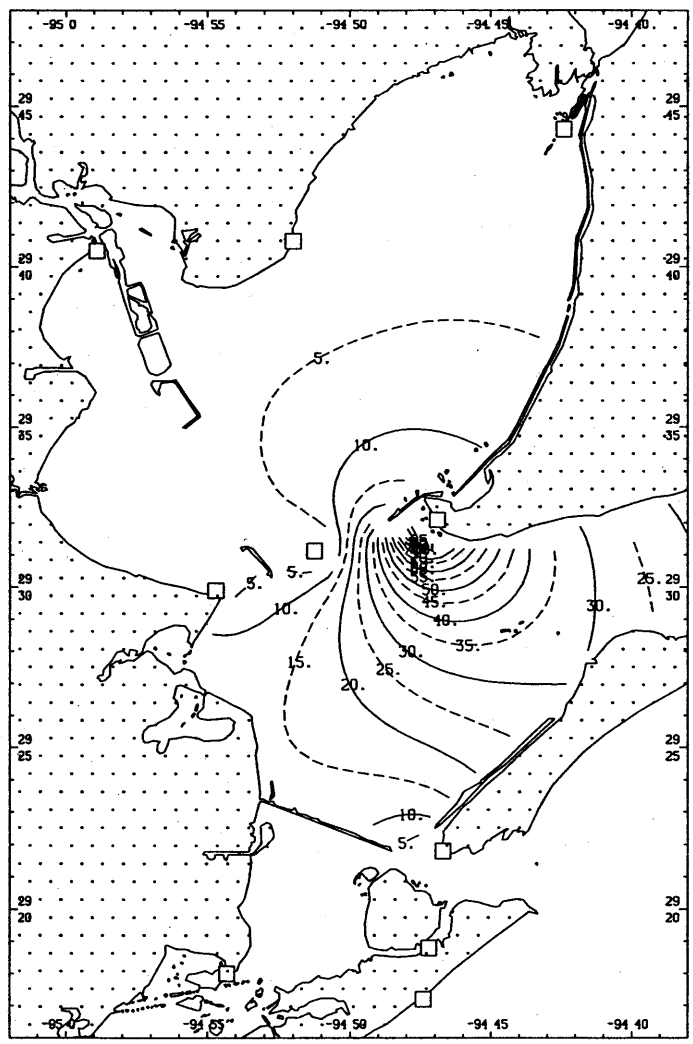

Figure 4.4. Weighting function *g(x, y)* for the water level station at Smith Point (877-0931). Contours are lines showing the percentage of the final interpolated field value that is due to the value at Smith Point.

4.4. Constituent Interpolation

The distribution of the M_2 tide was chosen for the first test. The distribution of the epoch angle as generated by the hydrodynamic model (Appendix C) and by the LE method are shown in Figure 4.5. The LE model parameter α (0.9) was calibrated to provide the best fit in the lower portion of the Bay where the phase increases from 110 degrees at the entrance to 210degrees in mid-bay. Remember that the LE distribution method matches the data at the water level gauge stations, while the modeled distribution does not necessarily match. For the stations in the portion of the Bay shown in the figure, the model's error ranges from -11.5 degrees at Morgans Point to 28.7 degrees at Eagle Point (Appendix C).

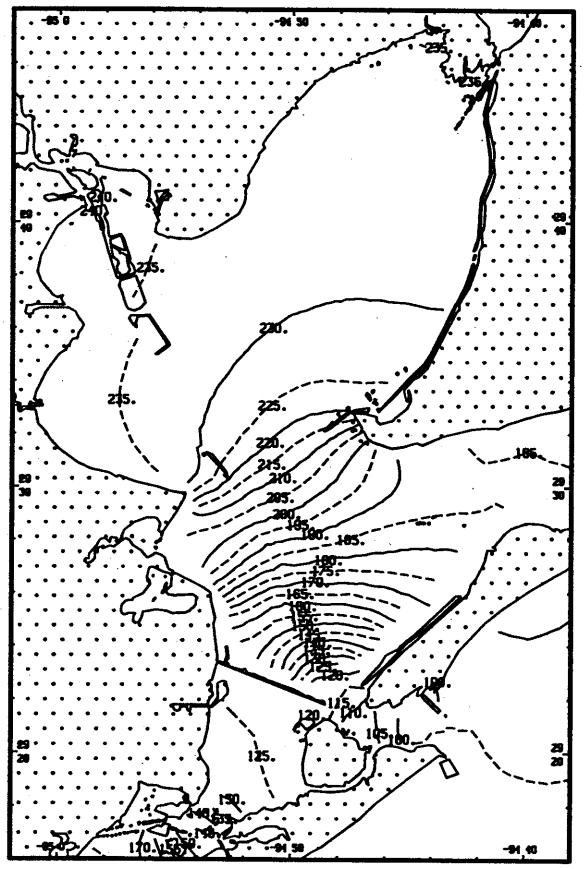

Figure 4.5a. Distribution of M_2 epoch (local) from the numerical model.

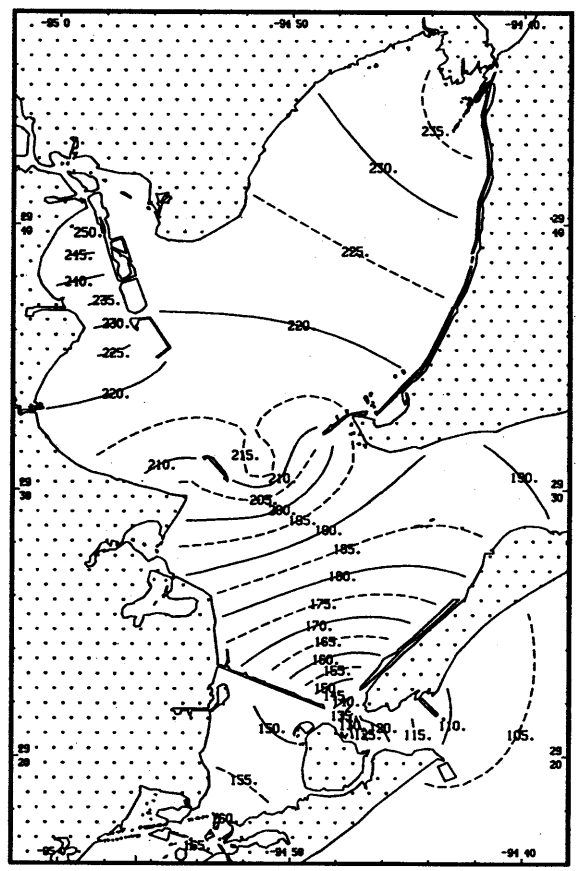

Figure 4.5b. Distribution of the M_2 epoch (local) from the LE interpolation method.

A comparison of the M_2 amplitudes generated by each method (Figure 4.6) show that the overall pattern of the distribution differs more than in the previous comparison, although the amplitudes are similar. For the stations in the portion of the Bay shown in the figure, the model's error ranges from -2 cm at Pleasure Pier to 0.7 cm at Eagle Point (Appendix C).

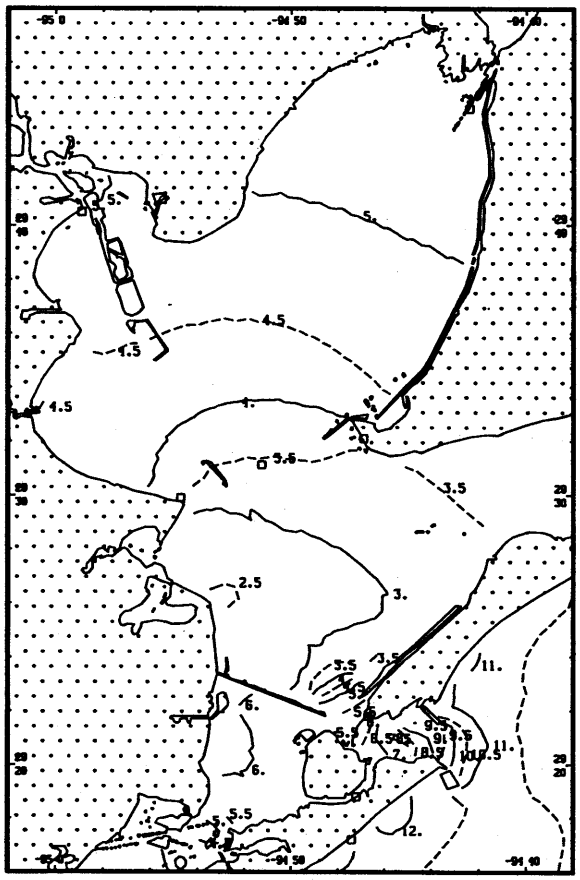

Figure 4.6a. Distribution of M_2 amplitude (cm) from the numerical model.

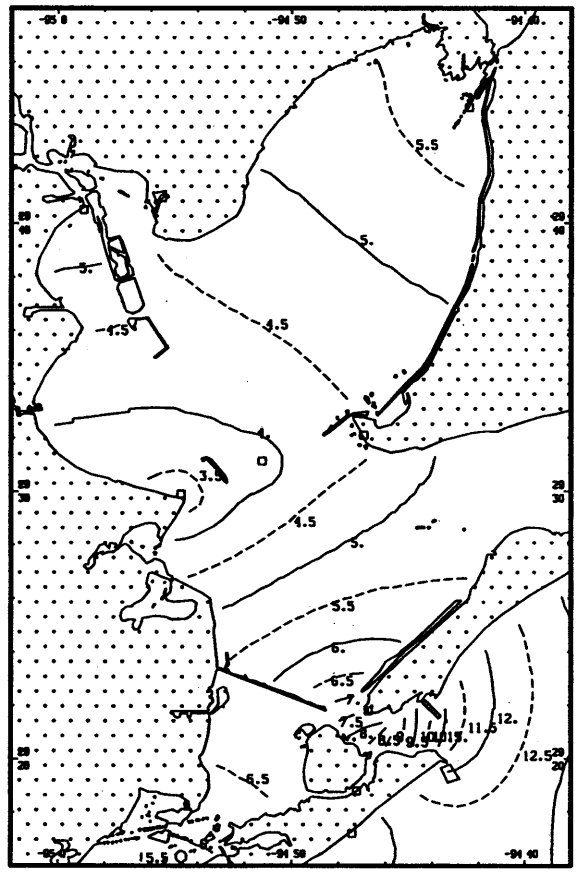

Figure 4.6b. Distribution of M_2 amplitude (cm) from the TCARI method.

Plots of the distributions of the epochs and amplitudes of the K_1, O_1, and P_1 constituents (which, along with the M_2, comprise the four largest in amplitude) generated by the numerical model and the TCARI method are shown in Appendix D.

4.5. Residual Water Levels

The residual water level is generated from Eqn. 2.10 using data taken at the set of tide gauges for which both constituents and an observed, hourly water level time series are available. The residual is the observed water level minus the reconstructed astronomical tide. A plot of the residual water levels for the period of the NOAA research project is shown in Figure 4.7. The water levels show events at Days 163 and 170 that seem to originate from outside the Bay, and an event at Day 187 that seems to be confined to inside the Bay.

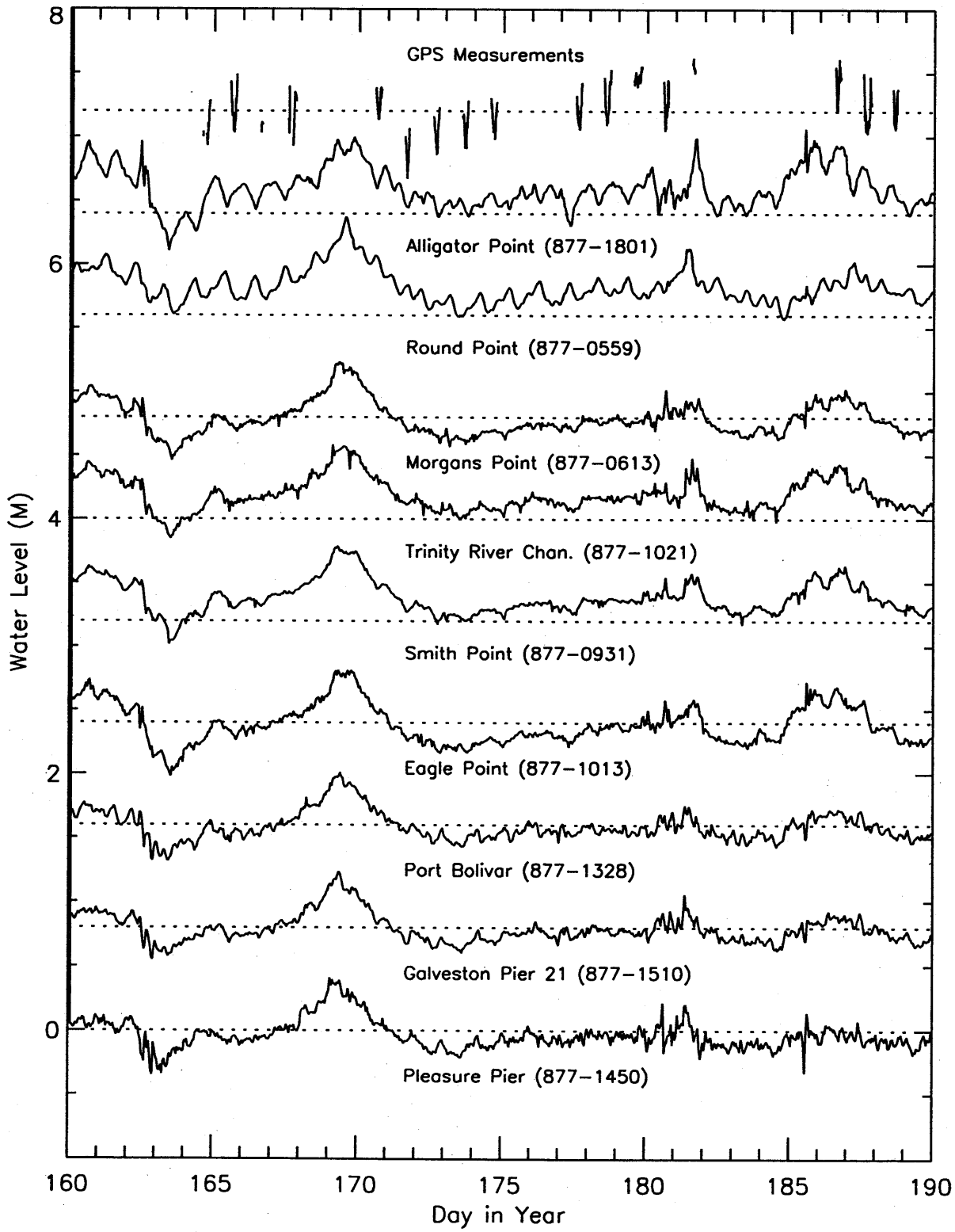

Figure 4.7. Residual water levels in Galveston Bay during 1995. Stations plotted nearer the bottom are nearer the Galveston entrance. The top row shows the demeaned kinematic GPS measurements.

4.6. The Offset and Datum

The offset, H_O, defined as the difference between MSL and MLLW (or the elevation of MSL relative to MLLW), and the datum, H_E, (the elevation of MSL relative to the WGS-84 ellipsoid) are shown in Figure 4.8. The distributions were generated by the LE method and used the values shown in Table 4.1.

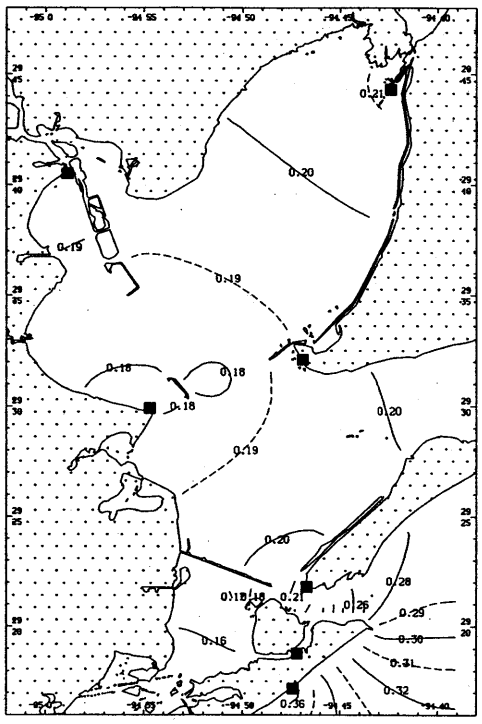

Figure 4.8a. H_O , the offset (m) (MSL minus MLLW). Contour interval is 0.01m.

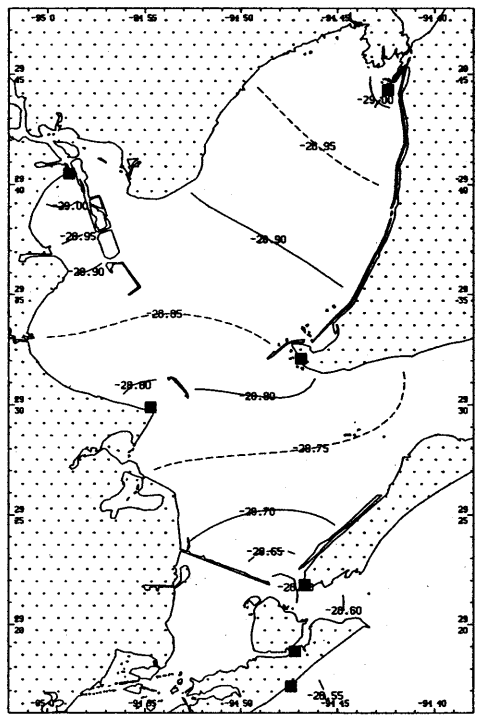

Figure 4.8b. H_E, the datum (m) (MSL relative to the ellipsoid). Contour interval is 0.10 m.

4.7. Sensitivity Tests

TCARI-generated, ellipsoidally-referenced water levels were computed according to the methods described in Section 2.5 and compared to the measured values in Galveston Bay. The operative equation for the ellipsoidally-referenced water levels is

$$D'_{GPS} = \eta_A + \eta_R + H_E \tag{2.13}$$

where D'_{GPS} is the ellipsoidally-referenced water level, η_A the astronomical tide relative to MSL, η_R the residual water level, and H_E is the ellipsoidally-referenced MSL. Because of the lack of reliability

in the values of the amplitude and phase of the long-period constituents (Mm, Mf, Msf, Ssa, and Sa), these constituents were masked out in the calculation of the astronomical tides; the net effect was to shift them to the residual water levels. At each time of a ship-based measurement, a TCARI prediction of the water level was made at the four grid cells surrounding the location of the ship; the water level value at the precise location of the ship was then computed using bi-linear interpolation.

Benchmark Tests

Tests of the sensitivity of the solution were carried out after a benchmark run was completed. Out of 618 observed values, 557 were used in the comparisons; values not used fell on grid land cells. For the benchmark run, which used hourly water levels observations, the mean error was 0.01 cm, the RMS error was 9.7 cm, and the maximum error was 27.1 cm. An analysis of the data showed that relatively large errors of consistent sign occurred for the water levels measured near the GPS-fitted buoy (the TCARI predictions were about 13 cm too low). This error is probably due to the absence of a measured offset for that location. When these measurements were excluded from the comparison, the RMS error dropped to 8.8 cm.

The first set of sensitivity tests involved changing the key parameters in the TCARI method. These are the following (the benchmark values appear in parentheses): the grid size, *wcell* (0.35 nmi); the boundary slope condition coefficient, α(0.9); the coastline Index (0); and the error ratio, ε(5 x 10^{-5}). The coastline index sets the coastline cells to either 0 for land or 1 for water. The new values tested were: *wcell* = 0.175 nmi, α= 1.0, Index=1, and ε= 5 x 10^{-4}. With the exception of excluding the GPS-fitted buoy values, the accuracy was only modestly affected by changes in the parameter values (Table 4.2).

Table 4.2. Results of the benchmark run and the sensitivity tests. Errors are in cm.

Run	Mean Error	RMS Error	Max. Error
Benchmark	0.01	9.7	27.1
Exclude GPS Buoy	1.5	8.8	27.1
Change *wcell* from 0.35 to 0.175	-0.6	9.9	27.7
Change α from 0.9 to 1.0	0.02	9.7	27.2
Change Coastline Index from 0 to 1	-1.7	9.6	28.8
Change ε from 5 x 10^{-5} to 5 x 10^{-4}	-0.2	10.1	27.3

Hourly vs. 6-Minute Water Levels

The second set of tests involved the use of 6-minute water level observations instead of the hourly values. During initial TCARI development, the 6-minute data were not used because there were significant gaps (greater than 2 hours) in the data files for stations 877-0931, 877-0559, and 877-1328.

The maximum gap was 44.7 hours. The TCARI program was revised so it uses the 6-minute data if they are available, and uses the hourly data if the 6-minute data are unavailable. The use of six-minute data gave a lower error (Table 4.3).

Table 4.3. Results from the use of hourly or 6-minute observed data for the calculation of the residual water levels. Errors are in cm. Skip Gaps means that when the water level data were missing, the ship track data were not used. Interpolate means that the water level for the required time was interpolated from the observed data, regardless of the time gap. Substitute means that when the water level interpolated from the 6-minute values was missing (the gap was greater than 1 hour), the water level interpolated from the hourly values was substituted. Num. Gaps is the number of data points that were skipped because of missing 6-minute data.

Run	Mean Error	RMS Error	Max. Error	Num. Gaps
Hourly (Benchmark)	0.01	9.7	27.1	0
6-Min, Skip Gaps	-0.01	8.4	24.6	112
6-Min, Interpolate	0.6	8.3	24.6	0
6-Min, Substitute	0.4	8.4	24.6	0

Interpolation Variables

A third test of sensitivity was to alter the parameters that were subject to interpolation. In full TCARI, the tidal component of the water level is generated from the interpolated constituent amplitudes and phases, and the residual water level is interpolated directly. For the first test, the tidal component was zeroed out and total water level at the gauges was interpolated directly. For the second test, the residual water level was zeroed out, so that the water level at the ship location was only the tidal component. The results (Table 4.4) show that full TCARI gave the smallest errors.

Table 4.4. Results for full TCARI, total water level interpolation, and ignoring the residual water level. Errors are in cm.

Run	Mean Error	Std. Dev.	RMS Error	Max. Error
Full TCARI	0.5	8.4	8.4	24.6
Interpolate Total W.L.	0.3	8.6	8.6	24.8
No Residual W.L.	-5.6	11.7	12.3	42.4

4.8. Accuracy Tests

Accuracy of the GPS Water Level Data

Huff and Gallagher (1996) estimated the error in the measurements using two sets of data, each subject to specific restrictions. For Set 1, the restrictions was: (1) the ship was within 2.5 km of one of four gauges (Port Bolivar, Smith Point, Trinity River Channel Platform, and Eagle Point), (2) ship speed was less than 0.5 m/s, (3) the GPS data for the relevant 6-minute interval had a relatively small number of erroneous values (less than 16%), and (4) the RMS deviation from the 6-minute mean of the 1-second samples measured at the water level gauge was less than 6 cm. Their result was that the GPS measurements of water level had a mean error of 0.07 cm and a standard deviation (SD) of 4.7 cm. For Set 2, the restrictions were: (1) the ship was within 5.0 km of one of the four gauges, (2) ship speed was less than 15 m/s, and (3) the RMS deviation was less than 30 cm. Their result was that the mean error was 2.13 cm, the RMS error was 9.1 cm, and the SD was 9.0 cm. The errors for the second set are probably more representative of errors in all the data.

Accuracy of TCARI Near the Tide Gauges

The TCARI method was applied to measurements that, for simplicity, met only the first two criteria of the second set. (Since TCARI will exactly match the measured water levels at the gauges, use of Set 1 data will not provide useful data.) The predicted water levels had a mean error of 3.0 cm, RMS of 8.3 cm, and an SD of 7.8 cm. Since these errors are approximately equal to those of the measurements, we conclude that the TCARI water levels are consistent with what was measured by post-processed kinematic GPS near the gauges (Table 4.5).

Table 4.5. Results from the accuracy tests. Errors are in cm. In Huff and Gallagher (1996), GPS measured water levels were compared to water levels observed at four gauges. In TCARI, the predicted water levels (which match exactly at the gauges) were compared to those measured in Huff and Gallagher, Set 2.

Method	Mean Error	Std. Dev.	RMS Error	Max. Error
Huff & Gallagher, Set 1	0.0	4.7	4.7	-
Huff & Gallagher, Set 2	2.1	9.0	9.1	-
TCARI	3.0	7.8	8.3	24.6

Accuracy of Discrete Tide Zoning

Tide zoning corrections, h_Z*, for the data were generated using the polygons shown in Figure 2.1, the 6-minute water level observations, and the range ratio and time lag data for each polygon. Not all the measured water level locations lie within the tide-zoned area; of the 618 measurements, 536 had corresponding corrections. A direct comparison of the tide corrections with the measured water levels

is not possible because tide zoning does not provide a distribution of the MLLW field relative to the ellipsoid. However, TCARI does. Therefore, an estimate of the ellipsoidally-referenced water level which incorporates the tide-zoned correction and the TCARI-generated offsets was computed as follows

$$D''_{GPS} = h_Z^* - H_O + H_E \tag{4.1}$$

where D''_{GPS} is the ellipsoidally-referenced water level and H_O is the spatially-interpolated (using LE functions) datum offset (MSL minus MLLW). As before, 481 points were used in the comparisons.

Three sets of estimated ellipsoidally-referenced water levels were generated. Each set consists of an estimate generated using the standard tide zoning method for corrections, and an estimate based on the standard method, but with spatially-interpolated corrections. In the second method, the interpolated value is the weighted mean of the original correction and the corrections in adjacent zones. The weights are equal to the fraction of the area of a circle that lies in the respective zones; the circle has an origin at the center of area of the original zone and has a radius equal to the area of the zone divided by its perimeter. The first set of estimates was based on the preliminary tide zoning corrections. Preliminary corrections were generated using the 6-minute water level observations from a single water level gauge, that at Pleasure Pier (877-1450). The corrections are termed preliminary because data from only a single water level gauge were used. The second set of estimates was based on the final zoning corrections. The final corrections had access to the 6-minute data from five stations (877-0613, 877-1013, 877-1021, 877-1450, and 877-1510); data from three of the eight locations (stations 877-0559, 877-0931, and 877-1328) were not used because they had gaps. The third set of estimates was like the second, but with access to all eight stations. The results are shown in Table 4.6.

Table 4.6. Errors (cm) based on water levels estimates using tide zoned corrections. Results are for preliminary tide zoning (one station), final zoning with five stations, and final zoning with eight stations.

Tide Zoning Method	Mean Error	Std. Dev.	RMS Error	Max. Error
Preliminary	-5.4	7.4	9.2	33.9
Preliminary, Interpolated	-5.4	7.4	9.2	34.2
Final, 5 Stations	-6.4	7.8	10.1	38.2
Final, 5 Stations, Interpolated	-6.4	7.6	9.9	38.8
Final, 8 Stations	-6.0	7.3	9.4	38.2
Final, 8 Stations, Interpolated	-6.0	7.0	9.2	38.8

The corrections from final tide zoning were less accurate than those from preliminary zoning. This may be partially due to the fact that, for GPS observations in the zone containing Galveston Pier 21 (877-1450), the water levels from the Port Bolivar (877-1328) gauge, not the Pier 21 gauge, were used to compute the corrections.

Comparison of TCARI with Tide Zoning

A major objective of this study is to compare the results of TCARI with those of discrete tide zoning. A plot of the corrections produced by each method is shown in Figure 4.9. Not all the measured water level locations lie within the tide-zoned area; of the 618 measurements, 536 had corresponding corrections, and of these, 481 also had a TCARI-generated offset value. The TCARI corrections are generally greater than the zoning corrections; the reason for this will be discussed below. This direct comparison has limited value because there is yet no way to determine which one is more correct.

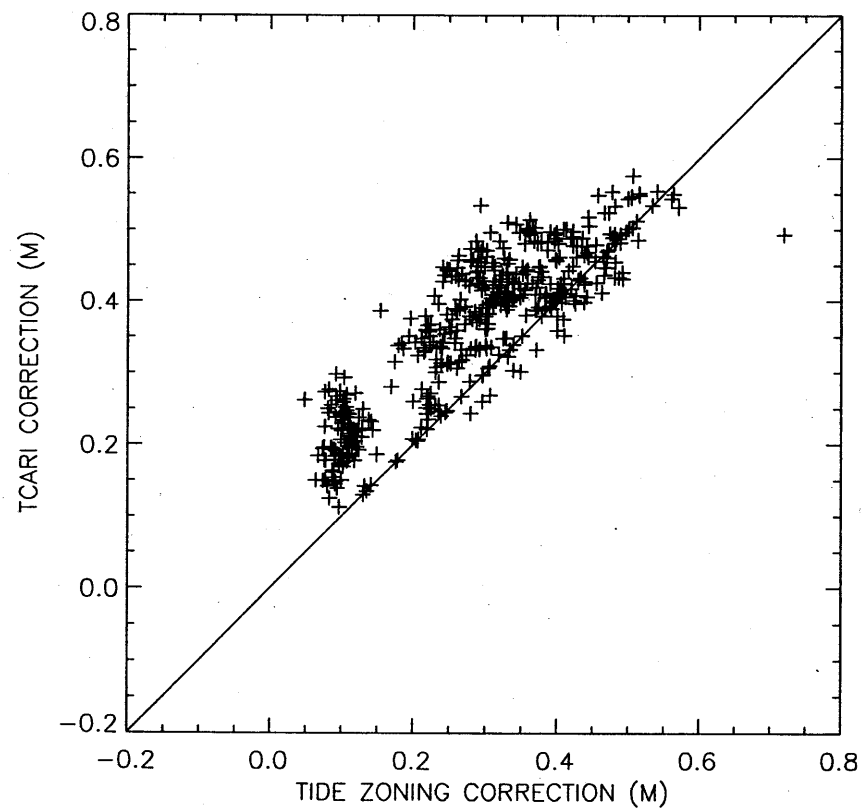

Figure 4.9. Scatter plot showing the corrections determined by tide zoning and those determined by TCARI. The correlation coefficient is 0.861.

However, since both the tide-zoned estimates and the TCARI estimates depend on H_E, a reliable assessment of the relative accuracies of discrete tide zoning and TCARI can be made *only if* the error contribution of H_O is small. A comparison of the errors for zoning and TCARI was made using only

the points where both were available. The results (Table 4.7) shown that tide zoning is generally less accurate than the TCARI method.

Table 4.7. Results from comparing errors in water level estimates using spatially-interpolated discrete tide zoning (both preliminary and final) corrections and TCARI when the same set of observations was used. Errors are in cm.

Method	Mean Error	Std. Dev.	RMS Error	Max. Error
Preliminary Zoning	-5.4	7.4	9.2	34.2
TCARI	1.9	7.3	7.6	24.6
Final Zoning (8 Stations)	-6.0	7.0	9.2	38.3
TCARI	1.6	7.3	7.5	24.6

Accuracy of the Numerical Model

The numerical model for Galveston Bay (Appendix C) was used to generate water levels for comparison with the kinematic GPS measurements. The model was run for the month of June 1995 and included tidal, density, and meteorological forcing. At each water level gauge the ellipsoidally-referenced model datum (corresponding to $z = 0$ in the model's coordinate system) was computed by assuming that the monthly mean of the modeled water level was equal to the monthly mean of the ellipsoidally-referenced observed water level. An ellipsoidally-referenced model datum field was generated by weighting the values of the ellipsoidally-referenced model datum at the water level gauges. The weight at each cell for each gauge was the square of the inverse distance to the gauge, normalized by the sum of the squares of the inverse distances to all gauges. The ellipsoidally-referenced instantaneous water level was then computed as the sum the instantaneous modeled water level and ellipsoidally-referenced model datum. Comparisons were made at 470 locations, and were stratified based on distance from the nearest water level gauge and the speed of the ship. The RMS difference for the numerical model was 15 cm, and there was no appreciable dependency on distance or speed. The TCARI RMS error for the 453 June measurements which were located within a numerical model water grid cell was 8.3 cm.

Summary

To summarize, TCARI has produced realistic estimates of the water levels measured with kinematic GPS (Huff and Gallagher, 1996). Better TCARI estimates are obtained when 6-minute observations at the gauges are used, rather than the hourly data. The TCARI estimates appear to be better than those produced by both preliminary and final tide zoning (without spatial interpolation), but those results are dependent on an estimate of H_o from TCARI and the assumption that H_o has negligible error. Results are summarized in Table 4.8 and a scatter plot of the measured water levels and the TCARI-predicted values appears in Figure 4.10.

Table 4.8. Mean and RMS error and standard deviation of the predicted water level as compared to the measured water level in Galveston Bay using various methods of prediction. Errors are in cm.

Method	Mean Error	Std. Dev.	RMS Error	Max. Error
Numerical Model	-	-	15	-
Final Zoning	-6.0	7.3	9.4	38.3
TCARI	1.6	7.3	7.5	24.6

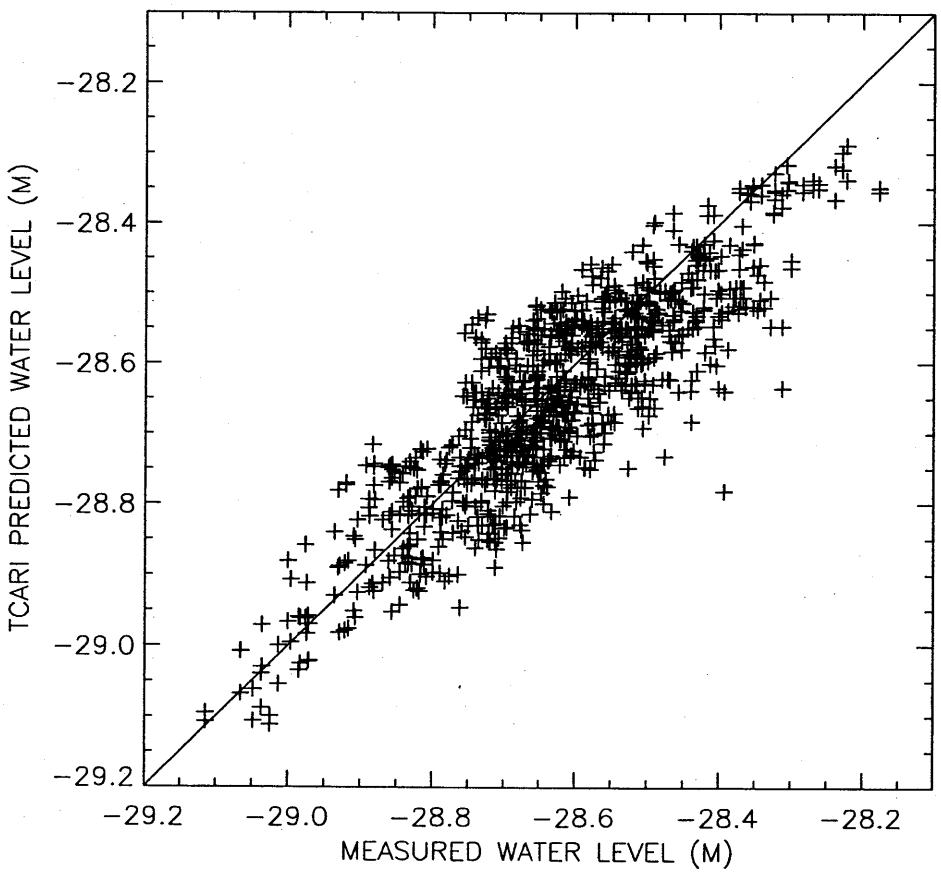

Figure 4.10. Scatter plot showing the kinematic GPS-measured water levels and the TCARI-predicted water levels, both referenced to the ellipsoid. The correlation coefficient is 0.863.

5. APPLICATION TO SAN FRANCISCO BAY

5.1. Ship Track Data

Water level data were gathered in San Francisco Bay during 1997 as part of a NOS-sponsored study (Huff et al., 1998). Figure 5.1 shows the location of the 968 locations where measurements of the water level [referenced to the NAD 83 (86) ellipsoid] were made during March 6 to 10 and June 10 to 23. The data were processed to account for settlement in the water, which is a function of ship speed.

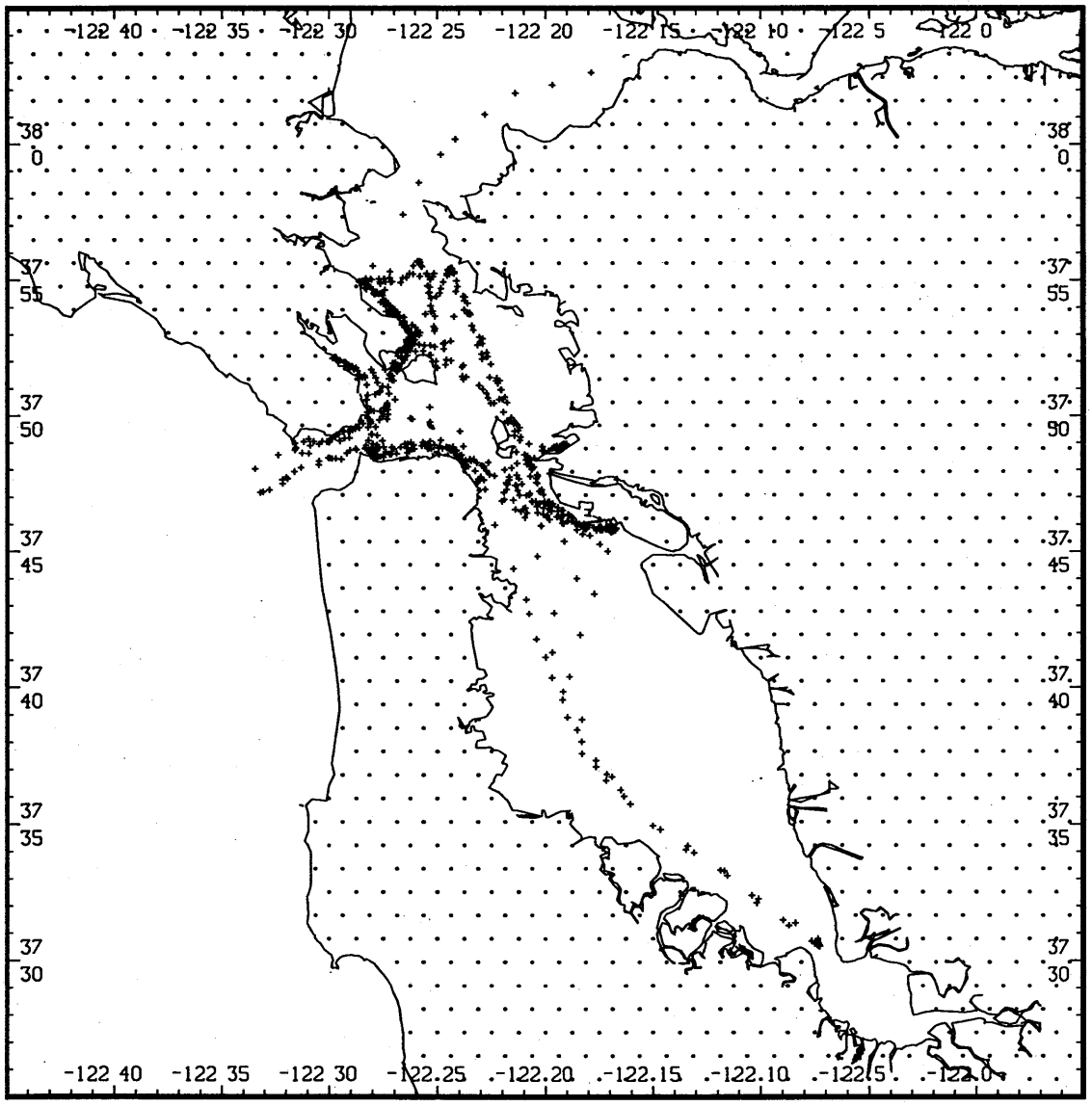

Figure 5.1. Location of water level measurements (denoted by a '+') in San Francisco Bay made by NOS during March and June of 1997.

5.2. Water Level and Model Data

Historical NOS water level data was available at the 42 stations shown in Figure 5.2. Real-time data were also available at three stations which are part of the NOS PORTS installation; these are San Francisco (941-4290), Alameda (941-4750), and Richmond Chevron Pier (941-4863). Additional water level data are available from Dumbarton Bridge (941-4509). Tidal constituent amplitudes and epochs, and information on the harmonic analyses is given in Appendix E.

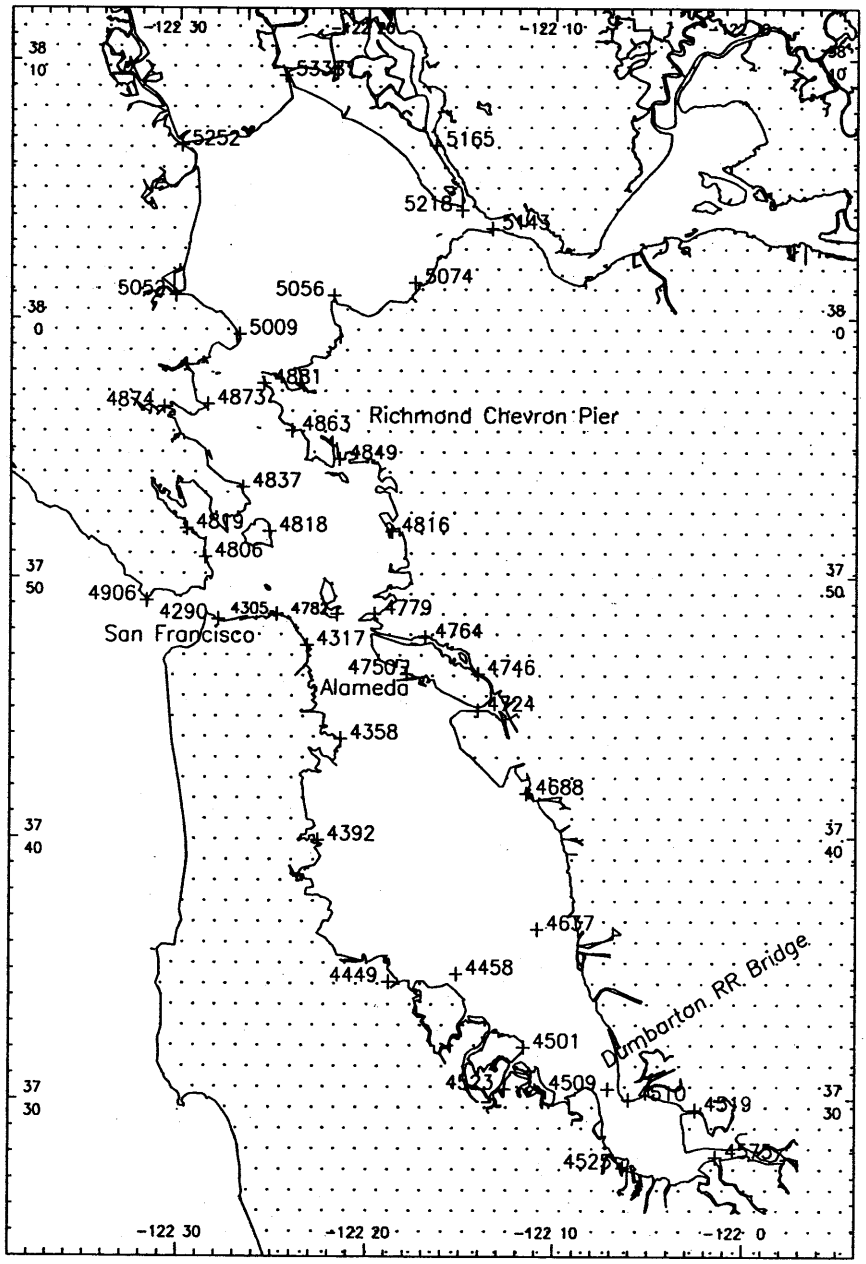

Figure 5.2. Present and past locations of NOS water level gauges in San Francisco Bay where tidal constituent and/or time series data were used. NOS station numbers are as above but preceded by a 941. Station names are given in Appendix E.

Ellipsoidally-referenced [NAD 83 (86)] MSL is available for the PORTS gauges. The values are -31.631 m for San Francisco, -31.462 m for Alameda, and -31.355 m for Richmond Chevron Pier.

A numerical circulation model for the Bay, called the Tidal, Residual, Intertidal Mudflat (TRIM) model (Cheng, et al., 1993), provides additional tidal data. The model was developed and calibrated for the astronomical tide, and plots were generated of the amplitudes and epochs of the M_2 and K_1 tidal constituents. The modeled distributions will be used for comparison to the TCARI-generated distributions. The TRIM model employs two-dimensional, depth-averaged Eulerian equations of water level, velocity, and density (which is related to salinity by a simplified equation of state that is independent of temperature). Horizontal advection of momentum is treated by an imbedded Lagrangian numerical scheme. Numerical calculations were made on two grids composed of square cells: a coarse-mesh grid with cell sides of 500 m and a fine-mesh grid with cell sides of 250 m. The model was driven by astronomical tide and variable density at the ocean boundary and without winds. Calibration consisted in adjusting the depth-dependent values of n in the Chezy-Manning bottom drag formulation, and altering the ocean boundary tidal constituents to provide the best match to constituent amplitudes and phases at 24 tide gauge locations and 11 current meter stations. Tidal data were collected in 1979 and 1980 during a joint USGS-NOS circulation survey (Welch et al., 1985). The modeled tides on the fine-mesh grid had the following accuracy: For the M_2 constituent, the amplitude had a mean error of 0.70 cm and a standard error of 1.61 cm, and the epoch had a mean error of -2.10 degrees and a standard error of 2.18 degrees. For the K_1 constituent, the amplitude had a mean error of -0.06 cm and a standard error of 0.80 cm, and the epoch had a mean error of 2.19 degrees and a standard error of 0.68 degrees.

5.3. Grid and Weighting Functions

A grid for the Bay, with a grid size of 0.25 nautical miles (chosen to represent small features such as the channels between islands in the central Bay) was generated (see Figure 5.3). The grid covers the areas where measurements were made, specifically the entrance to the bay, South San Francisco Bay, and San Pablo Bay. A typical weighting function is shown in Figure 5.4.

5.4. Constituent Interpolation

The distribution of tidal constituents was generated as in Section 4. The M_2 tide was studied for comparison. The TRIM (Cheng et al., 1993) model-computed amplitudes are shown in Figure 5.5a, and the TCARI-computed amplitudes are shown in Figure 5.5b. The patterns are similar, although TCARI amplitudes are generally greater in a narrow band along the eastern side of South Bay; this difference is most likely due to the shallowness of the water in that area. The TRIM (Cheng et al., 1993) model-computed M_2 phases are shown in Figure 5.6a, and the TCARI-computed phases are shown in Figure 5.6b. The patterns are similar. Comparisons for the K_1 tide and additional TCARI distributions are shown in Appendix F.

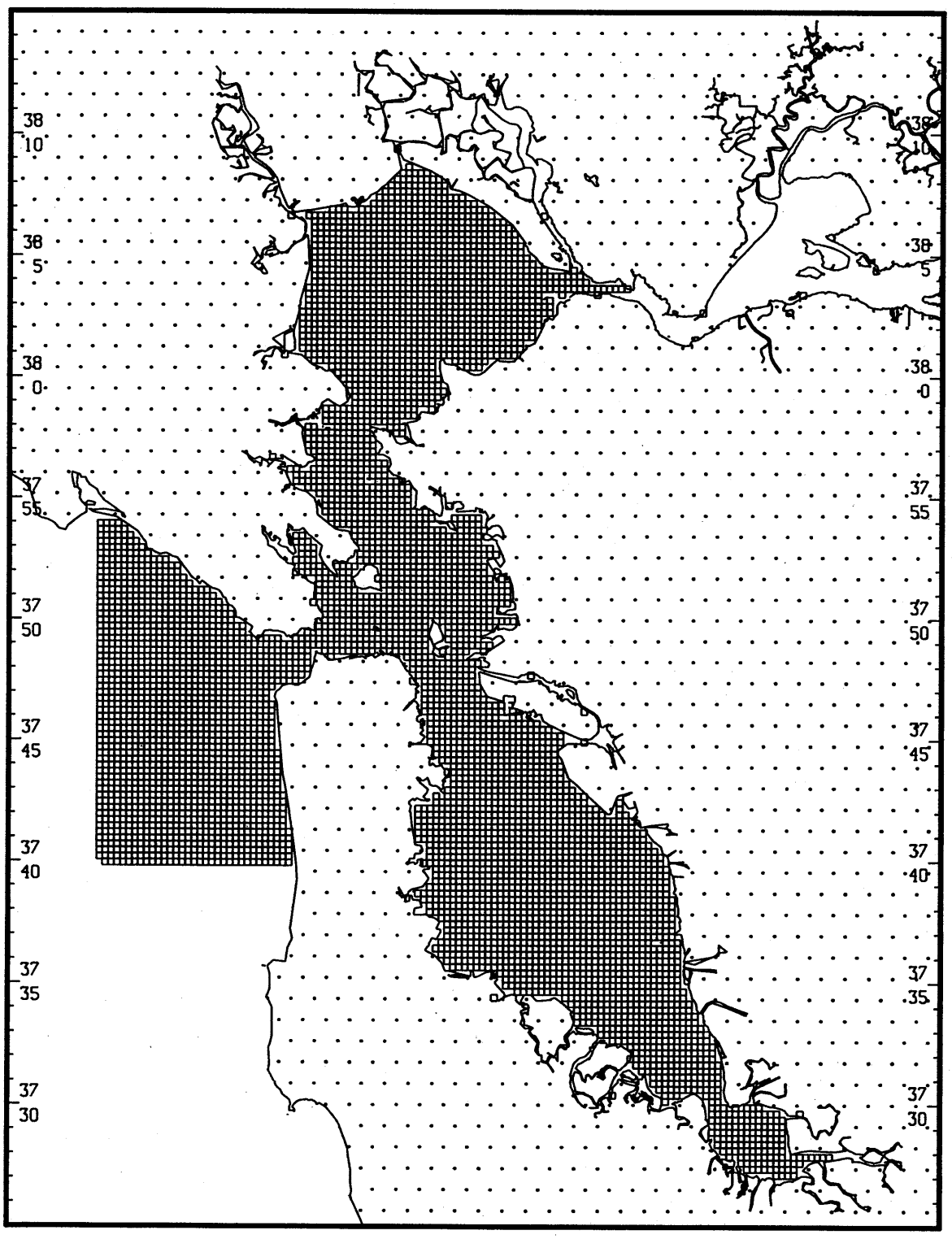

Figure 5.3. TCARI grid for San Francisco Bay. Cell size is 0.25 nautical miles.

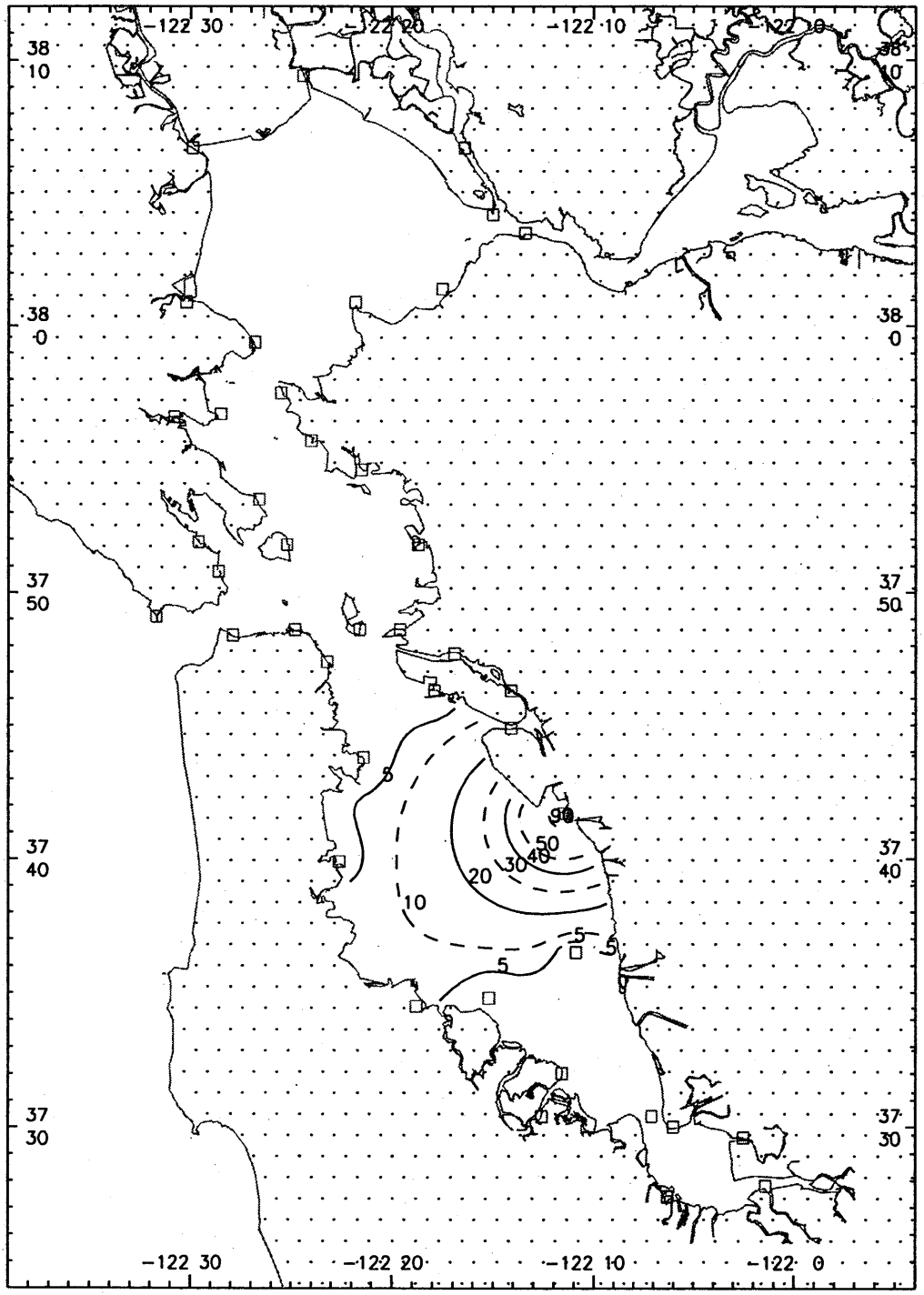

Figure 5.4. The weighting function, *g(x,y)*, for San Leandro Marina (941-4688) shown as a percentage.

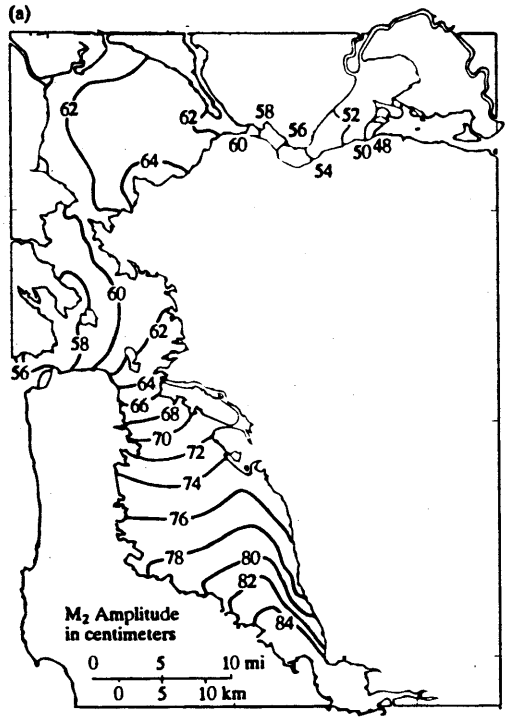

Figure 5.5a. M_2 amplitudes (cm) as generated by TRIM.

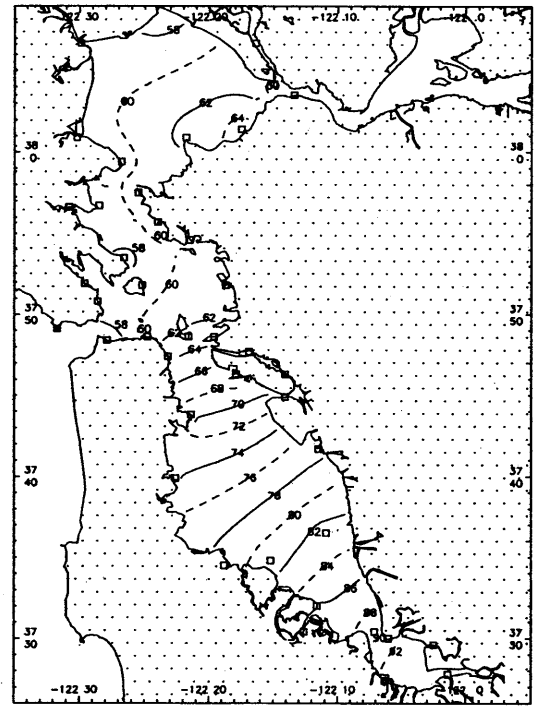

Figure 5.5b. M_2 amplitudes (cm) as generated by TCARI.

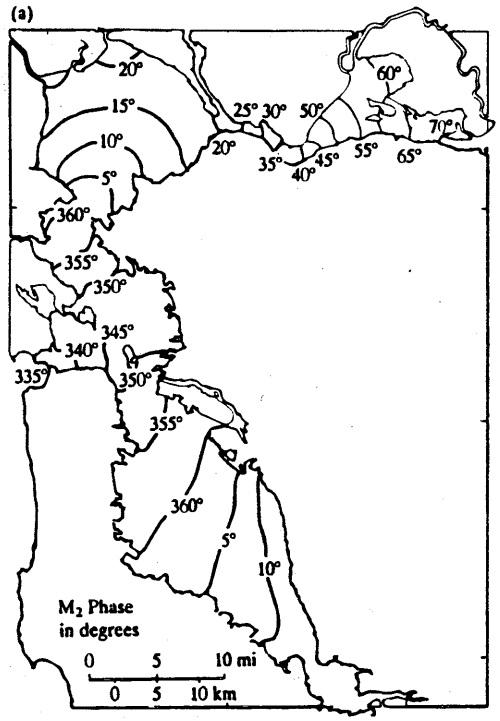

Figure 5.6a. M_2 local epoch (degrees) as generated by TRIM.

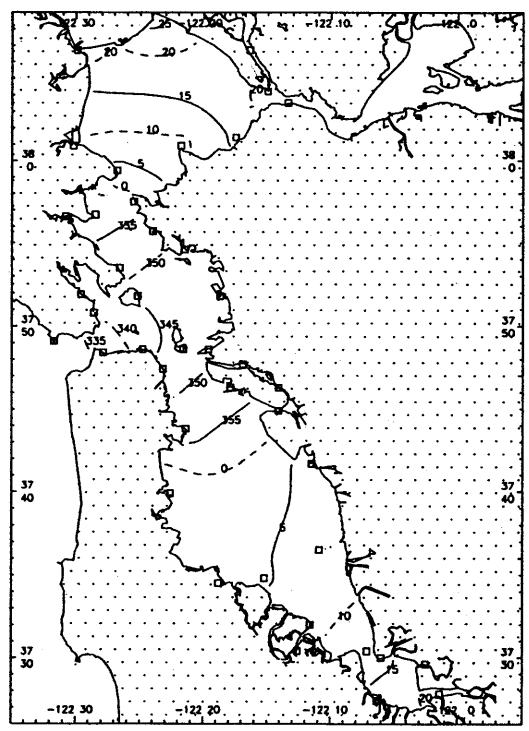

Figure 5.6b. M_2 local epoch (degrees) as generated by TCARI.

5.5. Residual Water Levels

The residual water levels at four stations and the GPS-measured water levels during the survey are shown in Figure 5.7. One panel of the figure represents a 5-day period in March and the other panel represents a 15-day period in June. The residual variations, which are the total water level from which the reconstructed tide has been subtracted, are relatively small (only a few centimeters), given that the tidal range is approximately 1 meter.

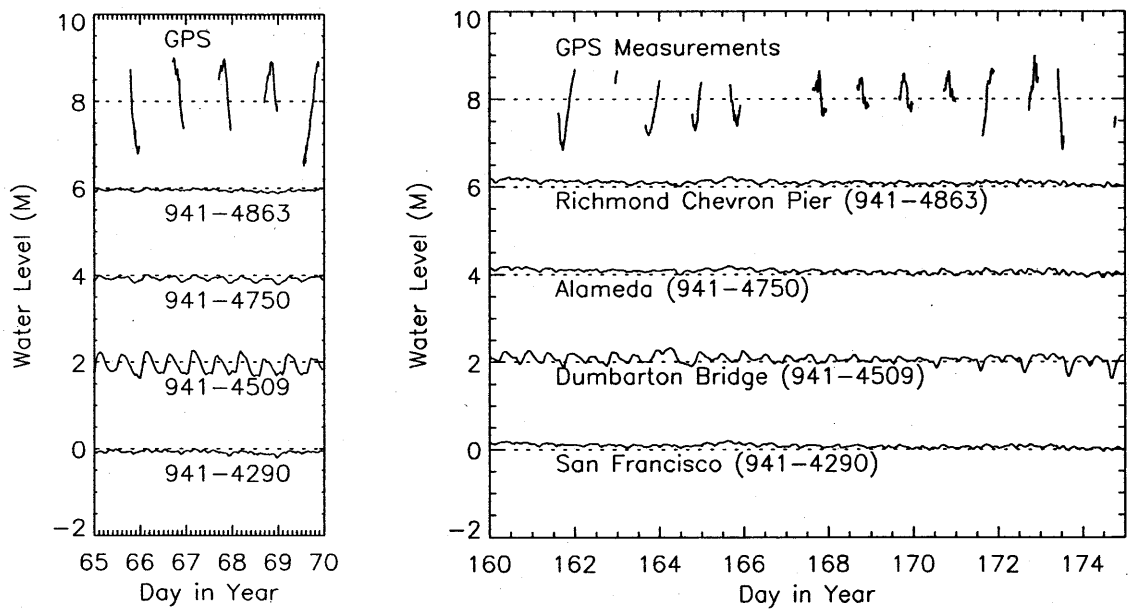

(a) (b)

Figure 5.7. Residual water levels at four locations in San Francisco Bay (four lower lines) and the demeaned kinematic GPS measured water level (top line) for (a) 5 days in March 1997, and (b) 15 days in June 1997.

5.6. The Offset and Datum

The offset, which is the difference between MSL and MLLW, and the MSL datum (the elevation of MSL relative to the ellipsoid) are shown in Figures 5.8 and 5.9, respectively. Values are discussed in Section 5.2.

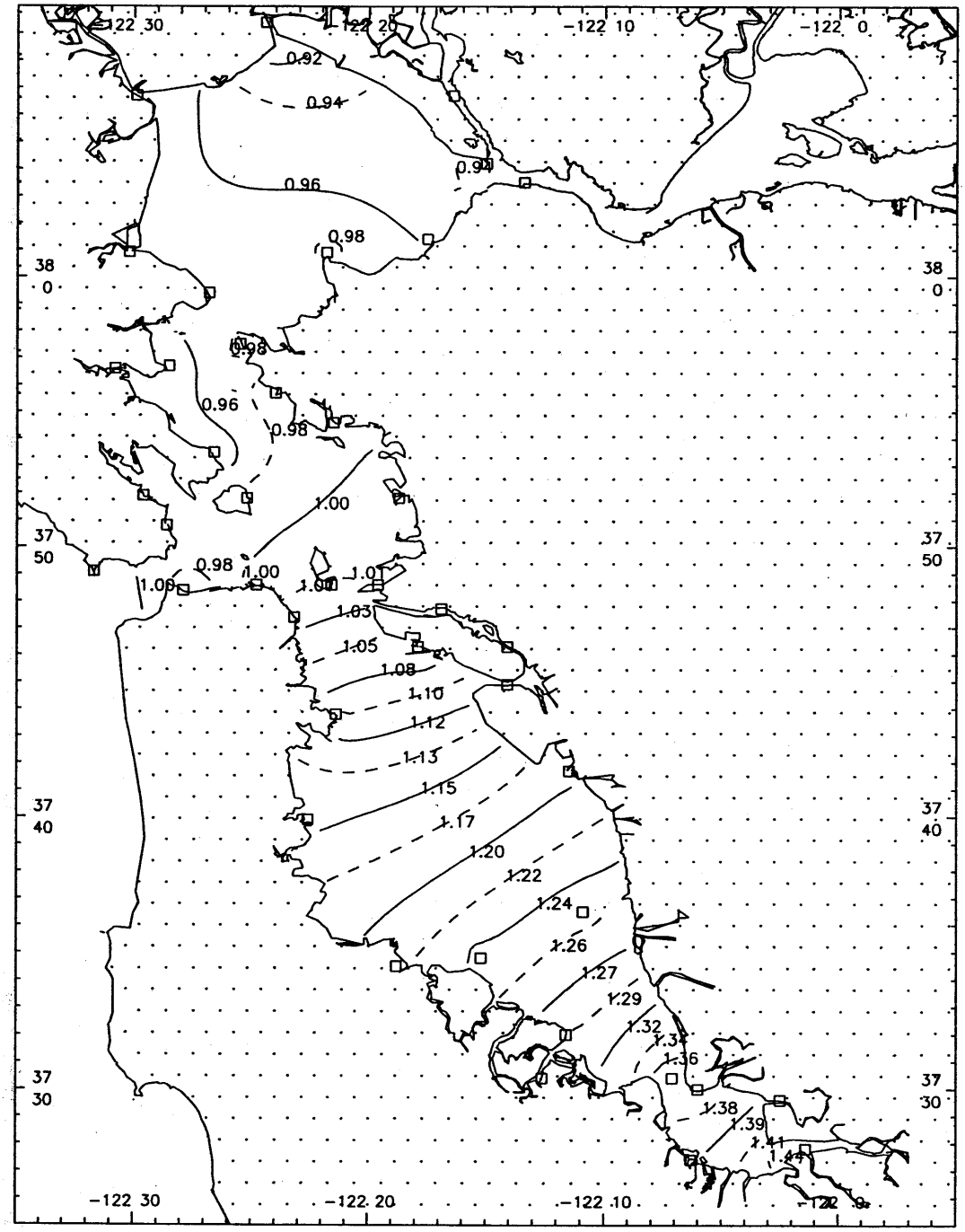

Figure 5.8. Distribution of the MSL-to-MLLW offset (m) in San Francisco Bay as generated by TCARI. Values range from 0.92 near the northwest part of the Bay to1.44 in the southern part of the Bay.

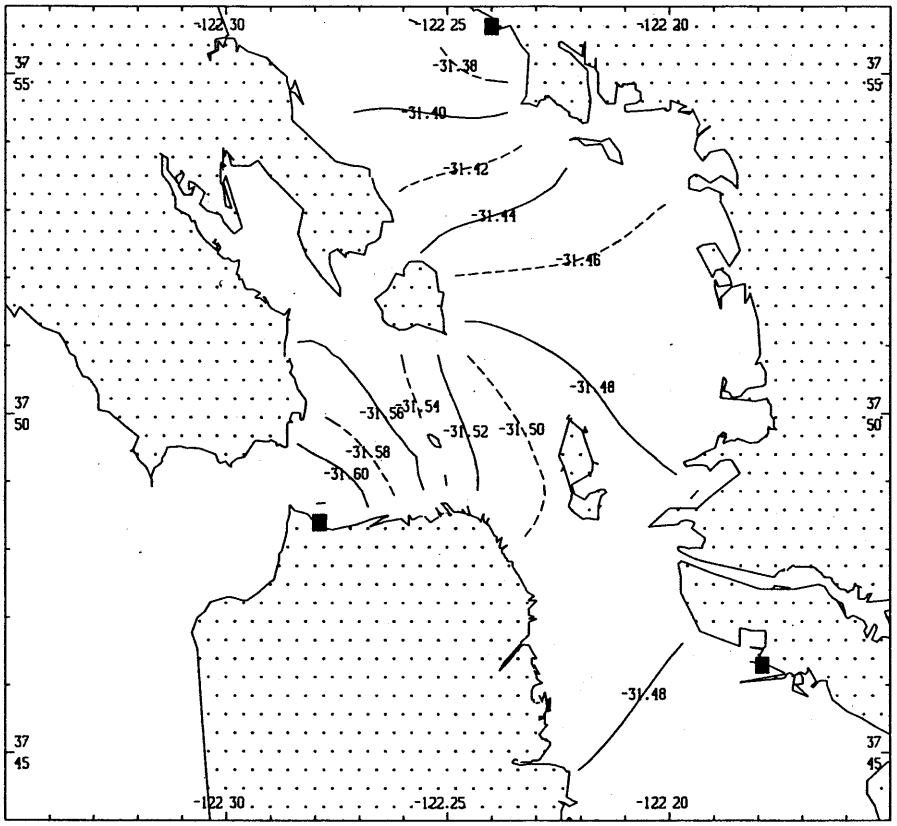

Figure 5.9. Distribution of ellipsoidally-referenced [NAD 83 (86)] MSL datum (m) computed with the TCARI method in central San Francisco Bay. The three locations where offset values are known are shown as filled squares. In the Bay, the values range from -31.63 m near the entrance to -31.36 m near the northern border of the plot. The contour interval is 2 cm.

5.7. Accuracy Tests

For the third test, TCARI-generated, ellipsoidally-referenced water levels were computed according to the methods described in Section 2.5 and compared to the measured values in San Francisco Bay. As in Galveston Bay, the long-term constituents were masked out. A total of 968 data values were available.

Benchmark Runs

Using the TCARI method and hourly water level data, the RMS error was 9.2 cm for the 939 points used (unused points lie outside the model grid). When the 6-minute observed water level time series

were used, the RMS error was 9.1 cm. The fact that there is very little difference when the hourly water levels were used is probably because the residual water levels are relatively small (see Figure 5.7). With the 6-minute data, the RMS error of 9.1 cm is slightly larger than for Galveston Bay (8.4 cm; see Table 4.3) because the tide range is larger (standard deviation of 16 cm for Galveston Bay and 55 cm for San Francisco Bay). A scatter plot of the results using the 6-minute data appears in Figure 5.10.

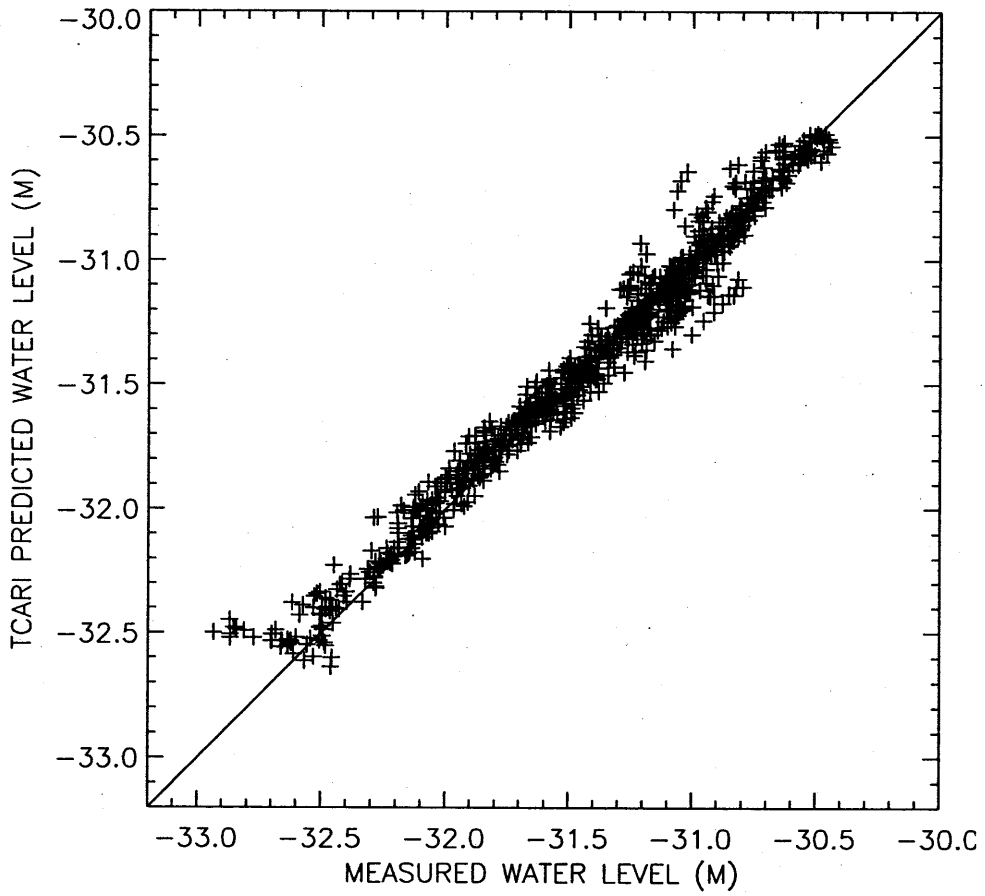

Figure 5.10. Scatter plot showing 939 ellipsoidally-referenced, measured water levels and the TCARI-predicted water levels for the same time and location. The correlation coefficient is 0.986.

Discrete Tide Zoning

An assessment of the discrete tide zoning method was also made. The tide zones for San Francisco Bay are shown in Figure 5.11. Zones in the bay south of the entrance are referenced to the water level gauge at San Francisco Presidio (941-4290), and zones north of the entrance are referenced to the Alameda gauge (941-4750). The RMS error for final zoning with 907 points was 10.1 cm, or about the same as for Galveston Bay. With the interpolated corrections (see Section 4.7), the RMS error was 9.8 cm.

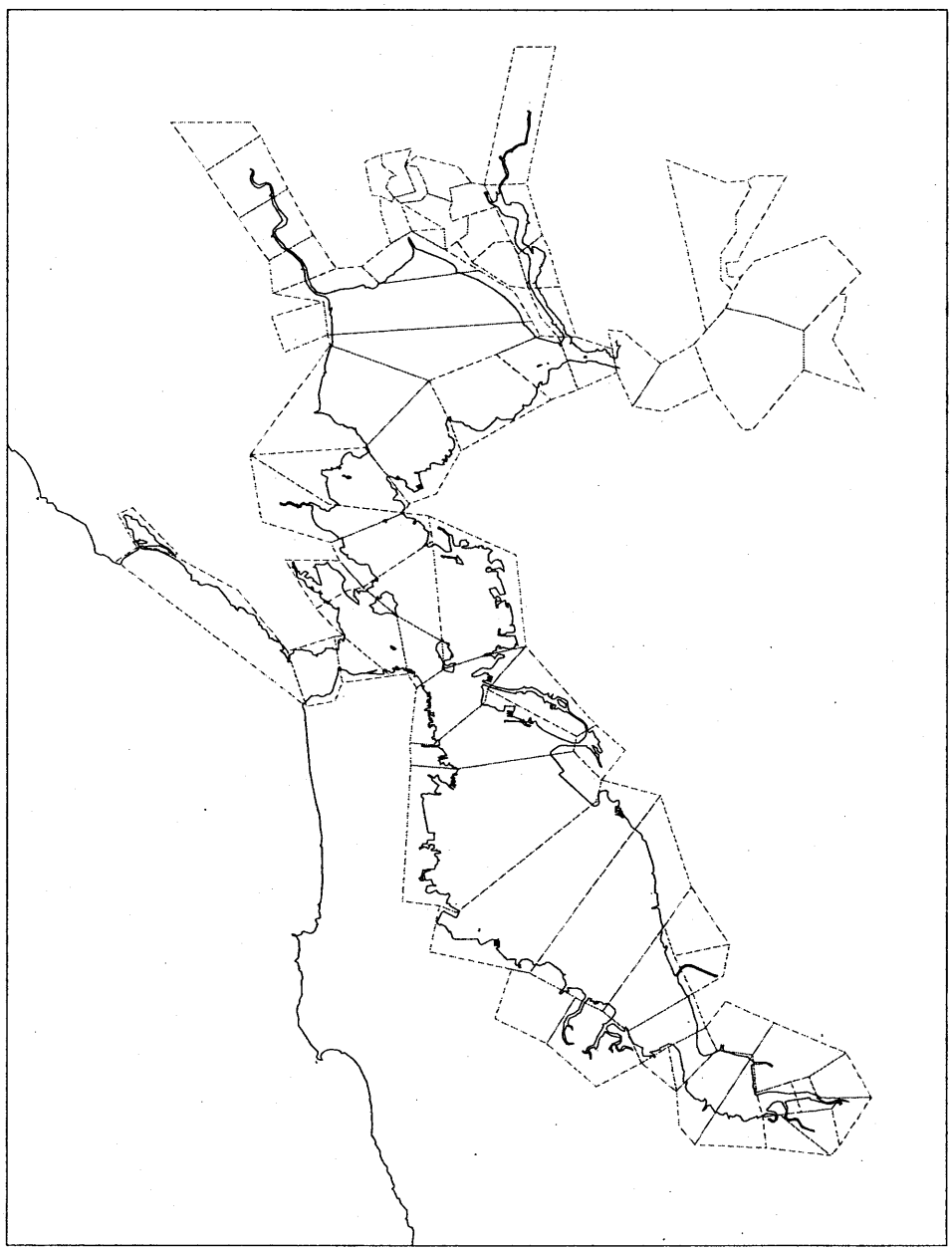

Figure 5.11. Tide zones (polygons bounded by dashed lines) for San Francisco Bay.

Comparison of TCARI and Tide Zoning

TCARI and discrete tide zoning were compared at locations where both estimates of water level were available. The results for all cases are shown in Table 5.1. TCARI has a lower RMS error and a lower maximum error than either tide zoning or interpolated tide zoning. RMS errors in the measurements (Huff, personal communication) were 6.8 cm, which probably establishes the lower bound on determining the accuracy of either method.

Table 5.1. Mean error, standard deviation, RMS error, and maximum value of the error (the predicted minus the measured) in water levels in San Francisco Bay (cm) for several methods of estimation as compared to the kinematic GPS measurements. WL is water levels. Results for tide zoning and TCARI are for 907 locations where both methods produced a value. GPS measurements vs. Gauge (Huff, personal communication) is an estimate of the error of the kinematic GPS water level when taken within a few km of an NOS water level gauge.

Method	Mean Error	Std. Dev.	RMS Error	Maximum Error
Tide Zoning	-0.4	10.1	10.1	46.7
Tide Zoning, Interpolated	-0.4	9.7	9.8	46.8
TCARI with Hourly WL	1.2	8.8	8.9	42.2
TCARI with 6-minute WL	1.4	8.6	8.8	41.5
GPS Measurements vs. Gauge	4.4	5.2	6.8	-

Summary

TCARI was used to estimate water levels for comparison to the kinematic GPS measurements of water levels in San Francisco Bay. The use of 6-minute observed water levels in generating the residual water levels gave only a modest improvement over the use of hourly data. This is because the tide range is large relative to the amplitude of the residual water levels. For the ship track locations where both estimates were available, the estimated water levels from TCARI had less RMS error (8.8 cm) than those from tide zoning (9.8 cm). The measured water levels had an estimated RMS error of 6.8 cm.

6. COMPUTER PROGRAMS

TCARI is implemented by the successive application of three Fortran programs, designated here as simply Program A (PA), Program B (PB), and Program C (PC).

The PA creates the numerical grid which will be used by PB to generate the weighting functions. PA reads in a control file that defines the grid limits in geographic coordinates and sizes, and a geography file that contains the digitized coastline data. The program then creates the grid, which is defined by an array of elements with a value 0 for land, a 1 for water, or 2 for ocean boundary. The control file contains both the input parameters and the names of the input and output files.

PB creates the weighting functions $g(x, y)$ and the offset functions $G(x, y)$ on the grid. The program reads the same control file that was read by PA, the grid, and the tide data and then creates the distributions. In general, the output files created by PA and PB are generated once for the area being surveyed, and need not be updated unless additional tidal stations are added.

PC creates the tide corrections along the ship track, and so is run after the survey data are collected. PC uses the data files generated by PA and PB, the tide data files, and the ship track file. PC has its own control file.

The program functions are explained in detail below.

6.1. PA: Grid Generation

The numerical solution requires a grid mesh with square cells representing land and water. This grid is generated by PA by reading the input values from the control file, following the steps in a process, and generating output files.

Input Data

The grid is generated from the following data:

- the grid window in latitude-longitude space,
- the digitized coastline (defined by a set of latitude-longitude pairs),
- the digitized ocean boundary (defined by a set of latitude-longitude pairs),
- the cell width (nmi),
- the latitude-longitude location of one water point, and
- the tide station locations

No bathymetric data are required.

The grid window is a rectangle in latitude-longitude space and it defines the limits of the grid. It is specified by the limits *lonmax, lonmin, latmax,* and *latmin*. The window is selected to (1) enclose the coastal area being surveyed, (2) be as small as possible to minimize computer time and storage requirements, and (3) minimize the crossing of water areas. For example, the grid window (shown as a dashed line) for the Galveston Bay region is plotted in Figure 6.1 along with the digitized coastline.

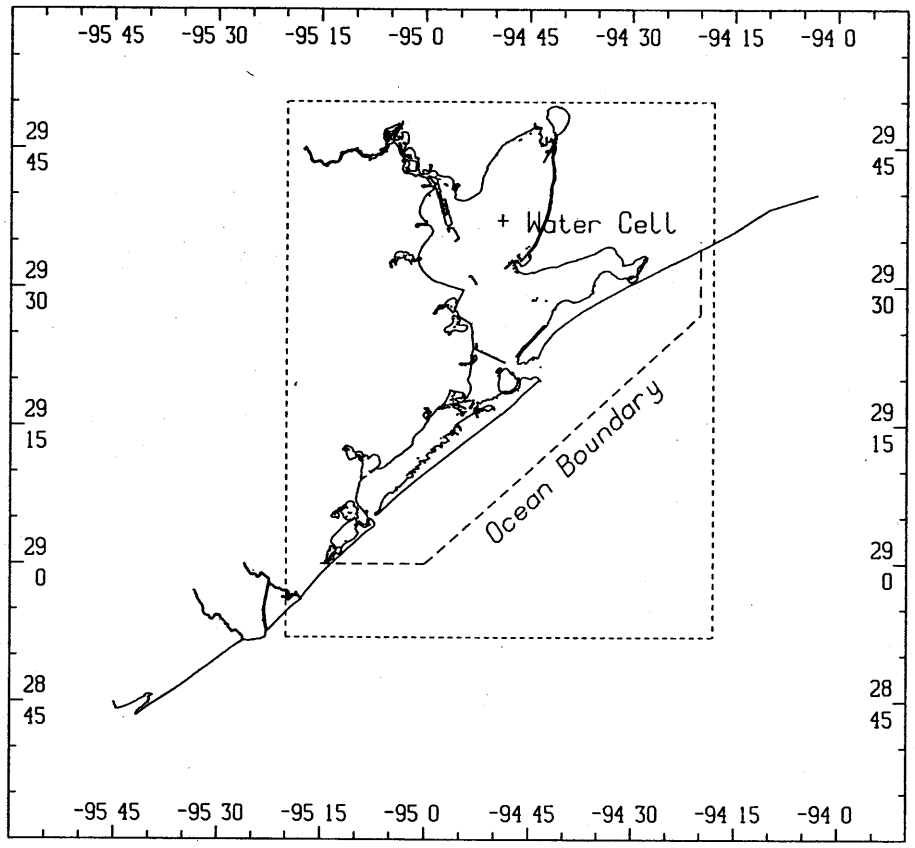

Figure 6.1. Galveston Bay region showing coastline data (solid lines), the grid window (dashed lines), the ocean boundary (dotted lines), and the location of the water cell. Note that, as required, the digitized coastline extends outside the grid window.

A digitized coastline file, such as used in plotting, is required. In this study the files are in ASCII format; each record contains a longitude, a latitude, and a pen up/down command. It is an important requirement that the coastline extend beyond the grid window.

The ocean boundary data determines the seaward extent of the grid. Because the grid window will often enclose a large portion of the coastal sea (which may have little useful data and may be outside the area to be surveyed), a way to exclude this area is needed. The removal is possible with the insertion of ocean boundaries, which are read from another digitized file.

The cell width specifies the resolution of the mesh in the region, and the location of a water cell is needed to start the solution. The area within the grid window and the ocean boundary lines are shown in Figure 6.1.

Finally, the locations of tide stations is required so they may be included in the grid.

The Process

The process for generating the grid proceeds as follows. The first step is the generation of the undifferentiated grid mesh using *wcell*. For a cell width, *wcell* (in nautical miles), a grid of undifferentiated (neither land nor water) cells is generated by dividing the width into *Imax* intervals and height into *Jmax* intervals, where

$$Imax = \frac{C_o}{wcell}(lonmax - lonmin)$$

$$Jmax = \frac{C_a}{wcell}(latmax - latmin) \tag{3.12}$$

where C_o and C_a convert degrees to nmi. Since *Imax* and *Jmax* are integer values, the division either of the width by *Imax* or the height by *Jmax* will result in actual cell widths that are slightly larger or smaller than *wcell*. Therefore, *wcell* should be considered a nominal value. This distortion is small (in the Galveston Bay and San Francisco Bay examples, it was less than 1%) when *Imax* and *Jmax* are large and is ignored in the numerical solution.

The next steps differentiate between land, water, and ocean boundary. Initially, all cells are given an Index equal to 0 (i.e., they are set to land). Then the land-water boundary in this grid is determined by checking all cells that (a) contain at least one point in the coastline data file, or (b) are intersected by a line drawn between points defining the coastline. These points are given an Index equal to 2. Then, the cells along the ocean boundaries are identified using the locations in the ocean boundary data file and interpolating; these cells are given an Index equal to 3.

Finally, the known water point is given an Index value of 1 (for water). Then, sweeping through the grid several times, all cells adjacent to a water cell (Index equals 1) which are not tagged as either land-water (Index equals 2) or ocean boundary (Index equals 3) are also set to a value of 1. At the end of all the sweeps, the unchanged cells remain as land. Then the land-water boundary cells (Index of 2) are set to land (Index equals 0), and the cells containing a tide station are set to water (Index equals 1).

Following the grid generation, two sets of checks are made. The first set of checks consists of determining the number of water cells that surround each tide station cell; an error flag appears if the number is zero (indicating a land-locked cell). The second set of checks consists of computing (a) the total number of land-locked tide gauge cells (which should be equal to zero), (b) the total number of coastline cells (which should be greater than zero), (c) the percentage of cells that are land (which

should be greater than 5% and less than 95%), and (d) the percentage of cells that are water (which should be greater than 5% and less than 95%). Another flag appears if any one of the above four values falls outside the acceptable range.

Running the Program

The program is run using a control file. The Unix command is

pa.x < gen.ctl

where gen.ctl is the input control file (see Figure 6.2). The output consists of a print file (which for Galveston Bay was a lengthy 53,000 lines) and the grid file. The control file contains the values of the necessary parameters *(latmax, latmin, lonmax, lonmin, wcell, latwat, lonwat, npmin, npsave)* and the names of the input files for the coastline data, the ocean boundary data, and the tide station location data. A sample of a coastline file is shown in Figure 6.3. The ocean boundary data file is shown in Figure 6.4.

```
9   Galveston Bay                                  Version, Title
 28 52.0  29 50.0  -95 20.0  -94 26.0              lat/lon window
 29 37.0 -94 48.0                                  lat/lon of water cell
0.35  .5e-4  0.90  1  10                           wcell, rerr, alfa, npsave, npmin
0 0 1   100                                        icon1,ires1,ioff,komega
/dir2/khess/Zone/Galv/Data/galv_sta.3.dat          Station data locations
/dir2/khess/Zone/Galv/Data/txshore.dat             Coastline data file
/dir2/khess/Zone/Galv/Data/oceanbnd.dat            Ocean Boundary data file
/dir2/khess/Zone/Galv/C/galv_grid.02               Grid file
/dir2/khess/Zone/Galv/C/galv_gc.02                 Con g file
/dir2/khess/Zone/Galv/C/galv_gr.02                 Residual
/dir2/khess/Zone/Galv/C/galv_go.01              Offset   (MSL   -   MLLW)
/dir2/khess/Zone/Galv/C/galv_ge.01                 Datum (MSL in ellipsoid ref)
0  95 153 100                                      mpr, print cell i, j, kstart
0  1  2  3  5  10 20  30  50 100 250  500          kpr, new kprnt
5 62 71 1  76 84 1  77 84 1  32 38 1 33 38 1 nedit, cell i, j, ifield
-------------------------------------------------------------------------------
wcell            cell width (nautical miles)
rerr             relative error
alfa             land boundary condition parameter
npsave           in coastline file, save every npsave
npmin            ", min number of for islands

icon1            1=generate gc, 0=do not
ires1            1=generate gr, 0=do not
ioff             1=generate gh, 0=do not
komega           keep omega constant (=1.5) until 'komega' iterations

mpr              number of i&js,
kpr
nedit            number of cells to be edited
```

Figure 6.2. Control file used to provide input to Program A and Program B as applied to Galveston Bay. Only data above the dashed line is read.

```
29.666666  -94.050000    1
29.640000  -94.166666    0
29.600155  -94.250023    0
29.592909  -94.269661    0
29.572519  -94.320297    0
29.567987  -94.334770    0
29.555073  -94.366287    0
29.538074  -94.415382    0
29.507248  -94.495209    0
29.506336  -94.500244    1
29.552580  -94.467934    1
29.552580  -94.470261    0
29.550766  -94.471809    0
29.551447  -94.472588    0
29.550537  -94.472839    0
29.549862  -94.471802    0
29.548500  -94.471283    0
29.551220  -94.468445    0
29.552580  -94.467934    1
```

Figure 6.3. Typical records from a coastline file. Data in each record are latitude, longitude (both in decimal degrees), and a pen index. An index of 1 denotes the start or end of a line segment.

```
29.00000  -95.25000   1
29.00000  -95.00000   0
29.45000  -94.33333   0
29.58333  -94.33333   1
```

Figure 6.4. All records from the ocean boundary file for Galveston Bay. Data in each record are latitude, longitude (both in decimal degrees), and a pen index. An index of 1 denotes the start of end of a line segment.

The tide station data for Galveston Bay (Figure 6.5) contains, among other things, the 7-digit NOS station number, the latitude (degrees, minutes), and the longitude (degrees, minutes) of each station.

```
4   14 Galveston Bay Tide Stations.
8770559 29 44.3  -94 42.4   1 1   0.213  -29.014  Round pt.
8771450 29 18.8  -94 47.2   1 1   0.253  -28.525  Pier 21 (in narrow channel)
8771510 29 17.2  -94 47.4   1 1   0.366  -28.537  Pleasure Pier
8771624 29 18.93 -94 36.56  1 0  99.      99.00   GPS buoy (est position)
8771328 29 21.8  -94 46.7   1 1   0.214  -28.624  Port Bolivar
8770971 29 31.1  -94 30.8   1 0   0.213  -28.725  Rollover  (lat was 29 30.9)
8771013 29 29.9  -94 54.7   1 1   0.174  -28.775  Eagle pt.
8771021 29 31.13 -94 51.25  1 1   0.177   99.00   Trinity Ri Chan (est posit)
8770923 29 32.9  -94 22.2   1 0   0.366   99.00   High Island
8770931 29 32.1  -94 47.20  1 1   0.195  -28.845  Smith Pt. (lon was -94 46.9)
8770613 29 40.5  -94 58.9   1 1   0.198  -29.053  Morgans pt. (new position)
8770625 29 40.8  -94 52.0   1 0  99.      99.00   Umbrella point
8771481 29 17.7  -94 54.3   1 0  99.      99.00   Tiki Is  (lat was 29 18.0)
8771801 29 10.0  -95 07.7   1 1   0.092   99.00   Alligator pt
0000000 00 00.0   00 00.0   0 0  00.0     00.00   << end delimiter
```

Figure 6.5. The Station file, showing tide station locations and other data for Galveston Bay. Following the header line, the data includes the 7-digit NOS station number, the latitude (degrees, minutes), the longitude (degrees, minutes), the indices icon and ires which denote whether data for tidal constituents or a residual water level are available, the offset (m) of MSL relative to MLLW (m), the offset (m) of MSL relative to the WGS-84 ellipsoid, and the station name. For the offsets, a value of 99 denotes a missing value.

The Output Files

Beside the screen print file, only one output file is created: the grid file. The file contains a header line with several grid parameters and is followed by records containing the cell row number and cell indices (3=ocean boundary, 1=water, 0=land). A sample appears in Figure 6.6. The header line contains the grid array limits (*Imax, Jmax*), the number of columns of data in each of the following records (*ncol*), and the latitude and longitude limits *(latmax, latmin, lonmax, lonmin*). The grid file is used by Program B to generate the weighting and offset functions.

6.2. PB: Weighting Function Calculation

Following the generation of the grid as described in the previous section, Program B generates the set of functions *g* that are required for the interpolation. The data and the *g* functions for the following are generated:

- Tidal Constituent Stations — *gc(i, j, m)*
- Residual Water Level Stations — *gr(i, j, m)*
- The Offset of MSL from MLLW — *go(i, j)*
- The Datum of MSL referenced to the ellipsoid — *ge(i ,j)*

```
134  162 60 28.86667 29.83333  -95.33334  -94.43333 i,jmax,nperl,0=land
162 000000000000000000000000000000000000000000000000000000000000
161 000000000000000000000000000000000000000000000000000000000000
160 000000000000000000000000000000000000000000000000000000000000
159 000000000000000000000000000000000000000000000000000000000000
158 000000000000000000000000000000000000000000000000000000000000
157 000000000000000000000000000000000000000000000000000000000000
156 000000000000000000000000001110000000000000000000000000000000
155 000000000000000000000000111111000000000000000000000000000000
154 000000000000000000000011111110000000000000000000000000000000
153 000000000000000000001111111111000000000000000000000000000000
152 000000000000000000111111111111100000000000000000000000000000
151 000000000000000001111111111111110000000000000000000000000000
150 000000000000000011111111111111111000000000000000000000000000
149 000000000000000111111111111111111100000000000000000000000000
148 000000000000001111111111111111111110000000000000000000000000
147 000000000000011111111111111111111111000000000000000000000000
146 000000000000111111111111111111111111100000000000000000000000
145 000000000000111111111111111111111111100000000000000000000000
144 000000000001111111111111111111111111100000000000000000000000
143 000000000001111111111111111111111111100000000000000000000000
142 000000000011111111111111111111111111100000000000000000000000
141 000000000011111111111111111111111111100000000000000000000000
140 000000000011111111111111111111111111100000000000000000000000
```

Figure 6.6. Sample portion of a grid file. The file contains a header line with several grid parameters, and is followed by records containing the cell row number and cell indices (0=land, 1=water, 3=ocean boundary). The header line contains the grid array limits (*Imax, Jmax*), the number of columns of data in each of the following records (*ncol*), and the latitude and longitude limits (*latmax, latmin, lonmax, lonmin*).

For each group, there is either a two-dimensional function or a three-dimensional function. The first two sets typically have three-dimensional *g* functions, representing at cell *i, j* a value of the weighting function for each individual tide station location, *m*. The second two sets have only a two-dimensional g function, which represents the offset value at each cell *i, j*.

Input Data

The program requires the following data, which are read in from the control file, gen.ctl (see Figure 6.2); relative error (ε), boundary condition factor (α), indices for the groups to be addressed (*icon1, ires1, ioff*), and an iteration parameter (*komega*). There are also print output control parameters.

The Process

For the three-dimensional *g* files, the process is as follows. First, the specific type of data (tidal constituents or residual water levels) is selected. Then one particular station location is selected. Next, all the water cells are given a flag; locations up to one cell away from all the tide stations in the group are given a special flag. Flags include -3 for land, -2 for ocean boundary, -1 for the tide stations, 0 for an interior water cell, 1 through 6 for various types of land-water boundary cells.

Then the numerical solution for g is computed by iteration. At the start of the iteration, the value of g at the selected station (and its adjacent cells tagged as a -1) are set to 100% (G^o_{max}), and the values at all other stations (and their adjacent cells) are set to 0% (G^o_{min}). Iteration begins at step k=1 and continues until (1) the convergence condition in Eqn. 6.1 is met,

$$\max\left|g_{i,j}^{k} - g_{i,j}^{k-1}\right| \le \varepsilon (G^o_{\max} - G^o_{\min}) \tag{6.1}$$

(2) k equals 15,000, or (3) the maximum difference gets too large

$$\max\left|g_{i,j}^{k} - g_{i,j}^{k-1}\right| > 4(G^o_{\max} - G^o_{\min}) \tag{6.2}$$

The iteration sequence depends on ω_k. For k less than or equal to *komega*, $\omega_k = 1$. Otherwise,

$$\omega_k = \frac{1}{1 - \frac{1}{4}\rho^2 \omega_{k-1}}$$

$$\rho = \tfrac{1}{2}[\cos(\frac{\pi}{Imax}) + \cos(\frac{\pi}{Jmax})] \tag{6.3}$$

However, if $k > komega$ and the maximum difference at step k exceed the maximum difference at step k - km (where km = 20), then ω_k is reset to 1.

Once the g field for that station has been computed and saved, the next tide station is selected and its g field is computed. This process is repeated until all stations in the group have been selected. Then the values for all functions in the group are written to the output file.

Then the numerical solution for the two-dimensional g functions is computed in a similar way. However, at the start of the iteration, the value of g at each tide station (and its adjacent cells which are tagged as a -1) are set to the value of the offset.

Output Files

Beside the print file, there are four output files, one each for: the weighting functions for tidal constituents (gc.out), the weighting functions for residual water levels (gr.out), the offset for MSL relative to MLLW (go.out), and the datum of MSL relative to the ellipsoid (ge.out).

Each file has the following format. The first line contains a brief text description. The second line contains grid array limits and latitude-longitude limits. The third line contains information on the water level stations used. The fourth and all succeeding lines contain, for a particular water cell, the indices, latitude, longitude, and numerical values for each weighting function. A sample output file is shown in Figure 6.7.

```
PB:   Galveston Bay w/ocean bnds.                    Version, Title
134 165  1 0.500E-02  28.86667  29.83333  -95.33334  -94.43333 0.90
        1        15        15   8770559   8771450   8771510   8771624
  8771328   8770971   8771013   8771021   8770931   8770613   8770625
  8771481   8771801   8772001   8772002
  15  19 1   28.97504997  -95.23594666   0.00000   0.00000   0.00000   0.00000
 0.00000   0.00000   0.00000   0.00000   0.00000   0.00000   0.00000   0.00000
 0.00000  100.00000   0.00000
  19  23 3   28.99848557  -95.20908356   0.00000   0.00000   0.00000   0.00000
 0.00119   0.00002   0.00002   0.00004   0.00002   0.00000   0.00000   6.55683
90.84222    0.60445   0.16547
  19  24 1   29.00434303  -95.20908356   0.00000   0.00000   0.00000   0.00000
 0.00118   0.00002   0.00002   0.00004   0.00002   0.00000   0.00000   6.55441
90.84204    0.60685   0.16547
  20  23 3   28.99848557  -95.20236206   0.00000   0.00000   0.00000   0.00000
 0.00118   0.00002   0.00002   0.00004   0.00002   0.00000   0.00000   6.55269
90.84083    0.60857   0.14714
  20  24 1   29.00434303  -95.20236206   0.00000   0.00000   0.00000   0.00000
 0.00117   0.00002   0.00002   0.00004   0.00002   0.00000   0.00000   6.55025
90.84016    0.61099   0.14714
```

Figure 6.7. Sample portion of the *g* field file. The first line contains a brief text description. The next line contains grid array dimensions (*Imax, Jmax*), and latitude-longitude limits *(latmax, latmin, lonmax, lonmin*), and the value of alpha used. The third line contains information on the water level stations used. Each data record contains, for a particular water cell, the indices, latitude, longitude, and numerical values for each weighting function.

6.3. PC: Calculation of the Tide Correction

Given a data file containing a ship's time and position, Program C uses the previously-derived weighting functions plus any contemporary observations of water levels to compute the tide correction for the time and place of the ship's observation. Program C also has the capability of generating a water level referenced to the ellipsoid that can be used for comparison with measurements.

Input Data

The input data required is as follows:

- Time and height units
- Local time reference (hours)
- Weighting function and offset files (see Section 6.2)
- Tidal constituent (amplitudes and phases) data
- Equilibrium argument and lunar node file
- Time series file of total water levels
- Ship time and position

The time and height units determine whether the tide correction output should be in Greenwich Mean Time (GMT) or Local Standard Time (LST) (*itime* =1 or 2, respectively), and whether the tide correction should be in meters or feet (*imetr* = 1 or 2, respectively). The local time reference is the

number of hours that is added to GMT to get LST; for Galveston Bay it is -6 hours and for San Francisco Bay it is -8 hours.

The tidal constituent data (Figure 6.8) is provided for all stations, and the file containing the equilibrium arguments and lunar node factor for 37 constituents (Figure 6.9). A sample of the residual tide series name file is shown in Figure 6.10. The tide series files themselves have records containing the year, the day of the year (for example, a value of 1.500 corresponds to noon on January 1), and the water level value (relative to MSL).

```
677-1510 Galveston, Pleasure Pier, Texas  T.M. 90 W.
    0.      94.8   0.     0 (= a, b, tlon, iunit (0=ft,1=meter,2=cm)x1000)
    0.      94.8   0.          (tlon= time meridian: 0=Greenwich, -90=local)
1510   1  4402748  1002730  1062571  551 287  0192008  507 207  0042337
1510   2  003  74  002 104  0081563  0212513  0022573  0151812  0252240
1510   3  024 705  0043385  0433295  043 417  034  91  1032652  365 571
1510   4  2591718  0883017  0102011  026 180  112  48  0142984  0072012
1510   5  005 435  162 251  003 282  005 434  0153186  0033423  0152734
1510   6  002 693  0122383
```

Figure 6.8. Tidal constituent data for a single station in a NOS standard format.

```
1995 0 11032 1821000   010323464 905 1561065 364 84535971099 546 934 338   1   1
1995 0 21000   01065  461032 6701000   01032 35310323147 566217210321494   1   1
1995 0 310001800 792  48 864 5021111 31810002004100028021032341 8 6911987   1   1
1995 0 4 845 486 84532801000  2710001773 845296210003498103234181048207 3   1   1
1995 0 512102293 964 208 78421031134 7281032 182 713  971032 284 872 673   1   1
1995 0 6 8453399 845   31065 3181065  46 8453496 8092285106533291289234 0   1   1
1995 0 712892657 8091921 6543358 979 979 634 788 8351179 654 924 8453597   1   1
1995 0 8 905 156 8723462 8092285103234641289265710 99 5461249247510653329   1   1
1995 0 912102293 899  44 899 361 964 520 934 338 73224411065 2621099 648   1   1
1995 010 964 2021032 1821099 2281065  461065 36413302204109935111249247 5   1   1
1995 01112892657 8092285133025221330283 9 8352467 928 226 995  66 899 361   1   1
1995 012 68322821099 2281099 5461065 3641134  931134 4101289265713733021   1   1
1995 01313302839 8612649 83524671027 2481027 5661027 884 995 7021171 592   1   1
1995 0141171 9101134 4101134 728133028391099 5461027 8841171 5921171 910   1   1
1995 015137330211134 728100035251000  7510002105 8723296 782 658 7133277   1   1
1995 016 964 208 7842103 692 314 6453439   0   0   0   0   0   0   0   0   1   1
1996 1 1103711831000   010373578 886 12210752366 812104811153548 9181305   1   1
```

Figure 6.9. A portion of the equilibrium arguments and lunar node factors file.

```
Residual wl station file names (10) for Galveston Bay. jtime:1=GMT,2=local
8770559  1  /dir2/khess/Zone/Galv/Data/Tides/8770559.ut
8770931  1  /dir2/khess/Zone/Galv/Data/Tides/8770931.ut
8771021  1  /dir2/khess/Zone/Galv/Data/Tides/8771021.ut
8771450  1  /dir2/khess/Zone/Galv/Data/Tides/8771450.ut
8771624  1  /dir2/khess/Zone/Galv/Data/Tides/8771624.ut
8770613  1  /dir2/khess/Zone/Galv/Data/Tides/8770613.ut
8771013  1  /dir2/khess/Zone/Galv/Data/Tides/8771013.ut
8771328  1  /dir2/khess/Zone/Galv/Data/Tides/8771328.ut
8771510  1  /dir2/khess/Zone/Galv/Data/Tides/8771510.ut
8771801  1  /dir2/khess/Zone/Galv/Data/Tides/8771801.ut
```

Figure 6.10. File with the residual file names.

The Process

The program is run using a control file (trak.ctl) to provide input as follows.

pc.x < trak.ctl

A sample of the control file trak.ctl is shown in Figure 6.11.

```
4   Input file for pc. NEW offset file
1   -6    1                                        itime,ihrref,imetr
1    0    1    88      10000        itcari,iskip,icallp,icallp2,icallmx
/dir2/khess/Zone/Galv/C/galv_gc.02                 Weighting for Constituents
/dir2/khess/Zone/Galv/C/galv_gr.02                 Weighting for Residual
/dir2/khess/Zone/Galv/C/galv_go.02                 Offset of MSL from MLLW
/dir2/khess/Zone/Galv/C/galv_ge.02                 Datum of MSL from Ellipsoid
/dir2/khess/Zone/Galv/Data/constit19.dat           Tidal Constituent File
/dir2/khess/Zone/Galv/Data/yyy.dat                 Tidal Constants File
/dir2/khess/Zone/Galv/Data/resid10a.dat            6-min Residual File Names
/dir2/khess/Zone/Galv/Data/resid10.dat             Hrly Residual File Names
/dir2/khess/Zone/Galv/Data/ship_gps.dat            Ship Track File
0 0                                                Time and Space Windows
-------------------------------------------------------------------------
itime   :      convert all times to 1=Greenwich, 2=local
ihrref  :      local time (hrs) in relation to Greenwich
imetr   :      1=all data converted to meters, 2=feet
itcari  :      1=full TCARI, 2=interpolate the total signal, 3=TCARI w/resid=0
iskip   :      skip over the first 'iskip' records in track file
icallp  :      print for icall LE icallp
icallp2 :      print for icall = icallp2
icallmx :      iterations will stop if 'icall' reaches icallmx
-------------------------------------------------------------------------
```

Figure 6.11. Control file for Program C.

After the files are opened and read in, a check for consistency of stations is made. Using the stations in the weighting functions for constituents file, a check of the stations numbers in the constituent data file (Figure 6.8) is made to insure sufficient data are available. Similarly, using the stations in the weighting functions for residuals, a check of the stations numbers in the residual names (Figure 6.7) and the residual data file is made. Also, since a tide prediction is needed to compute the residual, a check of the stations numbers in the constituent data file is made.

Next, the ship trackline file is read. Each record of the file contains the year (four digits), day in the year, latitude, and longitude. The day in the year is computed so that noon on January 1 has a value of 1.500. Using the year value, the astronomical constants (equilibrium phases and lunar node factors) are set.

Then the tide is computed. Using the weighting functions and data from the tide stations, the tidal constituent amplitudes and phases are computed for the four closest cells; then these are interpolated bi-linearly to produce amplitude and phase values at the precise location of the ship. Then the tide at the ship is computed by creating and summing the constituents.

The residual water level is computed. First the residual at each tide station is computed by subtracting the predicted tide from the observed tide. Then, using the weighting functions and the residual from the tide stations, the residuals at the four closest cells is computed; then these are interpolated bi-linearly to produce the residual water level at the precise location of the ship.

Then the offset and datum are computed. Values at the four closest cells are interpolated bi-linearly to produce the offset and datum at the precise location of the ship.

Finally, the tide correction and the estimated water level relative to the ellipsoid are computed and saved to an output file.

The Output Files

Besides the screen print file, two output files are created. The first is used for processing soundings and contains the ship's time and location, followed by the tide correction, and the estimated water level relative to the ellipsoid (Figure 6.12). The second is used for analysis and contains, in addition to the data in the first file, the tide, the residual, and the two offsets.

```
1995 164.59166  -94.9084   29.4977    0.1498  -28.7992
1995 164.59584  -94.9089   29.4984    0.1537  -28.7953
1995 164.72084  -94.7012   29.7291    0.5500  -28.6731
1995 164.72501  -94.7026   29.7275    0.5483  -28.6712
1995 164.72917  -94.7098   29.7190    0.5362  -28.6660
1995 164.73334  -94.7191   29.7083    0.5253  -28.6610
1995 164.73750  -94.7282   29.6978    0.5167  -28.6564
1995 164.74167  -94.7376   29.6869    0.5091  -28.6519
1995 164.74583  -94.7471   29.6758    0.5024  -28.6473
1995 164.75000  -94.7516   29.6706    0.5003  -28.6443
1995 164.75417  -94.7582   29.6630    0.4958  -28.6416
1995 164.75833  -94.7680   29.6516    0.4893  -28.6377
```

Figure 6.12. Sample of the Program C output file. Each record contains the year (four digits), day in year, longitude (degrees), latitude (degrees), tide correction (meters), and the estimated water level relative to the ellipsoid (meters).

7. SUMMARY AND CONCLUSIONS

7.1. Summary

The National Ocean Service's hydrographic survey data are processed to give water depth at the point of the measurement. To produce a depth relative to Mean Lower Low Water (MLLW), which is the chart datum, the measured depth must be corrected to account for the departure of the instantaneous water level from MLLW. This departure is due primarily to the astronomic tides, river flows, water density effects, and meteorological influences. At present, discrete tide zoning is used to provide this correction. Discrete tide zoning rests on the simplifying assumption that the water level in an entire zone has a fixed magnitude and phase relationship to the measured water level at a single nearby gauge. However, this method is difficult to apply because selection of zones is somewhat subjective, the method has known inaccuracies in its assumptions about how tides vary, it produces a discontinuity when crossing from one zone to the next, and the data it produces is not referenced to the GPS ellipsoid.

A new method, Tidal Constituent And Residual Interpolation (TCARI), has been developed to estimate the tide corrections for bathymetric data. TCARI separately interpolates:

- each tidal constituent's amplitude and epoch (phase) value,
- the residual, or non-tidal, water level,
- the Mean Sea Level (MSL) offset, which is the difference between local MSL and MLLW, and
- the MSL datum, which is the difference between MSL and the ellipsoid

This method has the advantages that it treats the astronomical tide and the residual water level separately, it eliminates the mismatch when moving between discrete zones, and it can be used in an ellipsoidal reference system. However, TCARI requires significant computer resources to generate the weighting functions, its accuracy is dependent on the existence of tide data at many locations in the survey area, and it does not alleviate the need for contemporary tide measurements.

The spatial interpolation at the core of this method is carried out by the use of a set of weighting functions that quantify the local contribution from each of the shore gauges. The weighting functions themselves are generated numerically by solving Laplace's Equation (LE) on a grid.
The LE approach provides a spatially-smooth solution that exactly matches the observations. There are four sets of weighting functions, one set each for each of the quantities in the above list of bullets. The LE is:

$$\frac{\partial^2 G}{\partial x^2} + \frac{\partial^2 G}{\partial y^2} = 0 \tag{7.1}$$

The variable G can be tidal constituent amplitude, constituent epoch, or an offset. The grid on which the LE is solved is generated rather easily from a digitized coastline file, and does not contain any depth information. The solution is by the method of successive over-relaxation (SOR), with convergence being defined as the acceptably small difference between solutions between iterations. Using the tide and water level data and the weighting functions, TCARI generates a tide correction for

the time of the depth measurement at the four cells in the grid that are closest to the location of the ship. The final correction is interpolated to the precise location of the ship.

TCARI's specific data needs to produce tide corrections for traditional surveys include (1) a digitized coastline file for the area, (2) tidal constituent amplitudes and epochs, the MSL-to-MLLW offset, and the ellipsoidally-referenced MSL datum at all water level gauge locations near the survey area, and (3) observations of total water level at gauges for the time of the survey. These are sufficient for producing the set of weighting functions relevant to the suite of water level gauges and, with (4) a ship trackline file, the corrections for the time of the survey. For shipboard processing of data in near-real-time (NRT), NRT water level observations are needed. The weighting functions can be generated before the survey and need not be updated. For a ellipsoidally-referenced survey that includes GPS measurements of the distance from the ellipsoid to the sea bottom, (5) the ellipsoid-to-MLLW offsets at locations near the survey area are needed.

Three Fortran computer programs were written to implement TCARI. The first, Program A,reads a digitized coastline file and generates the grid. Cells in the grid can be selectively added or removed to better represent the coastal region. The second. Program B,reads the grid and generates the weighting functions. This program requires the longest time to run and it produces the files containing the weighting functions. The third, Program C, reads the ship track file and generates the corrections as well as additional output that can be used for statistical analysis.

Initial tests of TCARI were carried out on a simple, semi- rectangular region (maximum height of the area of 30 nmi, maximum width of the area of 30 nmi, and a cell size of 0.50 nmi). Convergence of the solution is not guaranteed, but is somewhat dependent on geometry. The program was optimized for convergence, with the additional capability to force convergence (if necessary) by adjusting the SOR weighting factor and the convergence criteria. The solution was extremely sensitive to the value of the boundary parameter, α (see Eqn. 3.7). A small value (α=0) gave rise to a distribution similar to the temperature distribution with an insulated boundary, and a large value (α=1) gave a solution in which the contours were nearly parallel lines. The second solution was judged to be representative of co-tide and co-phase lines in nature. Errors in the numerical solution under the test case (rotation of the region by 45 degrees) with two input locations were about 5% of the maximum, or about 5 degrees in phase. Maximum errors occurred near the center of the computational region. It was determined that more accurate distributions of phase angles could be produced if the sine and cosine of the phase angle were interpolated separately, then combined by the arctangent to create the final distribution.

Further sensitivity testing and calibration of TCARI's solutions were made using the kinematic GPS water level data obtained in Galveston Bay. For the benchmark run, which used hourly water levels observations, the mean error was 0.01 cm, the RMS error was 9.7 cm, and the maximum error was 27.1 cm (there were four instances of errors 20 cm or greater). Out of 618 observed values, 557 were used in the comparisons; values not used fell on grid land cells. Many of the unused observations were in the Galveston Channel leading to Pier 21 and around the Port Bolivar gauge, and geographic features near these gauges were not included in the grid, which had a cell-size of 0.35 nmi. The value of α, which determines the land boundary condition, was selected to produce the best fit (visually) to contours of the M_2 epoch produced by the numerical model, especially in the lower bay near the entrance. Sensitivity tests were made on the following (nominal values appear in parentheses): the grid size, *wcell* (0.35 nmi); the boundary slope condition coefficient, α(0.9); the coastline index (0);

and the error ratio, ε (5×10^{-5}). The coastline index sets the coastline cells to either 0 for land or 1 for water. Results were not overly sensitive to changes in any of the above parameters. Errors for predictions of water levels near the GPS buoy (877-1624) averaged about -13 cm and were due mainly to the fact that the ellipsoidally-referenced MSL was not available (we can infer an value of -28.44 from the data). Finally, because of the lack of reliability in the values of the amplitude and epoch of the long-period constituents (Mm, Mf, Msf, Ssa, and Sa), these constituents were masked out in the calculation of the astronomical tides; the net effect was to shift them to the residual water levels.

In the application to Galveston Bay (cell size of 0.35 nmi), TCARI reproduced the measured water levels with a mean error of 0.4 cm, an RMS error of 8.4 cm, and a maximum error of 24.6 cm. The estimated RMS error on the kinematic GPS measurements ranges from 4.7 cm (light wave conditions and no forward ship motion) to 9.1 cm (all wave conditions and ship speeds up to 15 m/s). The use of 6-minute water levels produced a large improvement over the use of hourly water levels, probably because wind effects are large due to the shallowness of the bay.

In the application to San Francisco Bay (cell size of 0.25 nmi), TCARI reproduced the measured water levels with a mean error of 1.4 cm, an RMS error of 8.7 cm, and a maximum error of 41.5 cm. The grid cell size was 0.25 nmi, and of the 968 measurements, 939 were used. The use of 6-minute water levels produced only a small improvement over the use of hourly water levels, probably because wind effects are small due to the deepness of the bay.

7.2. Major Results

Major sources of error in TCARI appear to be (1) numerical interpolation errors in regions far from the input data of as much as 5 degrees in phase and 5% in amplitude, (2) the lack of tide data for locations not adjacent to land, (3) poorly-known constituent values at the gauges, and (4) the lack of water depth in determining the distributions.

TCARI and discrete tide zoning were compared, and TCARI had a lower error. A direct comparison of the tide corrections with the measured water levels is not possible because tide zoning does not provide a distribution of the MLLW field relative to the ellipsoid. However, TCARI does. Therefore, an estimate of the ellipsoidally-referenced water level which incorporates the tide-zoned correction and the TCARI-generated offsets was computed. Three sets of zoning methods were used: preliminary zoning, final zoning, and spatially-interpolated final zoning. Preliminary zoning for Galveston Bay is referenced to one gauge: Pleasure Pier (877-1510). Final zoning added references to four additional gauges: Port Bolivar (877-1326), Morgans Point (877-0613), Trinity River Channel (877-1021), and Pleasure Pier (877-1510). However, because of tide zoning station priorities, data from Pleasure Pier was not used in the final zoning. In spatially-interpolated tide zoning, the interpolated value is the weighted mean of the original correction and the corrections in adjacent zones. The weights are equal to the fraction of the area of a circle that lies in the respective zones; the circle has an origin at the center of area of the original zone and has a radius equal to the area of the zone divided by its perimeter. The results are summarized in the following table.

Table 7.1. Comparison of RMS errors (cm) in tide zoning and TCARI in estimating the post-processed water level data. NA means not applicable.

Method	Galveston Bay	San Francisco Bay
Tide Zoning, Preliminary	9.2	NA
Tide Zoning, Final	9.4	10.1
Tide Zoning, Interpolated	9.2	9.8
TCARI	7.5	8.7

TCARI was compared to numerical modeling, and TCARI had a lower error. The numerical model for Galveston Bay (Appendix C) was used to generate water levels for comparison with the kinematic GPS measurements. The model was run for the month of June 1995 and included tidal, density, and meteorological forcing. At each water level gauge the ellipsoidally-referenced MSL was computed as the monthly mean of the ellipsoidally-referenced observed water level minus the monthly mean of the modeled water level. An ellipsoidally-referenced MSL field (assumed here to be equivalent to the Mean Tide Level) was generated by weighting the values of the ellipsoidally-referenced MSL at the water level gauges. The weight at each cell for each gauge was the inverse distance to the gauge, normalized by the sum of the inverse distances to all gauges. The ellipsoidally-referenced instantaneous water level was then computed as the sum the instantaneous modeled water level and ellipsoidally-referenced MSL. Comparisons were made at 470 locations, and were stratified based on distance from the nearest water level gauge and the speed of the ship. The RMS difference was 15 cm, and there was no appreciable dependency on distance or speed. The TCARI RMS error for the June measurements which fell within both the TCARI and numerical model grid was 8.3 cm.

7.3. Production of Ellipsoidally-Referenced MLLW Fields

TCARI can be used to generate ellipsoidally-referenced MLLW fields, H_L (see Figure 1.1). The existing software generates the ellipsoidally-referenced MSL field (H_E) and the MSL-to-MLLW offset field (H_O). The new field can be generated by the difference in the two fields:

$$H_L = H_E - H_O \tag{7.2}$$

A second approach to generating H_L would be to subtract the H_O value from the H_E value at each station where both values exist, then create a MLLW field directly from the values at the stations. In either case, it is desirable to have both values at all stations. The fields for Galveston Bay and San Francisco Bay computed by the first method are shown below. Recall that in Galveston Bay, 7 stations have H_E values and 11 stations have H_O values. In San Francisco Bay, there are only three stations (all in the central bay) that have H_E values, and 37 stations have H_O values. Therefore, outside the central bay all the variation shown in the figure is due to variations in H_O.

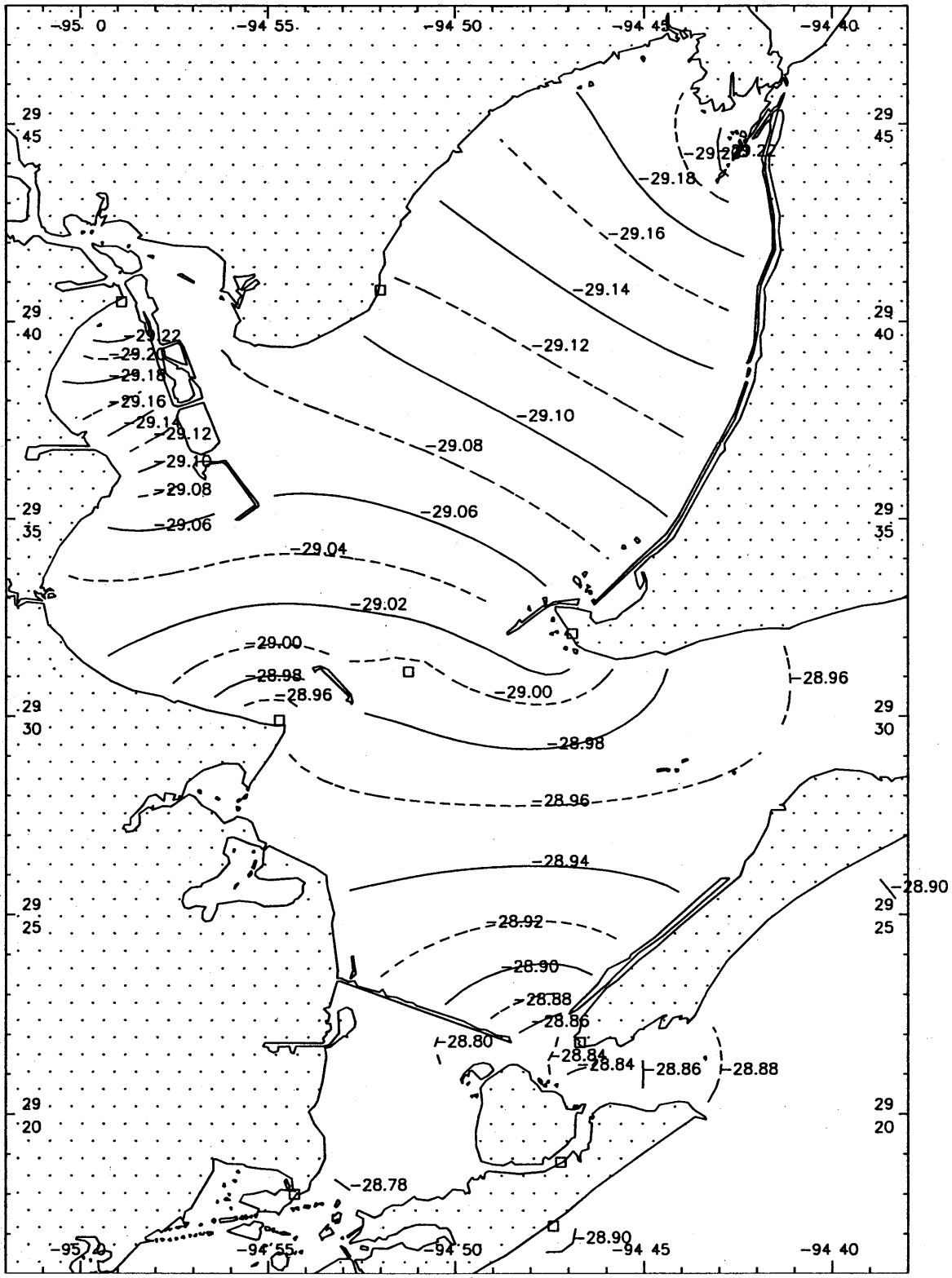

Figure 7.1. TCARI's ellipsoidally-referenced MLLW field (m) in Galveston Bay.

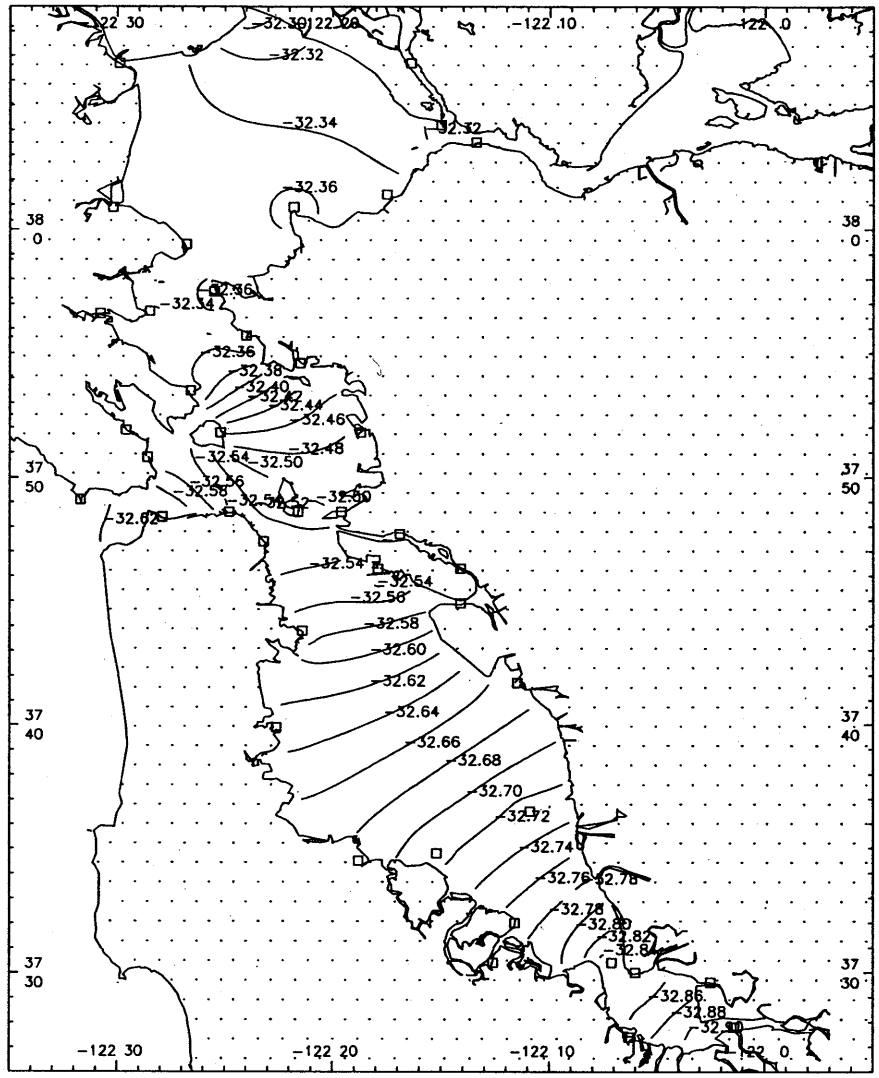

Figure 7.2. TCARI's ellipsoidally-referenced MLLW field (m) for San Francisco Bay.

7.4. Future Enhancements

Potential future enhancements of the TCARI method, in approximate order of greatest to least improvement in accuracy, are as follows: The use of the complex version of the shallow-water, uniform-depth, single-constituent tide wave equation rather than the LE, which would include depth and tidal frequency differences into the solution. The use of variable grid spacing in the LE solution to obtain better resolution in narrow entrance areas. The use of depth weighting in the present LE solution to account (in an indirect way) for tidal dependence of phase on gravity wave speeds. The use of an equation other than the LE (such as a fourth-order differential equation) for spatial interpolation.

TCARI and numerical model-generated fields can be combined to produce more accurate information. First, the numerical model's simulation of ellipsoidally-referenced water levels now relies on a

Barnes (1964) interpolation scheme. Since this scheme does not account for the presence of land, there will be errors in the water levels. However, it is likely that the errors can be reduced by using TCARI's LE-based method of interpolation for this field. Second, TCARI's tidal constituent and other fields were generated without information on the local bathymetry. Since the numerical model's tidal constituent fields were generated using the bathymetry, the model fields contain the influence of depth. The modeled fields could be used in TCARI after subtracting an error field which would be generated by spatially-interpolating the errors (with the LE method) at the gauges.

ACKNOWLEDGMENTS

Dr. Bruce Parker, Chief of the Coast Survey Development Laboratory (CSDL), provided many of the key concepts of spatial interpolation of tidal constituents. CSDL's Douglas Martin provided invaluable assistance in accessing NOS historical data and in defining terms like GPS and ellipsoid. CSDL's Dr. Lloyd Huff organized the field surveys that collected the water level measurements. Steven Gill of NOS's Center for Operational Oceanographic Products and Services (CO-OPS) provided information on tides and tide zoning policy, and CO-OPS's Mike Gibson and Cary Wong provided zoning data for Galveston Bay and San Francisco Bay.

REFERENCES

Barnes, S. L., 1964: A Technique for Maximizing Details in Numerical Weather Map Analysis. **Journal of Applied Meteorology**, 3, 396 - 409.

Browne, D. R., and C. W. Fischer, 1988: Tide and Tidal Currents in the Chesapeake Bay. **NOAA Technical Report** NOS OMA 3, 84 pp + appendices.

Cheng, R. T., V. Casuli, and J. W. Gartner, 1993. Tidal, Residual, Intertidal Mudflat (TRIM) Model and its Applications to San Francisco Bay, California. **Estuarine, Coastal and Shelf Science**, 36, 235 - 280.

Collier, W. C., G. Glang, and L.C. Huff, 1999: Managing Tide Information for Hydrographic Surveys. **Proceedings of the Eleventh Biennial International Symposium of the Hydrographic Society (HYDRO99)**, January 5-7, 1999, University of Plymouth, UK. (Special Publication No. 39). p. 1-1 to 1-7.

Defant, A., 1961: **Physical Oceanography, Volume II**. Pergamon, pp 598. (Esp. 202 - 216 and 364 - 456).

Gill, S., 1998: Description of Discrete Tide Zoning. NOS, Center for Operational Oceanographic Products and Services (personal communication).

Huff, L. C., B. J. Gallagher, and E. C. Snead, Jr., 1998. On-the-Fly GPS for Determination of Vertical Ship Motions. **Proceedings, Ocean Community Conference '98**, The Marine Technology Society Annual Conference. 785 - 791.

Huff, L. C., and B. J. Gallagher, 1996. On-the-Fly GPS for Vertical Control of Hydrographic Surveys. **Proceedings of Hydro '96** The Tenth Biennial International Symposium of the Hydrographic Society. Rotterdam, The Netherlands. 191 - 199.

Müller, T., and E. Groten, 1992. Accuracy Estimation of Mean Sea Level Determination in the Baltic Sea Using a Combined Method. Sea level Changes: Determination and Effects. **Geophysical Monograph** 69, IUGG Vol 11. 189-196.

National Ocean Service, 1999: NOS Procedures for Developing and Implementing Operational Nowcast and Forecast Systems for PORTS. **NOAA Technical Report** NOS CO-OPS 20. 33 pp.

Press, W. H., S. A. Teukolsky, W. T. Vetterling, and B. P. Flannery, 1992. **Numerical Recipes**. Cambridge University Press. 963 pp.

Schmalz, R. A., 1996: National Ocean Service Partnership: DGPS-Supported Hydrosurvey, Water Level Measurement, and Modeling of Galveston Bay. **NOAA Technical Report** NOS OES 12. 136 pp + appendices.

Schureman, P., 1958. Manual of Harmonic Analysis and Prediction of Tides. U.S. Department of Commerce, Coast and Geodetic Survey, **Special Publication** No. 98 [revised 1940 edition, reprinted 1988]. 317 pp.

Stawarz, M., and M. Metzner, 1994. Altimetric Geoid of the Indonesian Waters Derived from ERS-1 Radar Altimeter Data. **Proceedings, International Symposium on Marine Mapping (INSMAP)** 1994. 299 - 310.

Welch, J. M., J. W. Gartner, and S. K. Gill, 1985: San Francisco Bay Area Circulation Survey: 1979-1980. U.S. Department of Commerce, NOAA. **NOS Oceanographic Circulation Survey Report** No. 7. 180 pp.

Zervas, C. Z., (editor), 1993: Tampa Bay Oceanography Project: Physical Oceanographic Synthesis. **NOAA Technical Report** NOS OES 2. 184 pp.

APPENDIX A. TIDE WAVE SOLUTION

Another approach is to apply the equation for a simplified, shallow-water tide wave with gravity g, constant depth H, linearized friction γ, Coriolis acceleration f, and a single constituent frequency σ. Then for water level, η,

$$\eta = Ze^{i\omega t} \tag{A.1}$$

Z is the solution to the shallow water equation,

$$\frac{\partial^2 Z}{\partial x^2} + \frac{\partial^2 Z}{\partial y^2} + KZ = 0 \tag{A.2}$$

where complex K is

$$K = \left(\frac{(1 - i\frac{\gamma}{\sigma})^2 - (\frac{f}{\sigma})^2}{1 - i\frac{\gamma}{\sigma}} \right) \frac{\sigma^2}{gH} \tag{A.3}$$

(see Fang, Z., A. Ye, and G. Fang, 1991: Solutions of tidal motions in a semi-enclosed rectangular gulf with open boundary condition specified. In **Tidal Hydrodynamics**, B. Parker ed, 153 - 168). The finite difference expression of A.2 is

$$\begin{aligned} &(Z_{i+1,j} - Z_{i,j}) - (Z_{i,j} - Z_{i-1,j}) + (Z_{i,j+1} - Z_{i,j}) \\ &+(Z_{i,j} - Z_{i,j-1}) + BZ_{i,j} = 0 \end{aligned} \tag{A.4}$$

where $B = \Delta L^2 K$. Rearranging gives an estimate for Z

$$Z^*_{i,j} = \frac{1}{4 - B}(Z_{i+1,j} + Z_{i-1,j}) \tag{A.5}$$

This equation is analogous to that for the LE, Eqn. 3.10.

APPENDIX B. TIDE DATA FOR GALVESTON BAY

The following (Tables B.1, B.2, and B.3) list the tidal constituent amplitudes and epochs for 14 stations in Galveston Bay. Methods of harmonic analysis, time series data, and other notes appear in Table B.4. The locations and names of the stations appear in Figure 4.2.

Table B.1. Observed tidal constituent amplitudes (mm) in Galveston Bay.

	Station	559	613	625	923	931	971	1013	1021	1328	1450	1481	1510	1624	1801
1	M2	60	54	52	191	42	57	32	38	77	84	47	134	135	33
2	S2	13	13	12	53	15	16	10	9	23	23	17	30	37	7
3	N2	13	12	12	46	10	14	8	10	21	21	10	32	41	9
4	K1	116	123	113	205	114	118	109	107	126	129	117	168	177	78
5	M4	4	1	3	8	2	6	2	1	1	4	2	6	5	0
6	O1	119	114	113	189	119	109	102	116	127	119	110	155	173	79
7	M6	1	0	1	2	1	1	1	0	1	1	1	1	2	0
8	MK3	3	2	2	2	2	5	2	0	10	2	0	1	0	2
9	S4	0	1	0	3	1	1	0	1	1	1	2	1	3	0
10	MN4	3	1	1	3	2	4	1	0	1	2	0	2	0	1
11	NU2	2	3	3	5	3	2	1	2	3	3	2	6	8	1
12	S6	1	0	0	1	0	0	0	0	1	1	1	1	2	0
13	MU2	2	3	4	5	3	3	2	1	4	4	1	5	3	1
14	2N	6	4	5	9	8	1	3	1	9	6	1	8	6	2
15	OO	18	11	15	8	15	12	10	5	13	10	5	7	7	8
16	LAM2	2	1	1	2	1	2	1	0	3	1	0	1	1	1
17	S1	2	4	12	16	8	15	8	0	11	11	0	13	0	11
18	M1	11	13	8	17	10	13	10	8	5	8	8	13	12	4
19	J1	5	3	2	8	7	2	4	9	6	9	9	10	14	1
20	MM	21	35	25	24	51	17	34	0	9	31	0	31	0	22
21	SSA	119	116	35	183	170	131	114	0	117	113	0	111	0	153
22	SA	138	81	235	96	150	84	74	0	138	78	0	79	0	116
23	MSF	19	37	63	41	43	33	31	0	45	26	0	27	0	2
24	MF	7	19	21	3	44	9	11	0	36	1	0	3	0	51
25	RHO1	8	8	4	8	3	4	6	5	6	7	4	8	7	4
26	Q1	23	23	23	39	23	19	20	22	27	24	21	34	34	17
27	T2	2	2	3	5	3	2	1	1	5	3	1	4	2	1
28	R2	0	1	2	4	1	1	1	0	1	2	0	2	0	1
29	2Q	1	5	4	1	2	7	4	3	5	2	3	2	5	2
30	P1	32	35	27	61	31	37	31	35	35	39	39	49	59	22
31	2SM	2	1	2	1	0	1	2	0	2	1	0	1	0	1
32	M3	2	1	1	1	0	3	0	0	3	2	0	2	0	2
33	L2	5	6	3	9	2	4	3	1	2	2	1	5	4	2
34	2MK3	2	1	0	2	2	5	2	0	8	1	0	1	0	2
35	K2	12	11	10	10	9	9	5	2	14	4	5	5	10	6
36	M8	1	0	0	0	0	1	0	0	1	0	1	1	2	0
37	MS4	3	0	2	4	1	3	1	0	1	2	0	4	0	0

Table B.2. Observed tidal constituent Greenwich epochs (degrees) in Galveston Bay.

	Station	559	613	625	923	931	971	1013	1021	1328	1450	1481	1510	1624	1801
1	M2	53	67	59	272	9	18	19	31	292	296	331	275	275	25
2	S2	45	53	46	269	343	17	21	13	289	298	335	273	270	35
3	N2	29	48	33	249	349	348	354	359	266	278	307	257	259	7
4	K1	104	115	111	27	90	93	100	94	60	55	83	29	23	105
5	M4	355	352	339	219	220	331	209	238	21	257	266	201	223	335
6	O1	97	101	104	19	83	84	87	91	52	46	74	21	25	93
7	M6	326	46	241	232	61	208	45	0	307	263	123	234	310	270
8	MK3	53	97	26	339	270	332	259	0	135	156	0	7	0	105
9	S4	180	357	179	357	15	162	332	124	36	20	40	10	239	196
10	MN4	328	308	320	172	208	299	207	0	286	215	0	156	0	349
11	NU2	333	59	48	247	337	325	346	4	278	271	311	251	261	15
12	S6	136	258	169	129	62	248	29	0	66	285	226	257	204	149
13	MU2	296	283	260	186	280	293	265	211	242	219	135	181	92	198
14	2N	265	142	290	235	266	178	175	331	272	209	282	224	243	136
15	OO	112	121	118	48	93	113	112	98	113	98	91	71	21	106
16	LAM2	59	109	90	113	49	213	57	0	51	290	0	339	273	348
17	S1	205	260	274	288	316	336	348	0	353	360	0	330	0	66
18	M1	196	163	228	56	200	151	155	93	109	74	78	42	24	205
19	J1	68	47	127	43	359	11	51	96	32	29	87	9	22	53
20	MM	327	255	37	291	350	315	260	0	129	266	0	265	0	11
21	SSA	42	65	52	60	29	65	62	0	68	61	0	57	0	42
22	SA	121	150	141	140	119	141	166	0	185	176	0	172	0	146
23	MSF	188	327	196	293	144	328	319	0	192	308	0	302	0	219
24	MF	359	154	111	319	331	108	155	0	251	115	0	201	0	300
25	RHO1	43	81	142	49	87	118	82	89	25	56	70	18	26	124
26	Q1	66	88	72	6	55	66	75	89	29	27	69	5	26	79
27	T2	94	97	110	333	240	190	68	360	346	292	336	298	270	133
28	R2	183	58	93	191	156	331	170	0	18	216	0	201	270	37
29	2Q	266	152	287	205	173	202	147	87	306	120	65	44	27	222
30	P1	109	114	114	19	86	80	99	94	45	48	82	25	23	115
31	2SM	174	216	69	340	94	60	285	0	345	288	0	28	0	116
32	M3	274	331	239	260	36	194	61	0	248	73	0	43	0	223
33	L2	73	106	93	304	63	44	97	64	348	52	352	319	292	65
34	2MK3	40	156	57	277	240	347	253	0	117	196	0	342	0	78
35	K2	59	91	72	288	47	62	80	13	15	13	336	273	270	13
36	M8	83	106	295	262	262	91	351	0	180	170	178	69	137	148
37	MS4	326	285	344	230	227	344	226	0	24	280	0	238	0	299

Table B.3. Observed tidal constituent local epochs (degrees) in Galveston Bay.

	Station	559	613	625	923	931	971	1013	1021	1328	1450	1481	1510	1624	1801
1	M2	239	253	245	99	195	204	205	217	118	122	157	101	101	211
2	S2	225	233	226	89	163	197	201	193	109	118	155	93	90	215
3	N2	218	237	223	78	179	177	183	189	95	107	136	86	88	196
4	K1	14	25	20	297	360	3	10	4	330	325	352	298	293	15
5	M4	7	4	351	232	232	343	221	250	33	269	278	213	235	348
6	O1	13	17	20	296	359	0	4	7	328	323	350	297	301	10
7	M6	164	244	79	70	259	46	243	0	145	101	321	72	149	108
8	MK3	148	193	121	75	6	68	354	0	231	252	0	103	0	201
9	S4	180	357	179	357	15	162	332	124	36	20	40	10	239	196
10	MN4	343	324	336	187	223	314	223	0	301	231	0	172	0	5
11	NU2	162	247	237	76	165	154	175	192	107	100	140	80	90	204
12	S6	316	78	349	309	242	68	209	0	246	105	46	77	24	329
13	MU2	128	115	92	18	112	125	98	43	74	51	327	13	284	30
14	2N	98	335	123	67	98	10	7	164	105	42	115	57	75	329
15	OO	15	24	21	311	356	16	15	1	16	1	354	334	284	9
16	LAM2	243	292	273	296	233	36	240	0	235	113	0	162	96	171
17	S1	115	170	184	198	226	246	258	0	263	270	0	240	0	336
18	M1	109	76	141	329	113	64	68	6	22	347	351	315	297	118
19	J1	334	313	33	309	265	278	318	2	298	296	353	276	288	319
20	MM	323	251	33	288	347	312	256	0	125	262	0	262	0	7
21	SSA	41	64	51	60	28	64	62	0	68	61	0	57	0	41
22	SA	121	150	141	140	118	140	166	0	184	175	0	172	0	146
23	MSF	182	321	190	287	138	322	313	0	185	302	0	296	0	213
24	MF	353	147	105	312	325	101	148	0	244	108	0	195	0	294
25	RHO1	322	360	61	328	6	37	1	8	304	335	349	297	305	43
26	Q1	346	7	352	286	335	346	354	9	308	307	349	284	306	358
27	T2	274	277	291	154	60	10	248	180	166	112	157	119	90	314
28	R2	2	238	273	11	335	151	350	0	198	36	0	21	89	216
29	2Q	189	75	210	128	96	125	70	10	229	43	348	326	310	144
30	P1	19	24	25	290	357	350	9	4	316	318	352	295	293	25
31	2SM	348	30	243	154	267	234	99	0	159	102	0	202	0	290
32	M3	13	70	339	359	135	293	160	0	347	172	0	143	0	322
33	L2	255	289	276	127	246	227	280	247	171	235	175	141	115	248
34	2MK3	143	258	159	19	343	90	355	0	219	298	0	85	0	180
35	K2	239	271	252	107	227	241	259	193	195	192	156	93	89	193
36	M8	107	130	319	287	287	115	15	0	205	194	202	94	161	173
37	MS4	332	291	350	236	233	350	232	0	30	286	0	244	0	305

Table B.4. Methods of harmonic analysis and length of time series used.

* Drying occurs at low water levels. **Analyzed at Lamar University.

Station	Name	Harmonic Analysis	Begin	End	Days	Datum (feet)	Notes
0559	Round Point *	LSQHA	1/1/95	12/31/95	365	0.8	231 hours missing
0613	Morgans Point	LSQHA	1/1/94	12/31/94	365	0.7	
0625	Umbrella Point	LSQHA	9/1/95	5/31/96	274	0.7	
0923	High Island **	LSQHA	6/1/94	5/31/95	365	1.3	
0931	Smith Point	LSQHA	6/1/95	11/30/95	183	0.7	
0933	Clear Lake	LSQHA	1/1/94	1/1/94	365	0.6	
0971	Rollover Pass **	LSQHA	6/1/94	5/31/95	365	0.7	
1013	Eagle Point	LSQHA	1/1/94	12/31/94	365	0.6	
1021	Trinity River Channel Platform	HA29	5/21/95 6/19/95 7/18/95		29 29 29	0.6	Average of 3 H.A.
1328	Port Bolivar	LSQHA	1/1/96	12/31/96	366	0.8	
1416	Galveston Bay Ent., South Jetty	LSQHA	2/1/96	7/31/96	182	1.2	
1450	Galveston, Pier 21	LSQHA	1/1/94	12/31/94	365	0.8	
1481	Tiki Island	HA29	8/15/95 9/12/95 10/10/95		29 29 29	0.7	Average of 3 H.A.
1510	Galveston, Pleasure Pier	LSQHA	1/1/94	12/31/94	365	1.2	
1516	Offatts Bayou	HA29	9/22/95 10/20/95		29 29	0.7	Average of 2 H.A.
1624	Galveston GPS Buoy	HA29	7/13/95		29	1.3	
1801	Alligator Point *	LSQHA	1/1/95	12/31/95	365	0.5	71 hours missing
1904	Galveston Offshore	LSQHA	1/1/96	8/31/96	244	1.2	
2132	Christmas Bay	LSQHA	1/1/94	12/31/94	365	0.5	

APPENDIX C. GALVESTON BAY NUMERICAL CIRCULATION MODEL

Model Formulation

The NOS numerical model for Galveston Bay is an adaptation of the Princeton three-dimensional numerical circulation model (Blumberg and Mellor, 1987) [Note: references cited here appear at the end of this Appendix]. The model is capable of simulating water surface elevation fluctuations in Galveston Bay at small time scales (minutes) for long time periods (up to 3 months). To represent accurately the significant horizontal and vertical salinity and temperature gradients that were observed by NOS in Galveston Bay during the water density measurement component of the hydrosurvey, and to simulate density effects on water levels within and outside the navigation channels, the model includes:

- three-dimensional and time-dependent velocities, salinities, and temperatures;
- a free-surface;
- non-linear horizontal advection;
- horizontal and vertical density gradients; and
- variable grid spacing to resolve major navigation channels.

The model solves the equations of fluid motion (momentum balance, mass conservation, equation of state, salinity and temperature conservation, and hydrostatic balance) at all cells in the three-dimensional grid. The equations in three-dimensional Cartesian space are recast in generalized horizontal orthogonal curvilinear coordinates and further transformed using the dimensionless sigma coordinate. The model uses a level 2-1/2 turbulence closure scheme to compute vertical diffusion coefficients from turbulent kinetic energy and a mixing length. Details of the derivation are given in Blumberg and Mellor (1987), Blumberg and Herring (1987), and Mellor (1993).

The major focus of the model application in Galveston Bay in this study is on the accurate representation of the water surface elevation fluctuations due to astronomical and meteorological forcing. Since meteorological forcing are also considered, it is hoped that the modeling effort might also be used to provide nowcast and forecast of currents within the Houston Ship and Galveston Entrance Channels based on the Galveston Bay Physical Oceanographic real-Time System (PORTS) (NOS, 1995). A further potential use of the model would be to provide nowcast and forecast of salinity and temperature fields throughout the Bay to monitor the effects of freshwater inflows in conjunction with oyster population management. Thus the model developed here represents both water level fluctuations and circulation of shelf, Bay, and navigation channel waters.

The Model Grid

The Galveston Bay model runs on an orthogonal curvilinear grid closely fitted to the Bay's lateral boundaries (Figure G.1). A 181 x 101 = 18,281-cell, orthogonal curvilinear mesh was formed using an elliptic equation grid generation technique developed by Wilken (1988) based on the conformal mapping algorithm of Ives and Zacharias (1987). The actual grid generation code was obtained from Professor George L. Mellor, Princeton University.

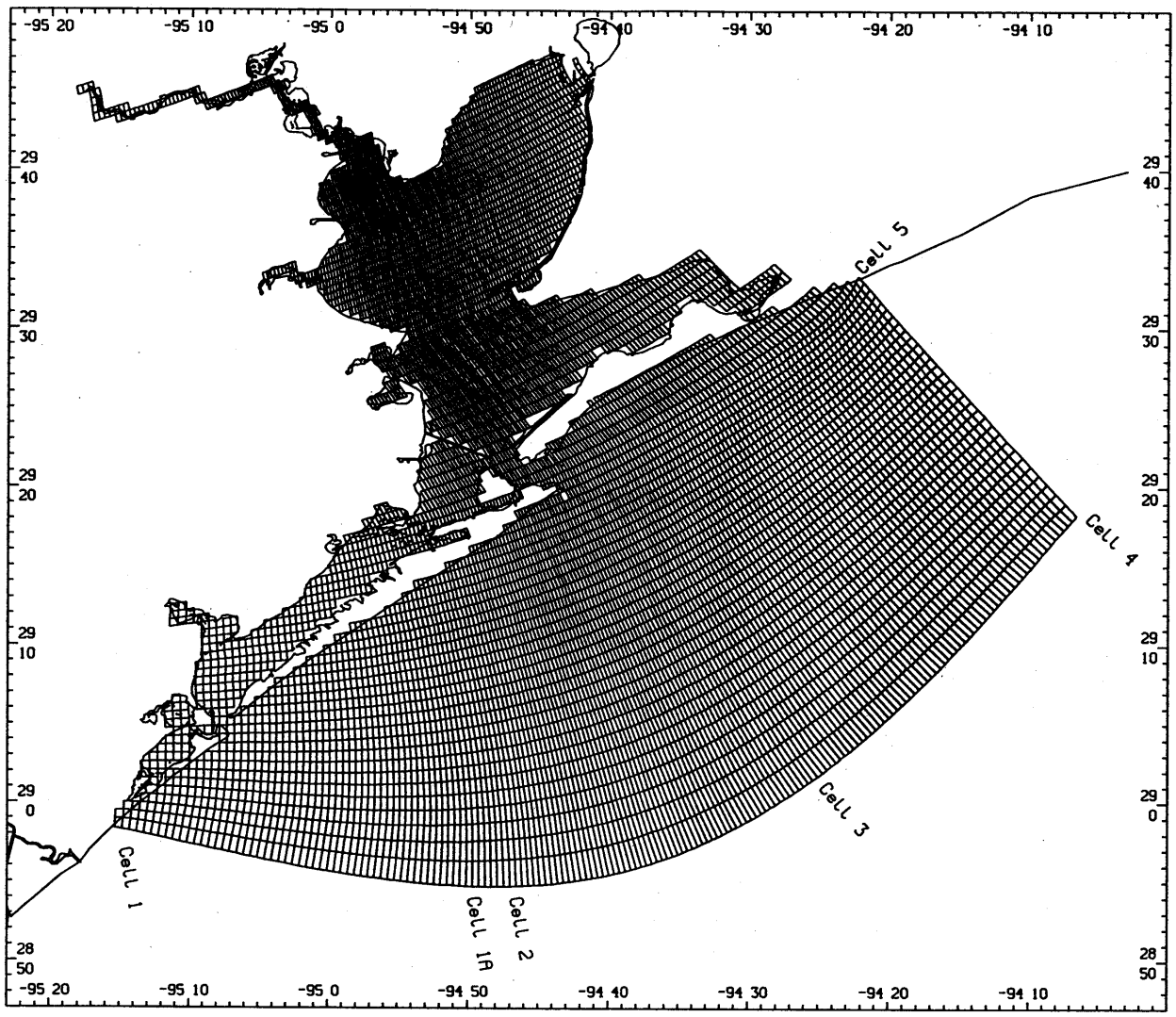

Figure C.1. Curvilinear grid used in the three-dimensional hydrodynamic model study. Cells 1 through 5 are the approximate locations in the grid where the boundary water level signals are supplied. Water levels at intervening cells along the ocean boundary are computed by interpolation.

Grid cells are closely spaced in regions where higher resolution is needed, such as near the major navigation channels, and through the Galveston Bay entrance. The grid configuration includes the two Entrance jetties to Galveston and the Texas City dike. Cell spacing varies from 254 meters to 2428 meters and from 580 meters to 3502 meters in the x and y directions, respectively. Each cell has a depth value obtained from bathymetric data for Galveston Bay available from NOAA's National Geophysical Data Center in gridded (15-second interval) format.

A substantial number of cells cover the Texas shelf region east of the Bay entrance. This placement of the boundaries allows for internal dynamics to dominate the simulation of currents and the density field in the bathymetrically complex Galveston Entrance region, rather than increase uncertainty by specifying the boundary condition in an oversimplified manner and risk imposing a dynamic

inconsistency. The grid has additional connections to the shelf through San Luis Pass at the entrance to West Bay and through Rollover Pass in East Bay.

The grid covers most of the water area of Galveston Bay, but cannot resolve all the small features along the shore such as the Gulf Intracoastal Waterway. The grid is detailed enough to represent the following features explicitly: Trinity River, San Jacinto River, Buffalo Bayou, and the Houston Ship Channel.

In the vertical, there are six sigma levels of varying thickness: $\sigma = (0.0, -.1667, -.4167, -.5833, -.7643, -.9167, -1.00)$. This is considered sufficient to resolve the density stratification observed. Considering cell lengths and depths, the model is run with an external-mode time step of 10 s and an internal mode time step of 60 s. A 30-day simulation requires approximately 15 hours on an SGI Challenge L computer using four CPUs at full utilization with level two (O2) optimization.

Ocean Boundary Conditions

The numerical model simulation requires driving forces (water levels, river discharges, winds) that are applied at the open boundaries on the grid. Each open boundary cell along the Texas shelf requires a water level value and salinity and temperature values at all vertical levels at each model time step. The river boundaries require discharge, salinity, and temperature values. The wind is applied at the surface of all cells. At the closed boundaries there is zero momentum, salt transfer, and heat transfer.

Water level signals at selected grid cells along the ocean boundary are computed at each step, and the water levels at the remaining cells are computed by linear interpolation based on distance. The signals at each of the cells consisted of (1) a tidal component, (2) a time-varying, non-tidal component, and (3) a constant offset. Tidal constituent amplitudes and phases were generated using values at the nearby coastal stations and applying an amplitude factor and a phase lag. The values for each constituent are given in Table 3.2 (pages 26 and 27) in Schmalz (1996). The time-varying non-tidal component was taken to be equal to the non-tidal component measured at Galveston Pleasure Pier. The offsets were generated by testing and analysis of the resulting signals at shore stations. Initially there were five selected cells (see Figure G.1), but a special adjustment was made at the southern boundary. An additional cell (Cell 1A) was added there; the signal at Cell 1A is identical to that at Cell 1. Further discussion of the open ocean and river boundary conditions appears in Sections 3 and 4 in Schmalz (1996).

Model Runs for Tidal Constituents

The NOS Galveston Bay model was run in two scenarios to simulate water levels for tidal constituent analysis. The first (Tide Only) scenario (May 1995) was focused on calibrating the model for the astronomical tide and so involved no winds. Climatological river inflows, salinities, and temperatures were included. The second (Tide-plus-Wind) scenario (June 1995) was focused on the total water level response and so involved the astronomical tide and included the winds. The results of the second scenario were used to determine the tidal constituent amplitudes and epochs.

For the Tide-plus-Wind scenario, the model was used to replicate the conditions encountered during the performance of the DGPS hydrosurvey during June 1995. Meteorological conditions were simulated as completely as possible. Seven meteorological gauge stations were used to develop surface wind and pressure fields for every 3 hours over the 30-day period. Salinity and temperature initial and boundary conditions were derived from measurements reported by Temple et al. (1977) and Orlando et al. (1993), which were used to define a climatology. In addition, sea surface temperature was specified in lieu of heat flux and was also based on this climatology. Daily average USGS observed flow rates were specified for inflows of the Trinity River, San Jacinto River, and Buffalo Bayou. Despite the climatological forcings for salinity and temperature and the use of a one day spin-up, the model reproduced the salinity fields to order 2-3 psu and the temperature fields to within 1-2 °C.

For each 30-day run, the model was initialized and run with a 1-day spin-up period. While it is possible to employ a longer simulation period to account for model spin-up of the density fields, the 1-day spin-up period used in this study appeared adequate due to the nearly dynamically consistent initial density fields. Hourly time series of water surface elevations at all 8672 water cells were saved for subsequent analysis. The standard NOS 29-day harmonic analysis program (Dennis and Long, 1971) was the used to determine amplitudes and phases for 24 tidal constituents.

The results of the Tide-plus-Wind run (Table C.1) show that the model demonstrated considerable skill in reproducing the tidal constituents throughout the Galveston Bay. Note that in comparing the model harmonic constants to the accepted constants, at most stations the accepted constants are based on a full year of observations enabling a least squares analysis (Schureman, 1958). However, as noted in Schmalz (1996), 29-day analyses were performed at Smith Point, Round Point, Galveston GPS Buoy, and at the Trinity River Platform due to length of observed series.

The agreement between the Tide Only results, which included river inflow influences, and the observations was order 2-3 cm rms. These rms values were determined from the differences between observed and modeled amplitude and phases for each of the 24 constituents after Hess (1994). A weighted gain (model vs. observation) and phase (model minus observation) are also reported in Table C.1 based on the magnitude of the observed constituent amplitudes; e.g., see Hess and Bosley (1992). The results for the Tide-plus-Wind run are also given in Table C.1. In comparing, these results with those obtained from the May 1995 astronomical calibration, one notes that at most station differences in constituent amplitudes are order 1 cm and phases are within 10 degrees. This range of differences is consistent with those obtained by comparing different 29-day harmonic analyses of observations themselves.

Model Runs for Ellipsoid Reference

Simulated water surface elevations with respect to the GPS ellipsoid and tidal epoch MLLW at 470 launch hydrosurvey track locations were generated for June 1995 for direct comparison with RTK GPS measurements. To obtain the ellipsoidally-referenced water level, the modeled water level (with respect to the model mean level of zero) was added to a spatially-interpolated value of the ellipsoidally-referenced MSL. Spatial interpolation was based on values at 10 shore stations and an inverse-distance weighting for each.

Table C.1. Tidal constituent amplitudes, A (cm), and local epochs, K (degrees). Values are shown for the Tide-Only (May 1995) run, NOS accepted values, the error, and values for the Tide Plus Wind run. The Gain, Phase, and Estimated RMS Difference are for the Tide-Only Run.

GALVESTON PLEASURE PIER 6771510

		NOS Accepted Values		Tide Only Values		Tide & Wind Values		Tide Only Error		Tide & Wind Error	
No.	Name	A	K	A	K	A	K	A	K	A	K
1	M(2)	13.0	100.9	12.7	91.6	11.9	93.3	-0.7	-9.3	-1.1	-7.6
2	S(2)	3.0	93.0	3.3	89.0	3.8	83.7	0.3	-4.0	0.8	-9.3
3	N(2)	3.0	86.5	3.3	78.7	3.0	70.5	0.1	-7.8	0.0	-15.9
4	K(1)	17.0	298.5	14.3	292.4	13.2	280.4	-2.5	-6.1	-3.8	-18.1
5	M(4)	1.0	213.0	0.4	203.9	0.5	142.8	-0.2	-9.1	-0.5	-70.2
6	O(1)	15.0	297.0	14.3	295.3	13.4	292.3	-1.1	-1.7	-1.6	-4.8
7	M(6)	0.0	72.0	0.2	61.4	0.7	281.3	0.1	-10.6	0.7	-150.7
8	S(4)	0.0	10.4	0.1	325.2	0.3	210.5	0.0	-45.2	0.3	-159.9
9	NU(2)	1.0	80.2	0.6	80.4	0.6	73.6	0.0	0.2	-0.4	-6.7
10	S(6)	0.0	77.3	0.1	34.1	0.3	158.5	0.0	-43.2	0.3	81.2
11	MU(2)	0.0	13.4	0.0	0.0	0.4	47.7	-0.5	-13.4	0.4	34.3
12	2N(2)	1.0	56.6	0.4	65.8	0.6	268.5	-0.4	9.2	-0.4	-148.2
13	OO(1)	1.0	333.7	0.6	289.6	0.1	88.8	-0.1	-44.1	-0.9	115.1
14	LMD(2)	0.0	161.8	0.1	90.4	0.9	286.3	0.0	-71.4	0.9	124.5
15	M(1)	1.0	314.7	1.0	293.8	1.1	274.5	-0.3	-20.9	0.1	-40.3
16	J(1)	1.0	275.6	1.1	291.0	0.5	297.4	0.1	15.4	-0.5	21.8
17	RHO(1)	1.0	297.2	0.5	296.5	2.6	298.2	-0.3	-0.7	1.6	1.0
18	Q(1)	3.0	284.4	2.8	296.6	0.2	84.0	-0.6	12.2	-2.8	159.6
19	T2	0.0	118.7	0.2	89.1	0.0	83.3	-0.2	-29.5	0.0	-35.4
20	2Q(1)	0.0	326.4	0.4	298.0	0.4	304.1	0.3	-28.4	0.4	-22.3
21	P(1)	5.0	295.4	4.7	292.6	4.4	281.3	-0.2	-2.8	-0.6	-14.1
22	L(2)	0.0	141.4	0.5	72.2	0.4	64.0	0.0	-69.2	0.4	-77.4
23	K(2)	0.0	92.9	0.9	88.8	1.0	82.9	0.4	-4.1	1.0	-10.1
24	M(8)	0.0	93.7	0.1	344.9	1.0	302.6	0.0	-108.8	1.0	-151.0

GAIN (-): 0.91 PHASE (HR): -0.25 EST. RMS (M): 0.03

GPS BUOY 8771021

		NOS Accepted Values		Tide Only Values		Tide & Wind Values		Tide Only Error		Tide & Wind Error	
No.	Name	A	K	A	K	A	K	A	K	A	K
1	M(2)	14.0	101.5	12.9	91.9	11.7	94.5	-0.6	-9.6	-2.3	-7.0
2	S(2)	4.0	89.9	3.3	85.0	3.2	73.7	-0.4	-4.9	-0.8	-16.2
3	N(2)	4.0	88.5	3.4	74.5	2.9	72.8	-0.7	-14.0	-1.1	-15.7
4	K(1)	18.0	292.5	14.4	296.0	13.4	285.9	-3.3	3.5	-4.6	-6.6
5	M(4)	0.0	234.9	0.4	213.7	0.4	178.5	-0.1	-21.2	0.4	-56.4
6	O(1)	17.0	301.2	14.8	297.8	13.8	297.9	-2.5	-3.4	-3.2	-3.4
7	M(6)	0.0	148.6	0.2	58.4	0.6	283.8	0.0	-90.2	0.6	135.3
8	S(4)	0.0	239.1	0.1	345.2	0.4	199.2	-0.2	106.1	0.4	-39.9
9	NU(2)	1.0	90.2	0.7	76.8	0.6	75.7	-0.1	-13.4	-0.4	-14.5
10	S(6)	0.0	24.2	0.1	29.2	0.2	224.8	-0.1	5.0	0.2	-159.4
11	MU(2)	0.0	283.9	0.0	0.0	0.4	51.1	-0.3	76.1	0.4	127.2
12	2N(2)	1.0	75.3	0.5	57.0	0.6	274.0	-0.1	-18.3	-0.4	-161.4
13	OO(1)	1.0	283.9	0.6	294.3	0.1	84.8	-0.1	10.4	-0.9	161.0
14	LMD(2)	0.0	96.2	0.1	88.7	1.0	291.9	0.0	-7.5	1.0	-164.3
15	M(1)	1.0	296.8	1.0	296.9	1.1	280.0	-0.2	0.1	0.1	-16.8
16	J(1)	1.0	288.3	1.2	295.2	0.5	303.0	-0.2	6.9	-0.5	14.7
17	RHO(1)	1.0	305.0	0.6	298.6	2.7	303.8	-0.1	-6.4	1.7	-1.2
18	Q(1)	3.0	305.5	2.9	298.7	0.2	74.5	-0.5	-6.8	-2.8	129.0
19	T2	0.0	90.3	0.2	85.2	0.0	72.8	0.0	-5.2	0.0	-17.5
20	2Q(1)	0.0	309.8	0.4	299.6	0.4	309.7	-0.1	-10.2	0.4	0.0
21	P(1)	6.0	293.1	4.8	296.2	4.5	286.8	-1.1	3.0	-1.5	-6.3
22	L(2)	0.0	114.6	0.5	67.9	0.4	66.3	0.1	-46.7	0.4	-48.4
23	K(2)	1.0	89.0	0.9	84.4	0.9	72.0	-0.1	-4.6	-0.1	-17.0
24	M(8)	0.0	161.4	0.1	352.5	0.8	283.0	-0.1	-168.9	0.8	121.6

GAIN (-): 0.86 PHASE (HR): -0.11 EST. RMS (M): 0.04

Table C.1. Continued.

HIGH ISLAND 8770923

No.	Name	NOS Accepted Values A	NOS Accepted Values K	Tide Only Values A	Tide Only Values K	Tide & Wind Values A	Tide & Wind Values K	Tide Only Error A	Tide Only Error K	Tide & Wind Error A	Tide & Wind Error K
1	M(2)	16.0	98.6	14.9	97.4	13.1	100.0	-1.1	-1.2	-2.9	1.4
2	S(2)	4.0	89.1	4.2	82.0	3.2	77.0	-0.2	-7.1	-0.8	-12.1
3	N(2)	4.0	78.5	3.8	74.6	3.5	77.9	0.0	-3.9	-0.5	-0.6
4	K(1)	17.0	296.9	15.5	300.3	14.7	291.6	-1.6	3.5	-2.3	-5.3
5	M(4)	1.0	231.7	0.6	224.9	0.3	281.7	0.0	-6.8	-0.7	50.0
6	O(1)	16.0	295.6	16.0	300.5	15.2	300.1	0.2	4.9	-0.8	4.5
7	M(6)	0.0	70.3	0.3	57.4	0.1	168.7	0.1	-12.9	0.1	98.4
8	S(4)	0.0	357.1	0.2	13.0	0.4	166.0	0.0	15.9	0.4	168.9
9	NU(2)	0.0	75.6	0.7	77.7	0.7	80.9	0.2	2.1	0.7	5.3
10	S(6)	0.0	309.3	0.1	5.1	0.3	151.4	0.0	55.8	0.3	-157.9
11	MU(2)	0.0	18.0	0.0	0.0	0.5	55.8	-0.5	-18.0	0.5	37.8
12	2N(2)	1.0	67.4	0.5	51.8	0.7	283.1	-0.3	-15.6	-0.3	-144.4
13	OO(1)	1.0	311.4	0.7	300.2	0.1	89.4	0.0	-11.2	-0.9	138.0
14	LMD(2)	0.0	296.0	0.1	90.3	1.1	295.8	-0.1	154.3	1.1	-0.1
15	M(1)	1.0	328.6	1.1	300.4	1.2	287.4	-0.3	-28.2	0.2	-41.3
16	J(1)	1.0	309.2	1.3	300.3	0.6	303.8	0.6	-8.9	-0.4	-5.4
17	RHO(1)	1.0	327.9	0.6	300.5	2.9	304.3	-0.1	-27.4	1.9	-23.5
18	Q(1)	3.0	285.6	3.1	300.5	0.2	77.9	-0.1	14.9	-2.8	152.3
19	T2	0.0	153.6	0.3	82.7	0.0	76.1	-0.2	-70.9	0.0	-77.5
20	2Q(1)	0.0	128.1	0.4	300.6	0.4	308.5	0.3	172.5	0.4	-179.5
21	P(1)	5.0	289.5	5.1	300.3	4.9	292.2	0.0	10.8	-0.1	2.7
22	L(2)	1.0	127.0	0.5	68.1	0.5	71.4	-0.3	-58.9	-0.5	-55.7
23	K(2)	1.0	107.1	1.2	80.8	0.9	75.2	0.3	-26.3	-0.1	-32.0
24	M(8)	0.0	286.6	0.1	331.2	0.3	1.7	0.1	44.6	0.3	75.1

GAIN (-): 0.96 PHASE (HR): 0.09 EST. RMS (M): 0.02

ROLLOVER PASS 8770971

No.	Name	NOS Accepted Values A	NOS Accepted Values K	Tide Only Values A	Tide Only Values K	Tide & Wind Values A	Tide & Wind Values K	Tide Only Error A	Tide Only Error K	Tide & Wind Error A	Tide & Wind Error K
1	M(2)	6.0	204.0	4.9	124.7	4.7	129.5	-0.8	-79.3	-1.3	-74.5
2	S(2)	2.0	197.3	1.3	118.8	1.6	88.6	-0.3	-78.5	-0.4	-108.7
3	N(2)	1.0	177.4	1.1	98.3	1.1	105.1	-0.3	-79.1	0.1	-72.2
4	K(1)	12.0	3.0	9.1	342.4	8.9	321.6	-2.7	-20.6	-3.1	-41.4
5	M(4)	1.0	343.5	0.3	269.0	0.3	260.4	-0.3	-74.5	-0.7	-83.1
6	O(1)	11.0	0.3	9.6	337.1	9.1	341.1	-1.3	-23.2	-1.9	-19.2
7	M(6)	0.0	46.4	0.2	87.2	0.1	150.5	0.1	40.8	0.1	104.1
8	S(4)	0.0	161.8	0.2	66.9	0.1	80.2	0.1	-94.9	0.1	-81.6
9	NU(2)	0.0	153.6	0.2	101.9	0.2	108.4	0.0	-51.7	0.2	-45.2
10	S(6)	0.0	68.0	0.1	6.1	0.2	185.0	0.1	-61.9	0.2	117.0
11	MU(2)	0.0	125.1	0.0	0.0	0.1	80.8	-0.3	-125.1	0.1	-44.3
12	2N(2)	0.0	10.1	0.2	72.0	0.4	302.1	0.1	61.9	0.4	-68.0
13	OO(1)	1.0	15.8	0.4	347.6	0.0	110.5	-0.8	-28.2	-1.0	94.7
14	LMD(2)	0.0	36.1	0.0	122.0	0.7	331.3	-0.2	85.9	0.7	-64.7
15	M(1)	1.0	64.4	0.7	339.7	0.7	311.9	-0.6	-84.7	-0.3	-112.5
16	J(1)	0.0	277.7	0.8	344.9	0.4	349.5	0.7	67.2	0.4	71.8
17	RHO(1)	0.0	37.2	0.4	334.9	1.8	350.8	0.0	-62.3	1.8	-46.4
18	Q(1)	2.0	345.7	1.9	334.6	0.1	90.3	0.0	-11.1	-1.9	104.6
19	T2	0.0	9.9	0.1	119.0	0.0	87.0	-0.1	109.1	0.0	77.0
20	2Q(1)	1.0	125.3	0.3	332.0	0.2	0.5	-0.4	-153.3	-0.8	-124.8
21	P(1)	4.0	350.3	3.0	342.0	2.9	323.1	-0.7	-8.3	-1.1	-27.2
22	L(2)	0.0	226.7	0.2	91.8	0.2	98.6	-0.2	-134.9	0.2	-128.1
23	K(2)	1.0	241.2	0.4	118.3	0.4	85.3	-0.5	-122.9	-0.6	-155.9
24	M(8)	0.0	115.5	0.1	64.0	0.4	295.9	0.0	-51.5	0.4	-179.6

GAIN (-): 0.81 PHASE (HR): -1.98 EST. RMS (M): 0.07

Table C.1. Continued.

CHRISTMAS BAY 6772132

No.	Name	NOS Accepted Values A	NOS Accepted Values K	Tide Only Values A	Tide Only Values K	Tide & Wind Values A	Tide & Wind Values K	Tide Only Error A	Tide Only Error K	Tide & Wind Error A	Tide & Wind Error K
1	M(2)	3.0	192.6	4.2	251.5	3.2	248.4	1.0	58.9	0.2	55.8
2	S(2)	1.0	201.9	0.5	89.9	1.1	350.8	-0.2	-112.0	0.1	148.9
3	N(2)	1.0	182.0	1.5	235.5	1.2	229.8	0.9	53.5	0.2	47.8
4	K(1)	7.0	1.3	8.0	31.6	7.6	11.9	0.5	30.4	0.6	10.6
5	M(4)	0.0	247.9	0.4	330.8	0.1	270.9	0.2	82.9	0.1	23.0
6	O(1)	7.0	358.0	7.2	29.0	7.5	35.0	-0.1	31.0	0.5	36.9
7	M(6)	0.0	251.2	0.0	275.5	0.1	53.2	0.0	24.3	0.1	162.0
8	S(4)	0.0	105.0	0.0	93.0	0.3	37.0	0.0	-12.0	0.3	-68.0
9	NU(2)	0.0	173.0	0.3	237.6	0.2	232.3	0.1	64.6	0.2	59.3
10	S(6)	0.0	19.2	0.0	32.7	0.1	42.7	0.0	13.5	0.1	23.5
11	MU(2)	0.0	28.9	0.0	0.0	0.2	211.3	-0.2	-28.9	0.2	-177.6
12	2N(2)	0.0	237.8	0.2	219.5	0.3	348.8	-0.1	-18.3	0.3	110.9
13	OO(1)	0.0	12.6	0.3	34.3	0.0	295.9	-0.2	21.7	0.0	-76.7
14	LMD(2)	0.0	215.9	0.0	176.5	0.5	23.4	-0.1	-39.4	0.5	167.5
15	M(1)	1.0	70.0	0.5	30.3	0.6	0.4	-0.1	-39.7	-0.4	-69.6
16	J(1)	0.0	9.7	0.6	33.0	0.3	44.9	0.4	23.3	0.3	35.2
17	RHO(1)	0.0	334.9	0.3	27.9	1.5	46.4	0.0	53.0	1.5	71.5
18	Q(1)	1.0	342.3	1.4	27.7	0.1	346.7	0.1	45.4	-0.9	4.4
19	T2	0.0	160.1	0.0	96.4	0.0	354.9	-0.1	-63.7	0.0	-165.1
20	2Q(1)	0.0	60.5	0.2	26.4	0.2	57.9	0.0	-34.1	0.2	-2.6
21	P(1)	2.0	3.3	2.6	31.4	2.5	13.6	0.4	28.1	0.5	10.3
22	L(2)	0.0	208.7	0.2	228.9	0.2	223.3	-0.1	20.2	0.2	14.5
23	K(2)	1.0	161.9	0.1	76.9	0.3	359.1	-0.5	-85.0	-0.7	-162.8
24	M(8)	0.0	263.3	0.0	216.6	0.1	27.7	0.0	-46.7	0.1	124.4

GAIN (-): 1.07 PHASE (HR): 1.63 EST. RMS (M): 0.05

GALVESTON PIER 21 6771450

No.	Name	NOS Accepted Values A	NOS Accepted Values K	Tide Only Values A	Tide Only Values K	Tide & Wind Values A	Tide & Wind Values K	Tide Only Error A	Tide Only Error K	Tide & Wind Error A	Tide & Wind Error K
1	M(2)	8.0	122.4	7.7	113.1	6.0	115.9	-0.7	-9.3	-2.0	-6.5
2	S(2)	2.0	117.7	2.3	108.0	1.8	102.5	0.0	-9.7	-0.2	-15.2
3	N(2)	2.0	107.3	2.2	94.4	1.9	113.0	0.1	-12.9	-0.1	5.7
4	K(1)	13.0	324.9	10.0	325.4	9.3	309.0	-2.9	0.6	-3.7	-15.9
5	M(4)	0.0	269.0	0.3	248.5	0.4	174.1	-0.1	-20.5	0.4	-94.9
6	O(1)	12.0	322.6	10.7	324.9	10.2	327.1	-1.3	2.3	-1.8	4.5
7	M(6)	0.0	101.5	0.2	85.4	0.3	337.0	0.1	-16.1	0.3	-124.5
8	S(4)	0.0	20.0	0.1	26.8	0.1	79.3	0.0	6.8	0.1	59.3
9	NU(2)	0.0	100.1	0.4	96.9	0.4	113.4	0.1	-3.2	0.4	13.2
10	S(6)	0.0	105.2	0.2	71.6	0.3	231.0	0.1	-33.6	0.3	125.8
11	MU(2)	0.0	51.3	0.0	0.0	0.3	110.1	-0.4	-51.3	0.3	58.8
12	2N(2)	1.0	41.8	0.3	75.7	0.4	290.8	-0.3	33.9	-0.6	-111.0
13	OO(1)	1.0	1.1	0.5	326.0	0.0	109.7	-0.5	-35.1	-1.0	108.6
14	LMD(2)	0.0	112.9	0.1	110.8	0.7	318.0	0.0	-2.1	0.7	-154.9
15	M(1)	1.0	347.1	0.8	325.2	0.8	300.0	0.0	-21.9	-0.2	-47.1
16	J(1)	1.0	295.9	0.8	325.7	0.4	334.9	-0.1	29.8	-0.6	39.0
17	RHO(1)	1.0	334.8	0.4	324.7	2.0	336.1	-0.3	-10.1	1.0	1.3
18	Q(1)	2.0	306.7	2.1	324.7	0.1	103.1	-0.3	18.0	-1.9	156.4
19	T2	0.0	111.8	0.1	108.2	0.0	102.0	-0.2	-3.7	0.0	-9.9
20	2Q(1)	0.0	42.7	0.3	324.4	0.3	345.1	0.1	-78.3	0.3	-57.6
21	P(1)	4.0	318.5	3.3	325.4	3.1	310.3	-0.6	6.9	-0.9	-8.1
22	L(2)	0.0	234.7	0.3	87.9	0.3	106.4	0.2	-146.8	0.3	-128.3
23	K(2)	0.0	192.4	0.6	107.6	0.5	101.4	0.2	-84.8	0.5	-91.0
24	M(8)	0.0	193.9	0.1	96.3	0.2	335.8	0.1	-97.6	0.2	141.9

GAIN (-): 0.87 PHASE (HR): -0.04 EST. RMS (M): 0.03

Table C.1. Continued.

PORT BOLIVAR 6771328

No.	Name	NOS Accepted Values A	NOS Accepted Values K	Tide Only Values A	Tide Only Values K	Tide & Wind Values A	Tide & Wind Values K	Tide Only Error A	Tide Only Error K	Tide & Wind Error A	Tide & Wind Error K
1	M(2)	7.0	119.5	6.6	110.6	5.6	113.9	-0.1	-8.9	-1.4	-5.6
2	S(2)	1.0	152.0	2.5	100.3	1.9	75.5	1.5	-51.7	0.9	-76.5
3	N(2)	2.0	93.5	1.8	95.9	1.6	110.2	-0.1	2.4	-0.4	16.8
4	K(1)	11.0	333.8	10.0	329.0	8.9	313.2	-1.0	-4.8	-2.1	-20.6
5	M(4)	0.0	89.5	0.1	160.7	0.4	148.8	-0.1	71.2	0.4	59.3
6	O(1)	12.0	335.2	10.7	328.5	9.7	331.5	-1.0	-6.7	-2.3	-3.8
7	M(6)	0.0	135.9	0.1	93.8	0.3	279.8	-0.1	-42.1	0.3	143.9
8	S(4)	0.0	102.7	0.1	309.1	0.1	42.9	0.0	-153.6	0.1	-59.8
9	NU(2)	1.0	66.9	0.3	97.8	0.3	110.7	-0.2	30.9	-0.7	43.8
10	S(6)	0.0	120.3	0.1	56.9	0.3	222.0	0.1	-63.4	0.3	101.7
11	MU(2)	0.0	51.9	0.0	0.0	0.2	106.5	-0.2	-51.9	0.2	54.6
12	2N(2)	0.0	22.8	0.2	81.1	0.4	294.9	-0.3	58.3	0.4	-88.0
13	OO(1)	2.0	9.6	0.5	329.6	0.0	96.1	-1.0	-40.0	-2.0	86.5
14	LMD(2)	1.0	270.6	0.0	105.8	0.7	322.3	-0.6	-164.8	-0.3	51.7
15	M(1)	1.0	341.8	0.8	328.7	0.8	304.1	-0.3	-13.1	-0.2	-37.7
16	J(1)	0.0	349.1	0.8	329.3	0.4	339.3	0.3	-19.8	0.4	-9.8
17	RHO(1)	1.0	312.4	0.4	328.2	1.9	340.6	-0.7	15.8	0.9	28.2
18	Q(1)	3.0	317.6	2.1	328.2	0.1	77.0	-0.5	10.6	-2.9	119.4
19	T2	1.0	93.6	0.1	100.7	0.0	74.0	-0.5	7.2	-1.0	-19.6
20	2Q(1)	0.0	115.8	0.3	327.9	0.3	349.6	-0.1	-147.9	0.3	-126.1
21	P(1)	4.0	356.0	3.3	329.0	3.0	314.5	-0.4	-27.0	-1.0	-41.5
22	L(2)	0.0	220.7	0.3	89.3	0.2	103.7	-0.1	-131.4	0.2	-117.0
23	K(2)	2.0	176.2	0.7	99.5	0.5	72.4	-1.6	-76.7	-1.5	-103.8
24	M(8)	0.0	213.6	0.0	91.0	0.3	321.8	0.0	-122.6	0.3	108.2

GAIN (-): 0.86 PHASE (HR): -0.72 EST. RMS (M): 0.03

EAGLE POINT 6771013

No.	Name	NOS Accepted Values A	NOS Accepted Values K	Tide Only Values A	Tide Only Values K	Tide & Wind Values A	Tide & Wind Values K	Tide Only Error A	Tide Only Error K	Tide & Wind Error A	Tide & Wind Error K
1	M(2)	3.0	204.6	3.8	235.2	3.7	233.3	0.6	30.6	0.7	28.7
2	S(2)	1.0	200.6	1.0	162.2	0.4	107.1	0.0	-38.4	-0.6	-93.5
3	N(2)	1.0	183.3	1.2	217.9	1.1	187.3	0.4	34.6	0.1	4.0
4	K(1)	11.0	10.1	10.3	18.8	8.3	4.8	-0.6	8.8	-2.7	-5.2
5	M(4)	0.0	220.9	0.1	14.5	0.2	264.1	-0.1	153.6	0.2	43.2
6	O(1)	10.0	3.6	10.0	11.9	9.5	18.1	-0.2	8.3	-0.5	14.5
7	M(6)	0.0	243.1	0.1	280.4	0.1	68.7	0.0	37.3	0.1	-174.4
8	S(4)	0.0	332.4	0.0	53.7	0.1	61.0	0.0	81.3	0.1	88.6
9	NU(2)	0.0	174.9	0.2	220.2	0.2	193.5	0.1	45.3	0.2	18.5
10	S(6)	0.0	208.9	0.0	44.0	0.2	49.9	0.0	-164.9	0.2	-159.0
11	MU(2)	0.0	97.6	0.0	0.0	0.2	141.3	-0.2	-97.6	0.2	43.7
12	2N(2)	0.0	7.4	0.2	200.5	0.4	351.5	-0.1	-166.9	0.4	-15.9
13	OO(1)	1.0	15.4	0.4	25.7	0.0	174.8	-0.6	10.3	-1.0	159.4
14	LMD(2)	0.0	240.3	0.0	201.3	0.7	11.5	-0.1	-39.0	0.7	131.2
15	M(1)	1.0	67.6	0.7	15.3	0.8	358.2	-0.3	-52.3	-0.3	-69.4
16	J(1)	0.0	317.9	0.8	22.2	0.4	23.9	0.4	64.3	0.4	66.0
17	RHO(1)	1.0	1.5	0.4	8.9	1.9	24.8	-0.2	7.4	0.9	23.3
18	Q(1)	2.0	354.4	1.9	8.4	0.0	112.2	-0.1	14.0	-2.0	117.8
19	T2	0.0	247.9	0.1	165.2	0.0	102.1	0.0	-82.8	0.0	-145.9
20	2Q(1)	0.0	70.0	0.3	5.0	0.3	31.4	-0.1	-65.0	0.3	-38.6
21	P(1)	3.0	8.8	3.4	18.3	2.7	5.8	0.3	9.6	-0.3	-2.9
22	L(2)	0.0	280.1	0.2	211.3	0.2	180.8	-0.1	-68.8	0.2	-99.4
23	K(2)	1.0	259.4	0.3	156.3	0.1	96.9	-0.2	-103.1	-0.9	-162.5
24	M(8)	0.0	15.3	0.0	236.6	0.0	330.9	0.0	-138.7	0.0	-44.4

GAIN (-): 0.97 PHASE (HR): 0.32 EST. RMS (M): 0.03

Table C.1. Continued.

TRINITY RIVER CHANNEL PLATFORM 8771021

No.	Name	NOS Accepted Values A	NOS Accepted Values K	Tide Only Values A	Tide Only Values K	Tide & Wind Values A	Tide & Wind Values K	Tide Only Error A	Tide Only Error K	Tide & Wind Error A	Tide & Wind Error K
1	M(2)	4.0	216.6	3.4	216.8	3.4	218.2	-0.1	0.2	-0.6	1.6
2	S(2)	1.0	214.2	1.1	149.0	0.6	106.4	0.1	-65.2	-0.4	-107.8
3	N(2)	1.0	192.4	1.0	200.7	1.1	174.1	0.1	8.3	0.1	-18.2
4	K(1)	10.0	4.3	10.0	12.4	8.1	357.4	-0.1	8.1	-1.9	-6.9
5	M(4)	0.0	257.5	0.1	234.8	0.2	228.1	-0.1	-22.7	0.2	-29.4
6	O(1)	12.0	4.8	9.9	5.9	9.3	12.2	-1.7	1.1	-2.7	7.3
7	M(6)	0.0	282.8	0.1	275.3	0.1	45.1	0.0	-7.5	0.1	122.3
8	S(4)	0.0	187.5	0.1	106.4	0.1	28.4	0.0	-81.1	0.1	-159.1
9	NU(2)	0.0	195.6	0.2	202.9	0.2	180.1	0.0	7.3	0.2	-15.6
10	S(6)	0.0	237.4	0.0	53.3	0.1	24.3	-0.1	175.9	0.1	146.9
11	MU(2)	0.0	29.3	0.0	0.0	0.1	130.0	-0.1	-29.3	0.1	100.7
12	2N(2)	0.0	168.1	0.1	184.6	0.4	342.6	0.0	16.5	0.4	174.4
13	OO(1)	0.0	3.8	0.4	18.9	0.0	166.3	-0.1	15.1	0.0	162.6
14	LMD(2)	0.0	215.5	0.0	185.3	0.7	4.8	0.0	-30.2	0.7	149.3
15	M(1)	1.0	4.6	0.7	9.2	0.7	350.0	-0.1	4.6	-0.3	-14.6
16	J(1)	1.0	4.0	0.8	15.7	0.4	18.5	-0.1	11.7	-0.6	14.6
17	RHO(1)	0.0	5.1	0.4	3.2	1.8	19.5	0.0	-1.9	1.8	14.5
18	Q(1)	2.0	5.1	1.9	2.7	0.0	110.9	-0.4	-2.4	-2.0	105.8
19	T2	0.0	214.3	0.1	151.7	0.0	101.9	0.0	-62.5	0.0	-112.3
20	2Q(1)	0.0	5.4	0.3	359.5	0.2	26.9	0.0	-5.9	0.2	21.5
21	P(1)	3.0	4.3	3.3	12.0	2.7	358.5	0.0	7.7	-0.3	-5.9
22	L(2)	0.0	240.7	0.1	194.2	0.2	167.6	0.0	-46.5	0.2	-73.1
23	K(2)	0.0	214.0	0.3	143.5	0.2	97.3	0.0	-70.5	0.2	-116.7
24	M(8)	0.0	0.5	0.0	256.9	0.1	47.4	-0.1	-103.6	0.1	46.9

GAIN (-): 0.92 PHASE (HR): 0.16 EST. RMS (M): 0.02

SMITH POINT 8770931

No.	Name	NOS Accepted Values A	NOS Accepted Values K	Tide Only Values A	Tide Only Values K	Tide & Wind Values A	Tide & Wind Values K	Tide Only Error A	Tide Only Error K	Tide & Wind Error A	Tide & Wind Error K
1	M(2)	4.0	188.7	3.7	197.7	3.5	202.1	-0.4	9.0	-0.5	13.4
2	S(2)	1.0	163.5	1.3	135.5	0.7	102.5	0.2	-28.0	-0.3	-61.0
3	N(2)	1.0	162.9	1.1	182.5	1.1	167.5	-0.2	19.6	0.1	4.6
4	K(1)	10.0	353.9	10.1	5.7	8.2	350.2	-0.4	11.9	-1.8	-3.6
5	M(4)	0.0	213.2	0.3	250.1	0.4	222.0	0.0	36.9	0.4	8.8
6	O(1)	12.0	359.4	10.0	359.5	9.3	6.8	-2.2	0.1	-2.7	7.4
7	M(6)	0.0	290.3	0.1	282.5	0.1	354.2	-0.3	-7.8	0.1	63.9
8	S(4)	0.0	286.1	0.1	165.1	0.2	3.5	0.1	-121.0	0.2	77.4
9	NU(2)	0.0	166.3	0.2	184.6	0.2	172.1	0.0	18.3	0.2	5.8
10	S(6)	0.0	73.4	0.0	32.6	0.2	3.9	-0.1	-40.8	0.2	-69.5
11	MU(2)	0.0	24.4	0.0	0.0	0.1	132.9	-0.1	-24.4	0.1	108.5
12	2N(2)	0.0	137.0	0.1	167.4	0.4	333.6	-0.1	30.4	0.4	-163.4
13	OO(1)	1.0	348.3	0.4	11.9	0.0	155.9	-0.1	23.6	-1.0	167.6
14	LMD(2)	0.0	177.1	0.0	168.8	0.7	358.5	0.0	-8.3	0.7	-178.6
15	M(1)	1.0	356.6	0.7	2.6	0.7	342.0	-0.2	6.0	-0.3	-14.6
16	J(1)	1.0	351.1	0.8	8.8	0.4	13.9	-0.2	17.7	-0.6	22.8
17	RHO(1)	0.0	1.9	0.4	356.9	1.8	15.0	-0.1	-5.0	1.8	13.2
18	Q(1)	2.0	2.3	1.9	356.5	0.0	106.5	-0.5	-5.8	-2.0	104.2
19	T2	0.0	164.6	0.1	137.9	0.0	98.5	0.0	-26.6	0.0	-66.0
20	2Q(1)	0.0	5.1	0.3	353.4	0.2	23.2	0.0	-11.7	0.2	18.2
21	P(1)	3.0	354.3	3.3	5.2	2.7	351.5	-0.2	10.9	-0.3	-2.8
22	L(2)	0.0	214.6	0.2	176.0	0.2	160.9	0.1	-38.6	0.2	-53.7
23	K(2)	0.0	161.5	0.4	130.4	0.2	94.4	0.1	-31.1	0.2	-67.1
24	M(8)	0.0	311.1	0.1	265.8	0.1	77.1	-0.1	-45.3	0.1	126.0

GAIN (-): 0.89 PHASE (HR): 0.31 EST. RMS (M): 0.02

Table C.1. Continued.

CLEAR LAKE 6770933

No.	Name	NOS Accepted Values A	NOS Accepted Values K	Tide Only Values A	Tide Only Values K	Tide & Wind Values A	Tide & Wind Values K	Tide Only Error A	Tide Only Error K	Tide & Wind Error A	Tide & Wind Error K
1	M(2)	4.0	283.5	4.9	236.9	4.6	238.1	1.1	-46.6	0.6	-45.4
2	S(2)	1.0	276.8	1.2	168.6	0.5	127.7	0.2	-108.2	-0.5	-149.1
3	N(2)	1.0	263.2	1.5	219.0	1.2	189.5	0.7	-44.2	0.2	-73.7
4	K(1)	11.0	42.3	10.8	19.5	9.0	11.6	-0.4	-22.9	-2.0	-30.7
5	M(4)	0.0	15.8	0.3	332.5	0.3	302.3	0.1	-43.3	0.3	-73.5
6	O(1)	10.0	33.8	10.4	12.5	9.7	19.1	0.1	-21.3	-0.3	-14.7
7	M(6)	0.0	73.1	0.3	294.8	0.2	70.1	0.3	-138.3	0.2	-3.0
8	S(4)	0.0	211.2	0.0	286.5	0.1	69.7	0.0	75.3	0.1	-141.5
9	NU(2)	0.0	282.3	0.3	221.4	0.2	196.0	0.1	-60.9	0.2	-86.3
10	S(6)	0.0	335.8	0.0	54.3	0.3	52.2	0.0	78.5	0.3	76.4
11	MU(2)	0.0	123.4	0.0	0.0	0.2	140.9	-0.3	-123.4	0.2	17.5
12	2N(2)	1.0	349.7	0.2	201.0	0.4	4.1	-0.3	-148.7	-0.6	14.3
13	OO(1)	1.0	31.8	0.4	26.6	0.0	186.9	-0.7	-5.2	-1.0	155.1
14	LMD(2)	0.0	266.5	0.0	205.2	0.7	15.4	0.0	-61.3	0.7	108.9
15	M(1)	1.0	98.4	0.7	16.0	0.8	7.9	-0.7	-82.4	-0.2	-90.5
16	J(1)	0.0	342.4	0.8	23.0	0.4	22.4	0.5	40.6	0.4	40.0
17	RHO(1)	1.0	16.3	0.4	9.4	1.9	22.9	-0.2	-6.9	0.9	6.6
18	Q(1)	2.0	31.0	2.0	9.0	0.0	132.2	0.0	-22.0	-2.0	101.2
19	T2	0.0	321.0	0.1	171.3	0.0	123.3	0.0	-149.6	0.0	162.4
20	2Q(1)	1.0	80.3	0.3	5.5	0.3	26.6	-0.3	-74.8	-0.8	-53.7
21	P(1)	3.0	42.5	3.6	19.0	3.0	12.2	0.5	-23.5	0.0	-30.4
22	L(2)	0.0	305.0	0.2	212.4	0.2	182.9	-0.3	-92.6	0.2	-122.1
23	K(2)	1.0	281.7	0.3	163.0	0.1	118.8	-0.7	-118.7	-0.9	-162.9
24	M(8)	0.0	177.7	0.0	265.9	0.2	229.3	0.0	88.2	0.2	51.6

GAIN (-): 1.00 PHASE (HR): -1.89 EST. RMS (M): 0.05

MORGANS POINT 6770613

No.	Name	NOS Accepted Values A	NOS Accepted Values K	Tide Only Values A	Tide Only Values K	Tide & Wind Values A	Tide & Wind Values K	Tide Only Error A	Tide Only Error K	Tide & Wind Error A	Tide & Wind Error K
1	M(2)	5.0	252.8	5.4	239.6	5.0	241.3	0.0	-13.2	0.0	-11.5
2	S(2)	1.0	233.3	1.3	172.1	0.5	143.2	0.0	-61.2	-0.5	-90.1
3	N(2)	1.0	237.1	1.6	222.2	1.2	191.4	0.4	-14.9	0.2	-45.6
4	K(1)	12.0	24.5	11.0	19.7	9.0	11.6	-1.3	-4.8	-3.0	-13.0
5	M(4)	0.0	3.7	0.3	341.9	0.2	297.8	0.2	-21.8	0.2	-65.9
6	O(1)	11.0	17.3	10.5	12.5	9.6	19.8	-0.9	-4.8	-1.4	2.4
7	M(6)	0.0	244.1	0.2	292.0	0.2	77.0	0.2	47.9	0.2	-167.1
8	S(4)	0.0	356.8	0.1	306.3	0.2	60.4	0.0	-50.5	0.2	63.6
9	NU(2)	0.0	247.4	0.3	224.5	0.2	198.1	0.0	-22.9	0.2	-49.3
10	S(6)	0.0	78.2	0.0	44.6	0.2	69.0	0.0	-33.6	0.2	-9.2
11	MU(2)	0.0	115.1	0.0	0.0	0.2	141.5	-0.3	-115.1	0.2	26.4
12	2N(2)	0.0	334.6	0.2	204.8	0.4	3.3	-0.2	-129.8	0.4	28.7
13	OO(1)	1.0	24.3	0.5	26.9	0.0	195.8	-0.6	2.6	-1.0	171.5
14	LMD(2)	0.0	292.5	0.0	208.3	0.7	15.6	-0.1	-84.2	0.7	83.2
15	M(1)	1.0	76.2	0.7	16.1	0.8	7.5	-0.6	-60.1	-0.2	-68.8
16	J(1)	0.0	313.5	0.8	23.3	0.4	23.3	0.5	69.8	0.4	69.8
17	RHO(1)	1.0	359.9	0.4	9.5	1.9	23.8	-0.4	9.6	0.9	24.0
18	Q(1)	2.0	7.4	2.0	9.0	0.0	147.1	-0.3	1.6	-2.0	139.7
19	T2	0.0	276.9	0.1	174.8	0.0	139.2	-0.1	-102.1	0.0	-137.6
20	2Q(1)	1.0	74.9	0.3	5.4	0.3	27.9	-0.3	-69.5	-0.8	-47.0
21	P(1)	4.0	24.5	3.6	19.2	3.0	12.2	0.1	-5.3	-1.0	-12.3
22	L(2)	1.0	288.9	0.2	215.7	0.2	184.9	-0.4	-73.2	-0.8	-104.0
23	K(2)	1.0	270.8	0.4	166.7	0.1	135.2	-0.7	-104.1	-0.9	-135.6
24	M(8)	0.0	130.0	0.0	333.7	0.2	229.9	0.0	-156.3	0.2	99.9

GAIN (-): 0.89 PHASE (HR): -0.68 EST. RMS (M): 0.03

Table C.1. Continued.

ROUND POINT 8770559

No.	Name	NOS Accepted Values A	NOS Accepted Values K	Tide Only Values A	Tide Only Values K	Tide & Wind Values A	Tide & Wind Values K	Tide Only Error A	Tide Only Error K	Tide & Wind Error A	Tide & Wind Error K
1	M(2)	6.0	238.0	5.7	229.6	5.3	231.6	-0.2	-8.4	-0.7	-6.4
2	S(2)	1.0	222.6	1.4	166.4	0.3	138.4	0.0	-56.2	-0.7	-84.2
3	N(2)	1.0	232.3	1.7	214.5	1.3	191.4	0.5	-17.8	0.3	-40.9
4	K(1)	14.0	25.3	11.2	15.7	8.7	2.3	-2.7	-9.6	-5.3	-23.0
5	M(4)	0.0	356.8	0.7	324.8	0.4	301.2	0.3	-32.0	0.4	-55.6
6	O(1)	12.0	4.8	10.7	8.6	9.8	17.1	-0.9	3.8	-2.3	12.2
7	M(6)	0.0	197.2	0.2	70.9	0.1	131.4	0.1	-126.3	0.1	-65.8
8	S(4)	0.0	231.9	0.2	255.3	0.4	34.5	-0.2	23.4	0.4	162.6
9	NU(2)	0.0	233.0	0.3	216.5	0.3	196.8	0.1	-16.5	0.3	-36.3
10	S(6)	0.0	38.0	0.0	39.7	0.0	24.2	-0.1	1.7	0.0	-13.8
11	MU(2)	0.0	64.0	0.0	0.0	0.2	151.1	-0.2	-64.0	0.2	87.1
12	2N(2)	0.0	226.5	0.2	199.4	0.4	347.5	0.1	-27.1	0.4	120.9
13	OO(1)	0.0	45.8	0.5	22.7	0.0	188.4	0.0	-23.1	0.0	142.6
14	LMD(2)	0.0	230.9	0.0	200.3	0.7	9.6	0.0	-30.6	0.7	138.8
15	M(1)	1.0	15.1	0.8	12.1	0.8	354.9	0.0	-3.0	-0.2	-20.2
16	J(1)	1.0	35.4	0.8	19.2	0.4	23.4	-0.1	-16.2	-0.6	-12.0
17	RHO(1)	0.0	356.0	0.4	5.5	1.9	24.4	0.0	9.5	1.9	28.4
18	Q(1)	2.0	354.6	2.1	5.1	0.0	142.2	-0.2	10.5	-2.0	147.6
19	T2	0.0	223.1	0.1	168.9	0.0	134.7	0.0	-54.3	0.0	-88.4
20	2Q(1)	0.0	344.5	0.3	1.6	0.3	31.8	0.0	17.1	0.3	47.3
21	P(1)	5.0	23.8	3.7	15.1	2.9	3.4	-0.9	-8.6	-2.1	-20.4
22	L(2)	0.0	243.7	0.2	207.9	0.2	184.8	0.1	-35.8	0.2	-58.9
23	K(2)	0.0	221.3	0.4	161.3	0.1	130.9	0.0	-60.0	0.1	-90.4
24	M(8)	0.0	183.4	0.0	251.6	0.2	324.1	-0.2	68.2	0.2	140.7

GAIN (-): 0.90 PHASE (HR): -0.32 EST. RMS (M): 0.03

Model References

Blumberg, A. F., and H. J. Herring, 1987: Circulation modeling using orthogonal curvilinear coordinates. in **Three-Dimensional Models of Marine and Estuarine Dynamics** (J. C. J. Nihoul and B. M. Jamart, eds), Elsevier Oceanography Series, 45, 55 - 88.

Blumberg, A. F., and G. L. Mellor, 1987: A description of a three-dimensional coastal ocean circulation model. **Three-Dimensional Coastal Ocean Models**, (ed. Heaps), American Geophysical Union, Washington, DC., 1 - 16.

Dennis, R. E., and E. E. Long, 1971: A user's guide to a computer program for harmonic analysis of data at tidal frequencies. **NOAA Technical Report** NOS 41. NOAA, National Ocean Service, Office of Oceanography and Marine Assessment, Rockville, MD, 31 pp.

Hess, K. W., 1994: Tampa Bay Oceanography Project: Development and Application of the Numerical Circulation Model. NOAA, National Ocean Service, Office of Ocean and Earth Sciences, **NOAA Technical Report** NOS OES 005, Silver Spring, MD.

___ and K. T. Bosley, 1992: Techniques for validation of a model for Tampa Bay, **Proceedings Second International Conference on Estuarine and Coastal Modeling**, Tampa, FL, November 11-13, 1991, 83-94.

Ives, D. C. and R. M. Zacharias, 1987: Conformal mapping and orthogonal grid generation, Paper No. 87-2057, **AIAA/SAE/ASME/ASEE 23rd Joint Propulsion Conference**, San Diego, CA.

Mellor, G. L., 1993: User's guide for a three-dimensional, primitive equation, numerical ocean model. Atmospheric and Oceanic Sciences Program, Princeton University, Princeton, NJ, (unpublished manuscript).

NOS, 1995. **Houston/Galveston Physical Oceanographic Real-Time System (PORTS): FY 95 Implementation Plan**, NOAA, National Ocean Service, Rockville, MD.

Orlando, S. P., L. P. Rozas, G. H. Ward, and C. J. Klein, 1993. **Salinity characterization of Gulf of Mexico Estuaries**, NOAA, Office of Ocean Resources Conservation and Assessment, Silver Spring, MD.

Schmalz, R.A., 1996: National Ocean Service Partnership: DGPS-Supported Hydrosurvey, Water Level Measurement, and Modeling of Galveston Bay–Development and Application of the Numerical Circulation Model. NOAA, National Ocean Service, Office of Ocean and Earth Sciences, Silver Spring, MD. **NOAA Technical Report** NOS OES 12. 136 pp plus appendices.

Schureman, P., 1958: **Manual of Harmonic Analysis and Prediction of Tides**. U.S. Department of Commerce, Coast and Geodetic Survey, Special Publication No. 98 [revised 1940 edition, reprinted 1988], Rockville, MD.

Temple, R. F., D. L. Harrington, J. A. Martin, 1977. Monthly temperature and salinity measurements of continental shelf waters of the northwestern Gulf of Mexico, 1963-1965., **NOAA Technical Report** NMFS SSRF-707, Rockville, MD.

Wilken, J. L., 1988: A computer program for generating two-dimensional orthogonal curvilinear coordinate grids, Woods Hole Oceanographic Institution, (unpublished), Woods Hole, MA.

APPENDIX D. SIMULATED CONSTITUENT FIELDS FOR GALVESTON BAY

Distribution of constituent amplitudes and Greenwich epochs computed with the numerical model (Appendix C) and the TCARI method. Locations where constituent data was used (tide gauges) are shown as open squares.

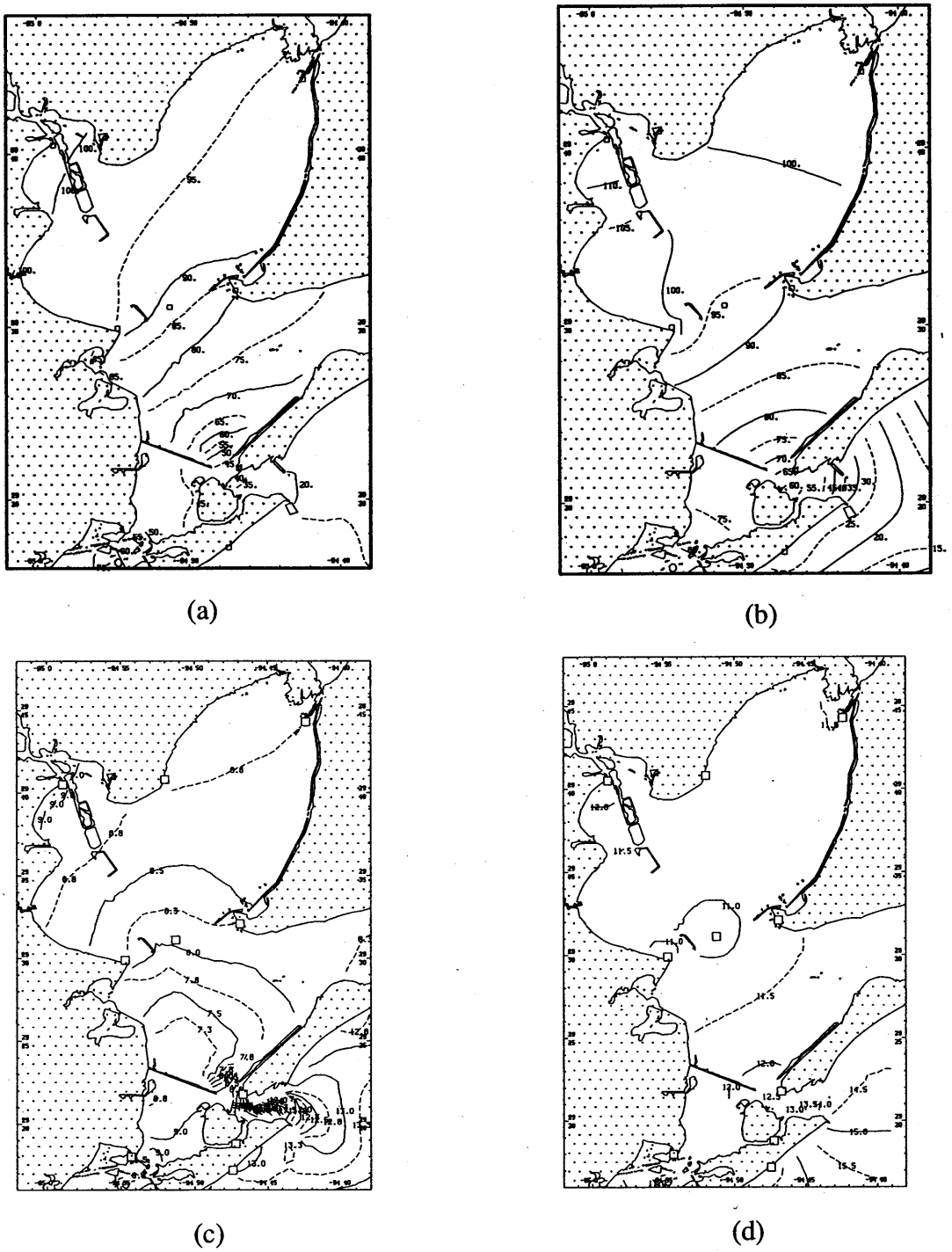

Figure D.1. For K_1, distribution of epoch from the numerical model (a) and TCARI (b), and amplitude from the numerical model (c) and TCARI (d).

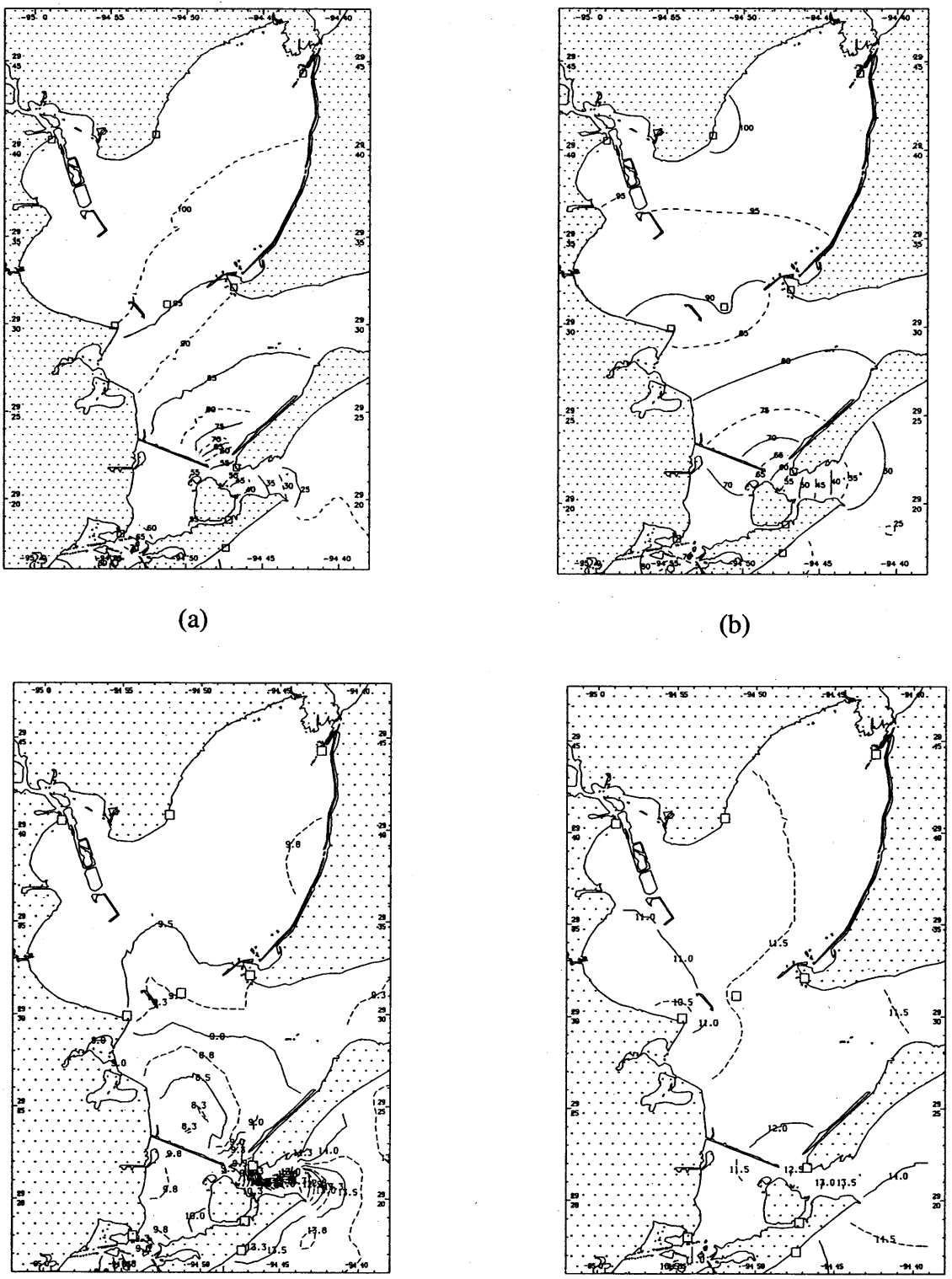

Figure D.2. For O_1, distribution of epoch from the numerical model (a) and TCARI (b), and amplitude from the numerical model (c) and TCARI (d).

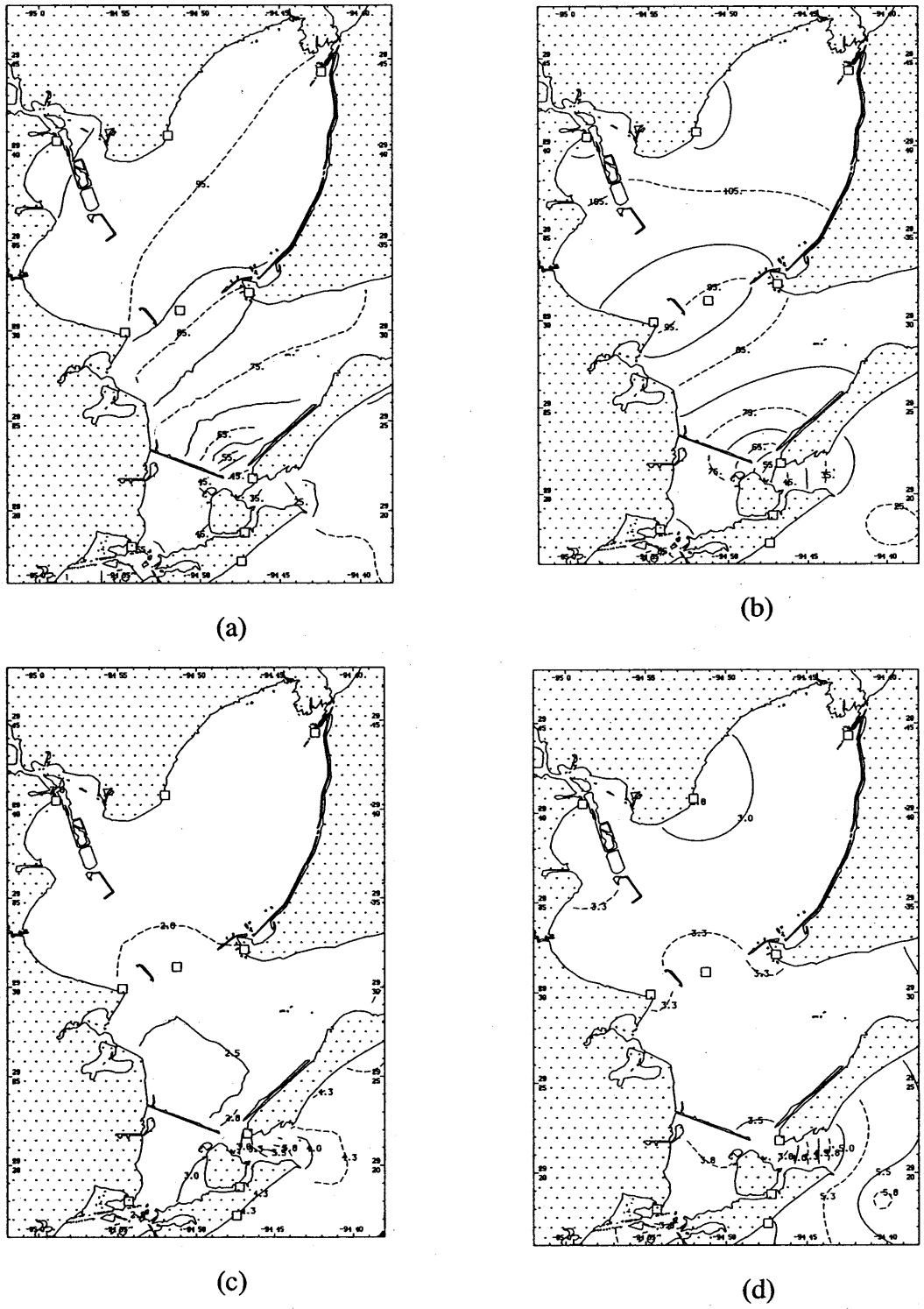

Figure D.3. For P_1, distribution of epoch from the numerical model (a) and TCARI (b), and amplitude from the numerical model (c) and TCARI (d).

APPENDIX E. TIDE DATA FOR SAN FRANCISCO BAY

The following (Tables E.1, E.2, and E.3) list the tidal constituent amplitudes and epochs for 44 stations in San Francisco Bay. Station numbers are the last four digits of the 7-digit NOS number; the first three digits are 941. Methods of harmonic analysis, time series data, and other notes appear in Table E.4.

Table E.1. Observed tidal constituent amplitudes (mm) in San Francisco Bay.

Station		4290	4305	4317	4358	4392	4449	4458	4501	4509	4510	4519	4523	4525	4575	4637	4688	4724
1	M2	570	607	647	699	738	786	812	862	894	918	929	879	862	960	831	774	778
2	S2	134	141	142	175	163	176	178	187	201	203	179	201	177	200	182	180	169
3	N2	122	129	133	143	153	159	164	173	182	188	170	185	161	191	165	162	155
4	K1	368	375	378	385	392	384	403	405	391	410	396	411	367	430	398	387	398
5	M4	26	29	23	20	9	1	3	13	17	18	45	12	52	67	13	3	5
6	O1	229	231	231	234	235	240	241	241	227	243	225	241	199	240	243	238	238
7	M6	2	2	5	6	7	6	8	12	12	16	21	10	10	30	10	3	8
8	MK3	20	26	27	24	21	27	26	31	44	28	0	20	85	56	25	24	28
9	S4	0	0	0	1	1	1	2	1	11	2	6	2	3	1	0	2	6
10	MN4	10	11	8	5	3	2	3	7	6	8	0	6	23	25	7	4	4
11	NU2	28	27	27	34	33	27	38	41	48	57	33	40	43	50	40	36	35
12	S6	1	0	0	1	1	0	1	0	9	1	4	0	1	1	0	0	4
13	MU2	10	7	9	5	9	19	17	25	34	21	22	17	39	41	26	12	14
14	2N	15	14	13	15	15	14	15	14	28	17	23	17	23	12	15	27	18
15	OO	14	13	13	12	12	17	14	14	38	16	10	16	13	12	29	16	9
16	LAM2	5	8	8	12	4	17	15	17	14	17	7	21	25	25	18	9	14
17	S1	5	7	2	16	18	21	12	15	20	19	0	23	14	44	0	12	11
18	M1	14	13	13	11	15	13	14	16	14	16	16	14	15	21	16	24	14
19	J1	21	19	16	17	18	16	17	16	30	19	18	19	13	18	21	19	15
20	MM	18	20	9	18	21	6	15	5	20	12	0	12	12	5	25	27	4
21	SSA	83	46	24	78	46	482	42	11	68	65	0	45	40	90	692	36	8
22	SA	47	27	47	95	27	1430	34	61	28	67	0	140	82	140	2182	126	61
23	MSF	2	18	16	9	5	9	6	4	15	14	0	8	45	14	19	4	1
24	MF	20	7	9	16	13	15	7	12	21	17	0	10	20	15	37	17	17
25	RHO1	10	10	7	13	10	10	11	7	25	10	9	11	11	6	5	7	9
26	Q1	40	40	39	40	43	45	44	42	26	47	44	47	37	38	43	44	42
27	T2	8	8	9	4	11	9	9	10	1	22	11	13	13	14	10	26	13
28	R2	2	2	2	22	12	24	3	2	17	11	1	6	5	4	0	28	1
29	2Q	6	5	3	4	6	3	5	3	12	9	6	11	6	1	2	9	3
30	P1	118	120	123	130	121	122	125	132	118	130	131	133	110	143	129	129	123
31	2SM	3	2	5	4	7	6	8	7	6	12	0	11	8	11	10	10	7
32	M3	3	9	8	9	8	8	6	7	16	10	0	7	30	15	3	5	5
33	L2	24	19	25	29	39	47	48	54	76	72	26	46	84	67	38	38	45
34	2MK3	16	19	21	24	26	33	33	41	55	46	0	35	93	65	38	33	34
35	K2	42	41	44	48	51	72	58	60	79	71	49	64	81	72	57	76	55
36	M8	0	1	1	1	1	1	2	2	5	4	4	3	4	9	0	1	0
37	MS4	12	12	7	6	2	5	5	9	3	12	0	7	23	31	8	3	6

Table E.1. Continued.

		4746	4750	4764	4779	4782	4806	4816	4818	4819	4837	4849	4863	4873	4874	4881	4906	5009
1	M2	659	669	662	626	635	550	614	590	564	571	601	610	587	574	610	580	593
2	S2	145	150	149	142	147	129	135	134	131	164	134	139	130	137	140	130	123
3	N2	136	137	141	131	131	122	127	125	120	122	129	129	124	130	128	124	120
4	K1	367	376	374	373	365	363	363	367	365	357	360	370	359	355	359	374	344
5	M4	25	20	19	16	15	19	12	18	17	14	9	12	14	8	16	24	15
6	O1	224	228	231	228	225	226	225	227	224	216	223	223	214	219	224	238	212
7	M6	3	6	5	4	4	2	4	4	4	2	5	5	6	4	6	1	10
8	MK3	28	23	20	18	16	15	10	15	11	14	0	12	0	11	0	0	24
9	S4	1	0	2	0	1	0	2	0	1	1	1	0	1	1	0	2	1
10	MN4	9	8	8	5	5	7	6	8	6	5	0	5	0	4	0	0	5
11	NU2	33	32	28	27	27	24	27	28	21	23	25	26	24	30	25	24	24
12	S6	1	0	0	1	0	1	2	1	0	0	1	0	1	0	1	1	0
13	MU2	5	4	12	7	8	7	6	11	7	6	14	6	14	4	11	14	11
14	2N	18	16	18	15	16	12	11	14	11	16	17	13	16	19	17	17	14
15	OO	14	12	14	14	13	10	14	13	12	12	10	11	9	7	10	10	11
16	LAM2	5	8	8	9	10	8	9	10	9	10	4	10	4	18	4	4	10
17	S1	11	11	4	13	16	5	14	5	8	4	0	13	0	3	0	0	23
18	M1	12	15	10	11	13	11	12	14	13	13	16	9	15	11	16	17	15
19	J1	19	21	17	18	19	20	19	19	20	17	18	19	17	14	18	19	14
20	MM	8	14	21	15	15	9	10	13	6	15	0	8	0	22	0	0	13
21	SSA	101	88	82	76	49	69	59	64	47	104	0	59	0	74	0	0	77
22	SA	49	49	42	127	98	73	19	15	46	126	0	25	0	91	0	0	43
23	MSF	9	5	10	8	1	7	6	4	6	9	0	16	0	7	0	0	9
24	MF	14	20	32	19	12	15	7	12	22	18	0	15	0	15	0	0	21
25	RHO1	10	10	6	13	9	7	10	11	7	9	8	9	8	8	8	9	7
26	Q1	38	40	39	39	39	39	38	40	37	38	43	38	41	37	43	46	37
27	T2	10	11	17	8	11	8	6	10	7	25	8	13	8	6	8	7	5
28	R2	1	2	6	4	3	1	8	2	2	28	1	3	1	6	1	1	16
29	2Q	5	6	6	5	2	6	5	4	1	3	6	2	6	6	6	6	5
30	P1	125	120	120	127	107	116	114	115	117	106	119	117	119	112	119	124	99
31	2SM	4	5	6	4	5	2	3	4	4	3	0	4	0	5	0	0	5
32	M3	7	6	5	7	5	0	2	3	1	4	0	2	0	3	0	0	6
33	L2	35	37	30	20	23	17	26	30	19	20	17	23	16	24	17	16	35
34	2MK3	25	24	21	18	16	11	13	14	12	12	0	13	0	13	0	0	27
35	K2	49	47	52	39	44	37	40	40	42	29	36	41	35	34	38	35	44
36	M8	1	0	0	2	0	1	1	2	1	1	2	2	2	1	0	1	1
37	MS4	9	8	8	6	6	9	3	9	8	5	0	5	0	4	0	0	6

		5052	5056	5074	5111	5143	5144	5165	5218	5252	5338
1	M2	612	634	650	525	607	508	636	597	594	537
2	S2	120	162	121	108	130	107	140	129	130	107
3	N2	121	153	126	99	118	95	130	120	109	100
4	K1	365	374	344	307	333	286	347	337	335	317
5	M4	9	6	16	8	16	11	6	12	35	42
6	O1	214	232	206	179	202	166	210	200	204	178
7	M6	8	4	11	7	11	10	10	10	4	5
8	MK3	21	0	22	17	12	28	21	19	59	68
9	S4	2	1	1	1	1	1	2	1	2	2
10	MN4	4	0	5	3	6	5	3	4	15	15
11	NU2	30	30	31	23	31	22	23	25	24	21
12	S6	0	0	1	0	1	0	0	0	0	0
13	MU2	13	15	21	18	18	18	13	16	29	25
14	2N	12	20	10	11	15	13	10	8	15	9
15	OO	17	10	11	11	8	9	15	12	16	13
16	LAM2	11	4	14	14	15	16	19	14	16	22
17	S1	34	0	16	8	23	13	12	16	15	14
18	M1	14	16	14	17	16	12	4	15	21	23
19	J1	18	18	14	7	9	7	11	14	12	14
20	MM	20	0	34	6	10	21	31	19	24	22
21	SSA	338	0	20	40	32	70	78	84	45	212
22	SA	1036	0	49	37	86	26	56	33	82	263
23	MSF	7	0	30	20	20	40	19	25	18	30
24	MF	32	0	28	29	28	24	46	23	23	27
25	RHO1	11	9	7	6	12	12	8	7	4	4
26	Q1	37	45	37	30	33	25	33	32	35	34
27	T2	6	10	13	10	12	6	19	5	1	4
28	R2	15	1	19	3	6	4	2	6	5	15
29	2Q	6	6	7	2	3	4	9	5	5	3
30	P1	97	124	104	90	95	78	110	99	101	91
31	2SM	5	0	5	6	5	6	5	4	8	9
32	M3	9	0	6	4	6	7	7	5	15	18
33	L2	35	18	26	33	42	30	27	23	33	26
34	2MK3	27	0	36	29	27	36	27	32	62	71
35	K2	42	44	55	45	49	43	57	51	61	69
36	M8	1	2	2	0	1	0	1	2	2	2
37	MS4	6	0	8	3	6	8	7	8	17	21

Table E.2. Observed tidal Greenwich epochs (degrees) in San Francisco Bay.

		4290	4305	4317	4358	4392	4449	4458	4501	4509	4510	4519	4523	4525	4575	4637	4688	4724
1	M2	209	213	219	223	235	236	236	241	245	246	249	239	250	255	239	239	240
2	S2	215	221	228	235	247	256	252	260	258	264	273	257	270	278	256	260	257
3	N2	184	187	194	199	213	215	215	221	221	227	224	219	233	237	217	221	221
4	K1	226	227	230	233	238	240	239	241	243	243	248	240	249	248	243	240	241
5	M4	143	136	134	138	179	133	14	14	57	358	31	297	85	46	14	98	80
6	O1	210	210	213	215	222	223	223	226	230	227	234	224	238	236	224	226	225
7	M6	91	59	58	66	79	23	33	50	89	48	60	31	153	75	51	46	74
8	MK3	130	124	117	113	115	100	90	92	103	102	0	102	95	82	87	92	78
9	S4	321	169	41	194	130	40	72	79	335	79	223	97	190	174	0	46	111
10	MN4	118	109	111	105	149	32	346	359	198	342	0	299	75	23	340	337	44
11	NU2	196	192	198	198	193	229	215	222	233	215	227	210	231	226	208	208	221
12	S6	166	62	132	181	220	118	263	266	133	10	15	157	349	346	0	299	357
13	MU2	135	88	68	52	45	4	6	6	350	360	204	345	23	7	15	35	3
14	2N	153	154	154	176	194	185	193	200	198	225	198	223	216	226	155	211	195
15	OO	242	263	264	271	291	266	282	294	281	289	262	296	288	332	304	291	281
16	LAM2	214	215	228	220	187	189	218	211	113	234	260	199	235	221	231	191	209
17	S1	221	277	259	282	281	191	235	186	180	236	0	239	187	205	0	210	262
18	M1	238	249	255	243	267	255	268	273	237	272	241	259	281	282	292	294	292
19	J1	246	249	249	266	272	262	274	275	309	289	255	273	331	294	282	266	289
20	MM	221	148	181	156	131	254	130	240	251	223	0	56	328	190	132	60	197
21	SSA	285	307	314	8	299	59	309	267	277	252	0	285	235	347	113	227	332
22	SA	279	129	123	261	76	120	102	132	323	178	0	201	176	251	323	286	131
23	MSF	269	175	146	211	138	137	166	95	74	21	0	318	22	38	355	36	222
24	MF	102	174	141	219	160	184	160	100	179	159	0	176	184	89	126	150	198
25	RHO1	209	199	217	184	195	244	202	216	206	209	228	208	217	198	233	212	198
26	Q1	203	203	210	210	220	219	221	227	210	227	227	224	247	235	222	223	224
27	T2	198	202	224	151	197	254	225	243	83	203	272	221	230	277	280	265	242
28	R2	328	7	261	249	24	155	55	355	126	55	274	54	60	139	0	181	316
29	2Q	202	186	225	194	229	261	221	288	153	266	221	242	283	334	173	221	230
30	P1	225	224	226	233	238	240	237	237	241	244	247	240	244	245	246	240	240
31	2SM	43	56	51	54	31	52	55	62	325	70	0	50	73	76	73	31	48
32	M3	210	30	34	36	43	359	4	359	213	11	0	23	355	344	119	21	10
33	L2	235	226	230	238	234	221	228	225	231	243	274	240	243	228	236	237	242
34	2MK3	94	92	84	82	87	64	69	68	74	81	0	71	77	76	55	70	70
35	K2	207	212	217	208	229	225	234	240	257	249	275	242	258	261	251	239	239
36	M8	350	274	252	252	126	63	68	120	211	106	141	96	315	153	0	5	0
37	MS4	151	147	150	158	203	331	357	10	285	25	0	344	116	63	9	80	54

		4746	4750	4764	4779	4782	4806	4816	4818	4819	4837	4849	4863	4873	4874	4881	4906	5009
1	M2	224	225	225	222	221	215	220	217	215	224	221	223	229	229	229	202	236
2	S2	234	235	230	229	230	222	232	225	222	231	230	234	237	242	242	205	242
3	N2	200	201	196	196	196	189	195	192	190	197	195	198	206	200	205	177	212
4	K1	233	233	235	232	230	229	231	230	231	232	231	233	239	237	236	224	238
5	M4	138	151	170	156	152	167	193	195	181	173	202	208	213	225	193	150	174
6	O1	217	217	216	215	215	213	215	213	213	217	217	217	219	222	219	207	221
7	M6	74	35	36	99	69	29	122	44	37	66	101	90	93	109	90	44	109
8	MK3	118	118	131	130	117	144	147	157	140	138	0	146	0	124	0	0	125
9	S4	49	124	69	160	292	287	330	25	251	330	331	23	186	14	0	277	152
10	MN4	113	125	155	142	130	150	178	167	161	152	0	188	0	205	0	0	138
11	NU2	204	210	205	199	203	198	208	201	200	203	199	202	209	195	208	180	215
12	S6	147	145	0	164	111	72	164	70	137	123	176	83	29	195	29	358	323
13	MU2	124	63	58	114	82	110	99	92	113	131	328	83	200	188	201	178	57
14	2N	181	172	165	167	151	161	168	156	161	163	169	166	182	198	181	151	180
15	OO	246	261	278	263	275	248	239	272	243	273	246	261	260	225	253	241	278
16	LAM2	271	213	206	214	210	224	249	230	215	209	225	223	233	215	235	204	241
17	S1	262	224	325	279	252	219	234	267	270	309	0	253	0	305	0	0	250
18	M1	246	251	281	244	244	236	237	239	239	240	224	236	229	269	228	216	262
19	J1	264	261	255	260	255	246	245	248	246	258	239	255	249	262	245	232	260
20	MM	239	224	162	137	184	50	31	204	224	203	0	127	0	75	0	0	191
21	SSA	277	284	183	29	196	305	278	312	303	246	0	282	0	296	0	0	301
22	SA	300	291	236	288	251	294	1	326	235	34	0	259	0	306	0	0	316
23	MSF	110	332	5	184	84	197	229	43	111	113	0	343	0	293	0	0	51
24	MF	145	106	117	216	155	254	324	167	281	132	0	138	0	164	0	0	170
25	RHO1	201	215	186	193	204	220	201	213	222	204	211	217	211	255	212	200	228
26	Q1	211	211	207	208	207	207	209	207	207	208	210	212	209	221	211	199	224
27	T2	194	201	262	215	203	204	192	211	239	249	229	205	237	292	241	205	181
28	R2	108	6	261	211	146	255	119	265	216	354	230	115	237	114	242	206	294
29	2Q	212	218	191	159	223	206	219	206	235	222	203	206	199	213	202	191	244
30	P1	232	233	234	231	227	227	228	228	228	230	230	231	238	233	235	223	238
31	2SM	62	57	51	62	59	44	83	47	41	42	0	62	0	108	0	0	75
32	M3	185	178	77	34	39	357	180	209	110	48	0	135	0	100	0	0	162
33	L2	249	235	248	236	227	243	247	234	245	223	248	249	252	234	252	228	250
34	2MK3	86	81	82	98	86	105	81	94	95	100	0	94	0	84	0	0	86
35	K2	224	224	227	215	218	214	211	216	213	246	230	224	238	221	243	206	252
36	M8	228	221	0	243	210	159	276	209	211	191	187	176	149	253	0	80	186
37	MS4	143	162	205	176	184	177	237	198	191	201	0	212	0	246	0	0	174

Table E.2. Continued.

		5052	5056	5074	5111	5143	5144	5165	5218	5252	5338
1	M2	247	240	247	274	258	285	260	255	257	264
2	S2	256	250	262	285	270	298	270	268	270	275
3	N2	222	212	221	248	233	259	235	228	238	242
4	K1	250	240	245	263	251	270	253	251	255	261
5	M4	12	118	10	16	334	123	50	19	80	109
6	O1	232	223	230	246	233	255	237	234	241	249
7	M6	138	118	122	187	132	240	144	130	196	294
8	MK3	95	0	90	125	105	134	114	108	89	104
9	S4	85	243	115	152	77	174	86	63	176	116
10	MN4	358	0	341	17	319	104	350	336	70	92
11	NU2	237	216	227	253	244	268	241	231	240	255
12	S6	345	169	251	317	211	18	320	212	353	165
13	MU2	49	210	58	87	73	99	71	61	48	52
14	2N	192	184	201	242	206	250	187	211	245	296
15	OO	306	257	282	325	328	332	311	293	300	310
16	LAM2	250	245	245	265	258	273	255	259	234	267
17	S1	24	0	173	300	249	266	291	226	152	249
18	M1	236	232	328	320	280	322	53	325	296	307
19	J1	275	248	272	315	288	325	268	285	335	324
20	MM	150	0	69	134	197	44	40	163	279	203
21	SSA	157	0	138	221	332	272	305	305	2	343
22	SA	169	0	117	238	128	24	333	307	22	285
23	MSF	21	0	52	14	31	11	25	69	66	72
24	MF	156	0	171	158	164	189	227	156	151	129
25	RHO1	234	216	232	239	237	230	278	224	217	241
26	Q1	232	215	234	257	240	264	241	232	249	263
27	T2	293	249	268	254	233	245	226	238	176	277
28	R2	16	250	17	149	178	198	281	187	170	127
29	2Q	273	206	230	152	263	328	246	219	252	325
30	P1	237	239	242	266	256	267	256	255	250	267
31	2SM	83	0	68	114	87	128	108	87	86	84
32	M3	175	0	158	178	163	29	177	153	312	327
33	L2	264	269	267	276	272	289	283	265	244	254
34	2MK3	65	0	75	111	93	120	84	84	68	82
35	K2	241	250	242	279	260	287	269	260	255	269
36	M8	339	344	289	261	243	90	45	317	44	122
37	MS4	23	0	37	77	14	138	61	54	93	114

Table E.3. Observed tidal local epochs (degrees) in San Francisco Bay.

		4290	4305	4317	4358	4392	4449	4458	4501	4509	4510	4519	4523	4525	4575	4637	4688	4724
1	M2	338	341	347	352	4	4	5	9	13	14	17	7	18	23	7	8	8
2	S2	335	341	348	355	7	16	12	20	18	24	33	17	30	38	16	20	17
3	N2	316	320	326	331	346	348	347	354	353	360	356	351	5	9	350	354	353
4	K1	106	107	109	112	118	120	118	121	123	122	128	120	129	128	122	120	121
5	M4	40	32	30	35	75	30	270	271	313	254	288	194	341	302	270	355	337
6	O1	98	98	102	104	110	112	112	115	119	116	123	112	126	125	112	114	114
7	M6	116	84	82	90	104	47	58	75	113	73	84	55	177	99	76	70	98
8	MK3	138	132	124	121	123	108	97	100	111	110	0	110	103	89	95	100	86
9	S4	201	49	281	74	10	280	312	319	215	319	103	337	70	54	0	286	351
10	MN4	19	9	12	6	50	293	247	260	99	242	0	200	336	283	241	238	305
11	NU2	328	324	330	330	325	1	347	354	5	347	359	342	3	358	340	340	353
12	S6	166	62	132	181	220	118	263	266	133	10	15	157	349	346	0	299	357
13	MU2	271	224	205	188	181	141	142	143	126	136	341	122	159	143	151	171	139
14	2N	290	291	291	313	331	322	330	337	334	2	335	360	352	3	292	348	331
15	OO	113	134	135	142	161	137	153	165	152	160	133	167	159	203	175	162	151
16	LAM2	339	340	352	344	312	313	342	336	237	358	24	324	359	346	355	315	334
17	S1	101	157	139	162	161	71	115	66	60	116	0	119	67	85	0	90	142
18	M1	122	133	139	127	151	139	152	157	121	156	125	143	165	166	176	178	176
19	J1	121	124	124	141	147	138	150	150	184	165	130	149	206	169	157	141	164
20	MM	217	144	176	152	127	250	126	235	247	218	0	52	324	186	128	56	193
21	SSA	284	307	314	7	299	58	308	266	277	252	0	285	234	347	113	226	331
22	SA	279	128	123	261	75	120	101	132	322	178	0	201	176	251	323	286	131
23	MSF	261	167	138	202	130	129	157	86	66	13	0	310	14	29	347	28	214
24	MF	93	165	133	210	152	175	151	91	170	150	0	167	176	80	117	141	190
25	RHO1	101	91	110	77	87	136	94	109	99	102	121	100	109	91	125	105	90
26	Q1	95	96	103	103	113	112	113	119	103	120	120	117	140	128	115	116	117
27	T2	318	322	345	271	317	14	346	4	204	323	32	341	350	38	40	25	2
28	R2	88	127	21	9	144	275	175	115	246	174	34	174	180	259	0	300	75
29	2Q	100	83	122	91	126	158	118	186	51	163	118	139	180	231	70	118	128
30	P1	105	104	107	113	118	121	117	117	121	125	127	121	124	125	126	121	120
31	2SM	155	168	162	166	143	163	167	174	77	182	0	162	185	188	185	143	160
32	M3	222	42	47	48	55	12	16	12	225	24	0	35	7	356	131	33	22
33	L2	358	349	354	1	358	344	351	349	355	7	38	4	7	351	360	1	5
34	2MK3	110	108	101	99	103	81	85	85	91	97	0	88	94	92	72	87	87
35	K2	327	331	336	327	348	344	354	360	16	9	34	1	18	20	10	359	358
36	M8	143	67	45	45	279	216	220	272	4	259	294	249	108	305	0	158	0
37	MS4	40	35	38	46	91	219	245	259	173	273	0	232	4	312	258	328	302

Table E.3. Continued.

		4746	4750	4764	4779	4782	4806	4816	4818	4819	4837	4849	4863	4873	4874	4881	4906	5009
1	M2	353	353	353	350	350	343	348	346	344	352	350	351	357	357	357	330	4
2	S2	354	355	350	349	350	342	352	345	342	351	350	354	357	2	2	325	2
3	N2	332	334	329	328	328	322	327	325	322	330	328	330	338	332	338	309	344
4	K1	113	113	115	111	110	109	110	110	110	112	111	113	119	117	116	104	118
5	M4	34	47	66	53	48	63	89	91	77	69	98	104	109	122	89	46	70
6	O1	106	105	104	103	104	101	103	101	102	105	106	105	108	110	108	96	110
7	M6	99	59	60	123	93	54	146	68	61	91	126	115	117	134	114	69	134
8	MK3	126	126	138	138	125	152	155	164	148	146	0	154	0	132	0	0	132
9	S4	289	4	309	40	172	167	210	265	131	210	211	263	66	254	0	157	32
10	MN4	14	25	56	42	31	51	78	67	61	53	0	89	0	106	0	0	39
11	NU2	335	342	337	331	335	330	340	333	332	335	331	334	341	327	340	312	347
12	S6	147	145	0	164	111	72	164	70	137	123	176	83	29	195	29	358	323
13	MU2	260	200	194	250	219	246	235	228	249	267	105	219	336	324	338	314	194
14	2N	318	308	302	304	288	297	305	293	298	300	306	303	319	334	318	288	317
15	OO	117	131	149	133	146	119	110	143	114	144	117	132	130	96	124	112	149
16	LAM2	35	338	330	338	335	348	13	355	340	333	350	348	357	340	359	328	5
17	S1	142	104	205	159	132	99	114	147	150	189	0	133	0	185	0	0	130
18	M1	130	135	165	129	128	120	121	124	123	124	108	120	113	153	112	100	146
19	J1	140	136	130	136	130	122	120	124	121	133	114	130	125	137	120	108	135
20	MM	234	220	158	133	180	46	26	200	219	199	0	123	0	70	0	0	186
21	SSA	276	283	183	29	195	305	278	311	302	245	0	282	0	296	0	0	300
22	SA	300	291	236	288	250	293	1	326	235	33	0	259	0	306	0	0	316
23	MSF	102	323	357	176	76	189	221	35	103	105	0	335	0	285	0	0	43
24	MF	136	97	108	207	147	245	315	158	272	123	0	130	0	156	0	0	161
25	RHO1	94	107	78	85	96	112	94	105	114	96	103	110	103	147	104	92	120
26	Q1	104	104	99	100	100	100	102	100	100	101	103	105	102	114	104	92	117
27	T2	314	321	23	336	323	324	313	331	360	9	350	325	357	52	2	326	302
28	R2	228	126	20	331	265	14	239	25	336	114	350	235	357	234	2	325	54
29	2Q	109	115	88	56	120	103	116	103	132	119	100	103	96	110	99	88	141
30	P1	113	113	114	111	107	108	109	108	109	110	111	112	118	113	115	103	118
31	2SM	174	169	163	174	171	155	195	159	153	154	0	174	0	220	0	0	187
32	M3	197	190	90	46	52	9	192	221	122	60	0	148	0	112	0	0	174
33	L2	13	359	12	360	351	7	11	358	9	347	11	13	16	358	16	352	14
34	2MK3	103	98	98	114	103	122	98	111	112	117	0	111	0	100	0	0	102
35	K2	343	343	346	335	338	333	330	335	333	6	350	344	357	340	2	325	11
36	M8	20	13	0	36	3	311	69	2	4	343	340	329	302	45	0	232	339
37	MS4	32	50	93	65	72	66	125	87	79	89	0	100	0	135	0	0	62

		5052	5056	5074	5111	5143	5144	5165	5218	5252	5338
1	M2	15	9	15	42	26	53	29	23	25	32
2	S2	16	10	22	45	30	58	30	28	30	35
3	N2	355	345	354	21	6	31	8	1	10	15
4	K1	130	120	125	143	131	149	132	131	134	141
5	M4	269	14	266	273	231	19	307	276	337	5
6	O1	120	112	119	134	122	143	126	123	130	138
7	M6	162	142	147	211	156	265	168	154	221	319
8	MK3	103	0	97	133	113	141	122	116	97	112
9	S4	325	123	355	32	317	54	326	303	56	356
10	MN4	259	0	242	278	220	5	251	236	331	353
11	NU2	9	348	359	25	16	40	13	3	12	27
12	S6	345	169	251	317	211	18	320	212	353	165
13	MU2	185	347	194	223	209	236	207	197	184	188
14	2N	328	321	338	19	343	27	324	348	22	73
15	OO	177	128	152	196	199	203	182	164	171	181
16	LAM2	15	9	10	30	23	38	20	23	358	31
17	S1	264	0	53	180	129	146	171	106	32	129
18	M1	120	116	213	204	164	206	297	209	180	191
19	J1	151	124	147	191	164	201	143	160	210	200
20	MM	145	0	65	130	193	40	35	158	275	199
21	SSA	157	0	138	220	331	271	304	304	1	343
22	SA	169	0	116	238	128	24	333	306	22	285
23	MSF	13	0	44	6	23	2	17	61	58	64
24	MF	148	0	163	149	155	180	219	147	142	120
25	RHO1	126	108	125	132	129	123	171	117	109	133
26	Q1	125	108	127	149	133	157	134	124	142	156
27	T2	53	10	29	14	353	6	347	358	296	37
28	R2	136	10	137	268	298	318	41	306	289	247
29	2Q	170	104	127	49	160	226	143	116	149	222
30	P1	117	119	123	147	137	147	136	136	130	147
31	2SM	195	0	179	226	199	240	220	199	198	196
32	M3	187	0	170	191	175	42	189	166	324	339
33	L2	28	33	31	40	36	53	47	29	8	18
34	2MK3	81	0	92	127	110	136	100	101	85	98
35	K2	0	10	1	39	19	47	29	19	14	29
36	M8	132	136	81	54	36	243	198	110	196	275
37	MS4	271	0	285	325	263	26	309	302	341	2

Table E.4. Methods of Harmonic Analysis and Length of Time Series Used.

Sta. No.	Name	Harmonic Analysis	Begin	End	Days	Datum	Notes
4290	San Francisco	LSQHA	1/1/80	12/31/80	366	3.18	
4305	North Point	LSQHA	1/1/75	12/31/75	365	3.29	
4317	Pier 22 ½	LSQHA	5/1/75	2/28/76	304	3.39	
4358	Hunters Point	LSQHA	10/22/74	4/13/75	174	3.61	
4392	Oyster Point	LSQHA	1/1/75	12/31/75	365	3.78	
4449	Coyote Point	LSQHA	5/9/75	9/29/75	144	3.94	
4458	San Mateo Bridge West End	LSQHA	1/1/75	12/31/75	365	4.08	
4501	Redwood Creek Channel Marker	LSQHA	6/1/75	3/31/76	305	4.27	
4509	Dumbarton Bridge	LSQHA	1/1/80	12/31/80	366	4.50	
4510	Dumbarton RR Bridge	LSQHA	1/1/84	12/31/84	366	4.49	
4519	Mowry Slough	HA29	12/1/84		29	4.55	
4523	Redwood City Wharf 5	LSQHA	8/16/83	5/17/84	276	4.30	
4525	Palo Alto Yacht Harbor	LSQHA	5/2/84	1/13/85	257	3.82	
4575	Coyote Creek	LSQHA	10/1/75	3/31/76	183	4.83	
4637	San Mateo Bridge East End	LSQHA	12/17/76	4/13/77	117	4.12	2 blocks of data
4688	San Leandro Marina	LSQHA	4/1/82	11/30/82	244	3.92	
4724	San Leandro Channel	LSQHA	10/14/74	3/31/76	383	3.60	7 blocks of data
4746	Oaklnd/Alameda Park St. Br.	LSQHA	11/9/79	8/19/80	285	3.46	
4750	Alameda	LSQHA	1/1/80	12/31/80	366	3.49	
4764	Oakland Inner Harbor	LSQHA	12/1/76	7/5/77	170	3.44	4 blocks of data
4779	Oakland Matson Wharf	LSQHA	11/1/74	4/30/75	181	3.33	
4782	Yerba Buena Island	LSQHA	3/2/93	9/20/93	203	3.34	
4806	Sausalito	LSQHA	1/1/78	12/31/78	365	3.10	
4816	Berkeley	LSQHA	2/7/79	8/31/79	201	3.35	3 blocks of data
4818	Angel Island	LSQHA	5/1/80	11/30/80	214	3.25	

Sta. No.	Name	Harmonic Analysis	Begin	End	Days	Datum	Notes
4819	Sausalito COE Dock	LSQHA	8/29/78	5/24/79	269	3.13	
4837	Point Chauncey	LSQHA	2/25/93	8/9/93	166	3.10	
4849	Richmond Inner Harbor	HA29	10/20/94 11/22/94 12/24/94 1/26/95		29 29 29 29	3.25	Average of 4 H.A.
4863	Richmond Chevron Pier	LSQHA	1/1/96	12/31/96	366	3.25	
4873	Point San Quentin	HA29	9/7/79 9/30/79		29 29	3.12	Average of 2 H.A.
4874	Corte Madera Creek	LSQHA	7/1/77	6/30/78	365	3.14	
4881	Point Orient	HA29	9/8/79 10/1/79 4/1/83 5/19/93 6/16/93 7/13/93		29 29 29 29 29 29	3.22	Average of 6 H.A.
4906	Point Bonita	HA29	4/10/80 5/15/80		29 29	3.34	Average of 2 H.A.
5009	Point San Pedro	LSQHA	5/1/80	11/30/80	214	3.16	
5052	Galinas	LSQHA	7/7/79	11/20/79	137	3.14	
5056	Point Pinole	HA29	4/1/83		29	3.23	
5074	Hercules	LSQHA	9/5/86	2/3/87	152	3.47	
5111	Benicia	LSQHA	1/1/81	12/31/81	365	2.75	
5143	Crockett	LSQHA	4/1/80	11/30/80	244	3.04	
5144	Port Chicago	LSQHA	1/1/93	12/31/93	365	2.55	
5165	Mare Island Strait	LSQHA	1/26/78	9/9/78	227	3.15	
5218	Mare Island Naval Shipyard	LSQHA	1/1/86	12/31/86	365	3.05	
5252	Petaluma River Ent.	LSQHA	7/1/85	1/31/86	215	3.24	
5338	Sonoma Creek Ent.	LSQHA	9/5/85	3/24/86	201	2.88	

APPENDIX F. SIMULATED CONSTITUENT FIELDS FOR SAN FRANCISCO BAY

Distribution of constituent amplitudes and epochs computed with the TRIM numerical model (Cheng et al., 1993) and the TCARI method. Tide stations are shown as open squares.

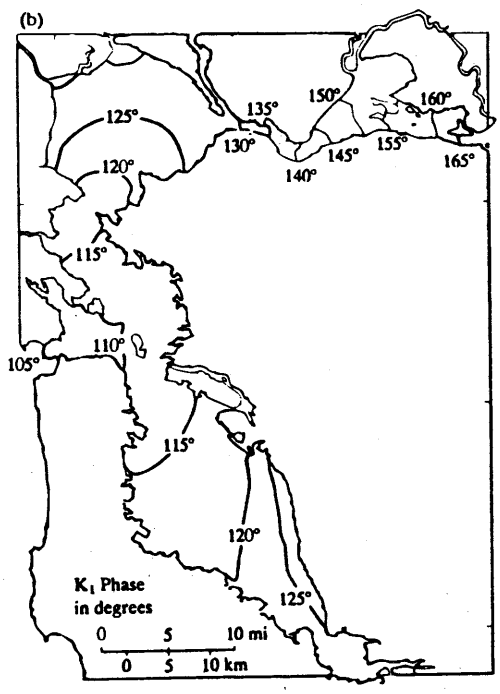

K_1 local epoch (degrees) from TRIM.

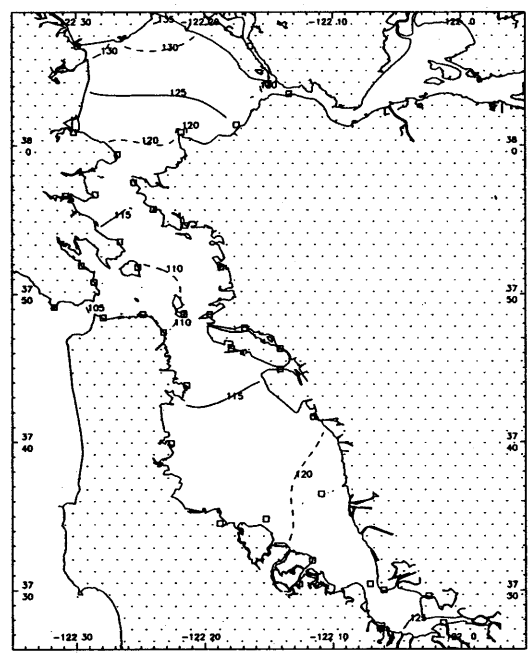

K1 local epoch (degrees) from TCARI.

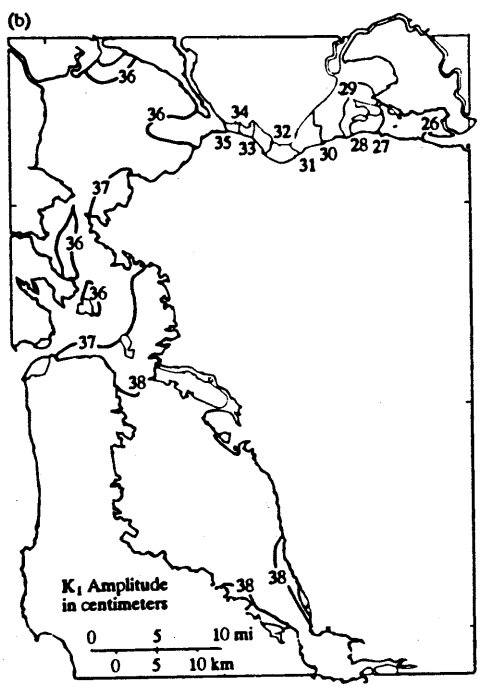

K_1 amplitude (cm) from TRIM.

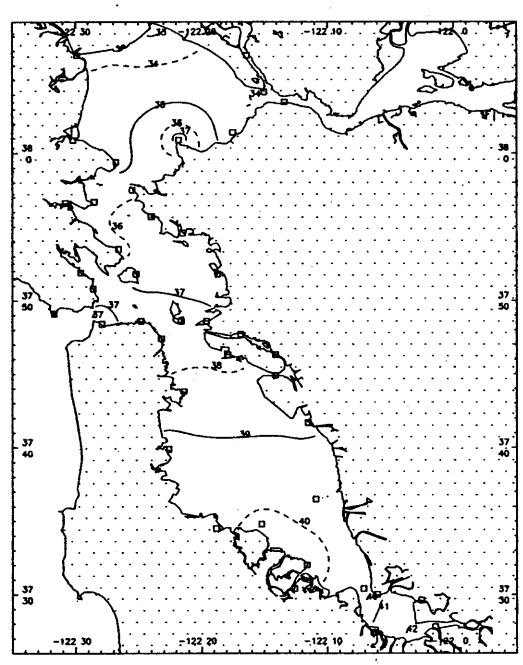

K_1 amplitude (cm) from TCARI.

Figure F.1. TRIM (left column) and TCARI (right column) fields for K_1 phase and amplitude.

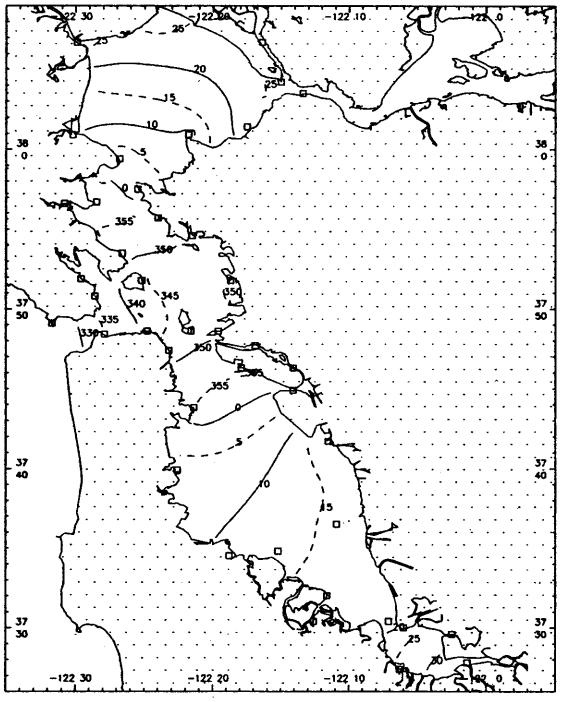

S_2 local epoch (degrees) from TCARI.

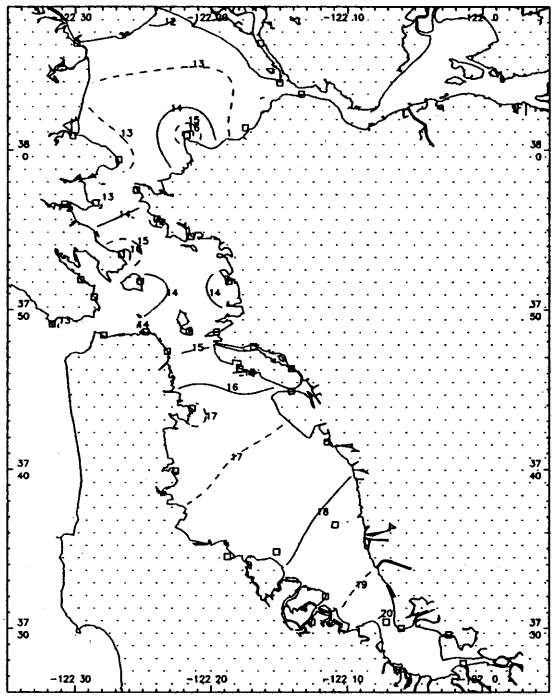

S_2 amplitude (cm) from TCARI.

Figure F.2. TCARI fields for S_2 phase and amplitude.

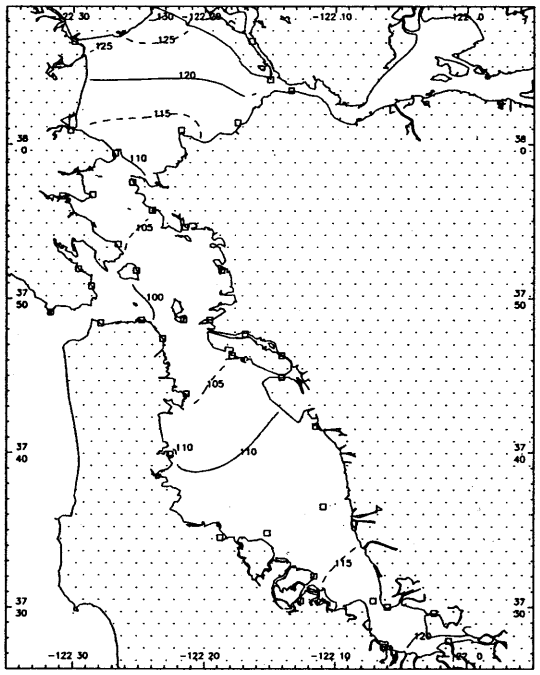

O_1 local epoch (degrees) from TCARI.

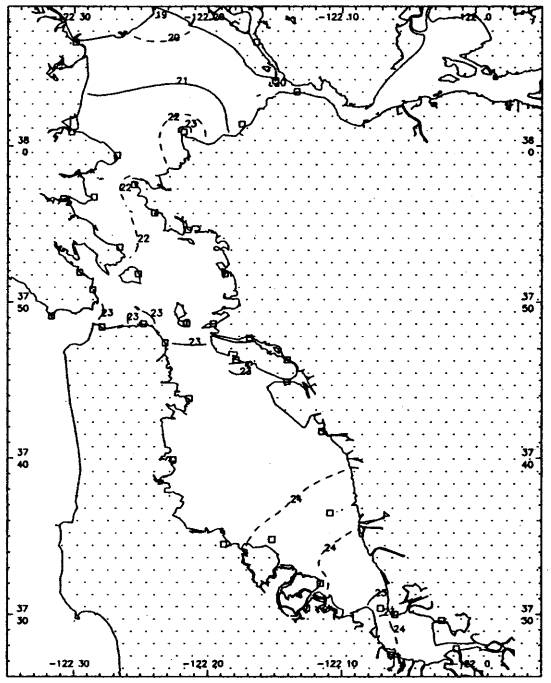

O_1 amplitude (cm) from TCARI.

Figure F.3. TCARI fields for O_1 phase and amplitude.

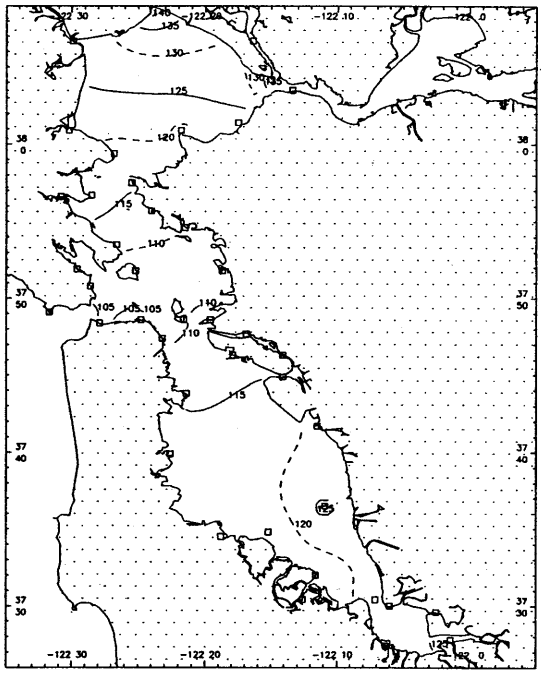

P_1 local epoch (degrees) from TCARI.

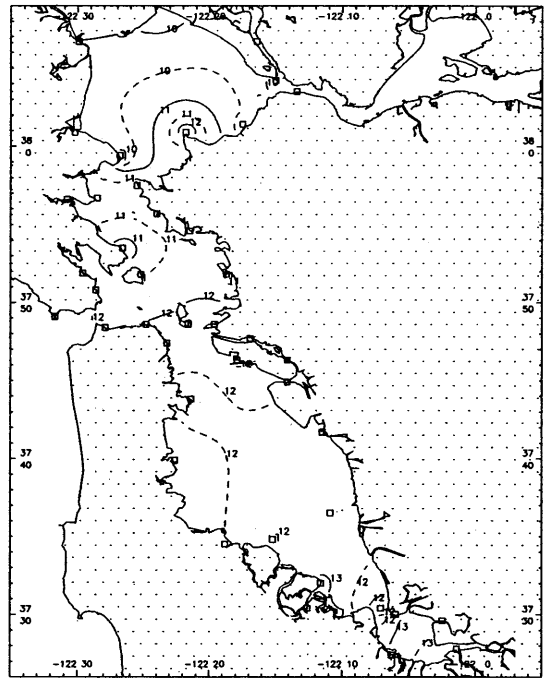

P_1 amplitude (cm) from TCARI.

Figure F.4. TCARI fields for P_1 phase and amplitude.

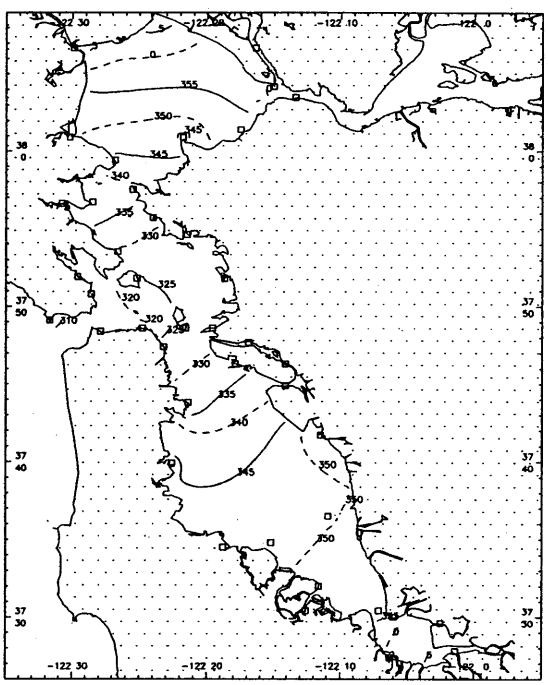

N_2 local epoch (degrees) from TCARI.

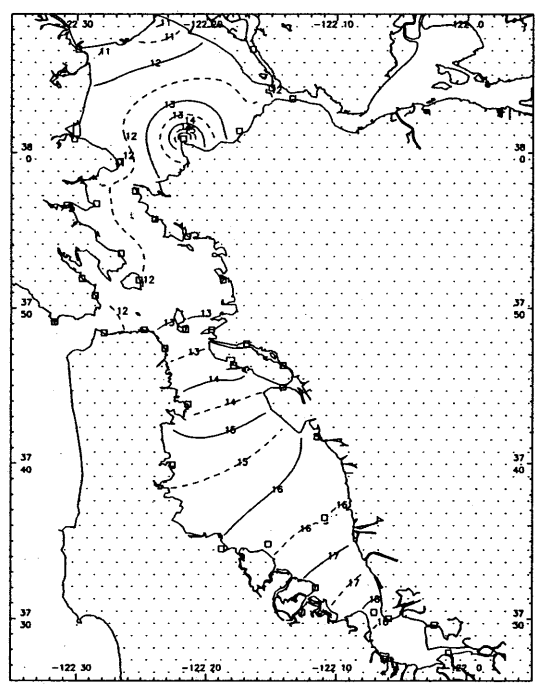

N_2 amplitude (cm) from TCARI.

Figure F.5. TCARI fields for N_2 phase and amplitude.